

Technical University of Crete
Faculty of Environmental Engineering

Passive Radiative Cooling: State-of-the-art materials

Master in Environmental Engineering: *Environmental Management, Sustainable Energy and Climate Change*

Postgraduate student: *Anastasiadou Alexandra*

Supervisor: *Kolokotsa Denia*

Examination committee: Kolokotsa Denia (supervisor)

Lazaridis Michalis

Xekoukoulotakis Nikolaos

Chania, Crete 2020

Credits

At the end of my dissertation thesis, I would like to thank all the people who helped, each in their own way, in its realization.

First of all, I thank my supervising professor Mrs. Kolokotsa for our cooperation during the postgraduate program of Environmental Engineering at the Technical University of Crete.

Also, Professors Mr. Lazaridis and Mr. Xekoukoulotakis, who agreed to be on the examination committee and evaluate the postgraduate thesis.

I owe a big thank you to Gobakis Konstantinos, Ioannis Moukazis as well as to Mr. Xekoukoulotakis and Konstantina Tyrovola for the help they offered during my dissertation.

Abstract

The environmental degradation has led to a quest for green and sustainable ways of living. In the built environment, the idea of cooling without energy input is very tempting and has been going around for years, while cool materials keep being more and more effective. Here we analyze two state – of – the – art passive radiative cooling coatings. Radiative cooling materials emit radiation that goes directly to outer space through the atmospheric window while the percentage of radiation that they absorb is as low as possible. The atmospheric window is the window of 8 – 13 μm , where the infrared radiation passes immediately to outer space without any significant absorption by the Earth’s atmosphere. Thus, it manages to acquire sub – ambient surface temperature which can contribute to improving the thermal comfort conditions in the buildings, the energy conservation, the mitigation of the urban heat island effect while it can also be used for low – grade heat dissipation from power stations

Based on the most recent research papers, we fabricate two radiative materials and we study their performances.

The first material is a porous polymer coating based on the research paper “*Hierarchically porous polymer coatings for highly efficient passive daytime radiative cooling*” by J. Mandal et al. Using a simple, scalable and cheap phase – inversion-based process, we construct a passive radiative coating and then try to merge it with different dyes.

The second material is a diffuse surface material for daytime radiative cooling based on the research paper “*Preliminary experimental study of a specular and a diffuse surface for daytime radiative cooling*” by Ao, X. et al. We first make the NaZnPO_4 powder and out of the powder we chemically prepare the surface.

In order to measure their performance, we test their reflective properties by a UV – Vis – NIR spectrophotometer. We also measure the porous polymer coating using a quantum cascade laser QCL. Finally, we test their performances by placing them on a rooftop and comparing their thermal qualities using a thermal camera.

Περίληψη

Η υποβάθμιση του περιβάλλοντος έχει οδηγήσει στην αναζήτηση πράσινων και βιώσιμων τρόπων ζωής. Στο δομημένο περιβάλλον, η ιδέα της ψύξης χωρίς κατανάλωση ενέργειας είναι πολύ δελεαστική και υπάρχει εδώ και χρόνια, ενώ η τεχνολογία των ψυχρών υλικών συνεχίζει να αναπτύσσεται. Στην παρούσα εργασία αναλύουμε δύο υπερσύγχρονα ψυχρά υλικά παθητικής ακτινοβολίας. Τα υλικά αυτά εκπέμπουν ακτινοβολία που φεύγει απευθείας στο διάστημα, μέσω του ατμοσφαιρικού παραθύρου, ενώ το ποσοστό της ακτινοβολίας που απορροφούν είναι όσο το δυνατόν χαμηλότερο. Το ατμοσφαιρικό παράθυρο είναι το παράθυρο των 8 - 13 μm , όπου η υπέρυθη ακτινοβολία φεύγει αμέσως στο διάστημα χωρίς σημαντική απορρόφηση από την ατμόσφαιρα της Γης. Έτσι, το υλικό καταφέρνει να αποκτήσει θερμοκρασία επιφάνειας χαμηλότερη από τη θερμοκρασία του περιβάλλοντος. Αυτό μπορεί να συμβάλει στη βελτίωση των συνθηκών θερμικής άνεσης μέσα στα κτίρια, στην εξοικονόμηση ενέργειας, στον μετριασμό του φαινομένου αστικής θερμικής νησίδας, ενώ μπορεί επίσης να χρησιμοποιηθεί για χαμηλού βαθμού απαγωγή θερμότητας από τα εργοστάσια.

Με βάση τις πιο πρόσφατες ερευνητικές αναφορές πάνω στο θέμα, κατασκευάζουμε δύο τέτοια υλικά και μελετάμε τις επιδόσεις τους.

Το πρώτο υλικό είναι ένα πορώδες πολυμερές επίχρισμα βασισμένο στην ερευνητική αναφορά των J. Mandal et al. Χρησιμοποιώντας μια απλή και φθηνή διαδικασία που βασίζεται σε αλλαγή φάσης, κατασκευάζουμε το υλικό και μετά προσπαθούμε να ενσωματώσουμε σε αυτό διάφορες βαφές.

Το δεύτερο υλικό βασίζεται στην ερευνητική αναφορά «Preliminary experimental study of a specular and a diffuse surface for daytime radiative cooling» από τους Ao, X. et al. Κατασκευάζουμε πρώτα τη σκόνη NaZnPO_4 και από τη σκόνη φτιάχνουμε την επιφάνεια.

Για να μετρήσουμε την απόδοσή τους, μετράμε τις ανακλαστικές τους ιδιότητες με ένα φασματοφωτόμετρο UV - Vis - NIR, ενώ το πολυμερές υλικό το μετράμε και με λέιζερ QCL (Quantum Cascade Laser). Τέλος, δοκιμάζουμε τις επιδόσεις τους στο εξωτερικό περιβάλλον, τοποθετώντας τα σε στέγη και συγκρίνοντας τις θερμικές τους ιδιότητες με τη βοήθεια θερμοκάμερας.

Table of Contents

Titles	1
Credits	3
Abstract	5
Περίληψη	6
Table of Contents	7
1. Introduction	10
1.1 Energy consumption in the built environment	10
1.2 Climate Change	11
1.3 Cool Materials	15
1.4 Thermal Comfort	16
1.5 Urban Heat Island Effect	19
1.6 Atmospheric Window	21
1.7 Which climates are best for passive cooling technologies?	22
1.8 What happens in winter?	23
1.9 Types of passive cooling materials	23
1.9.1 Photonic emitters	24
1.9.2 Plasmonics	24
1.9.3 Metamaterials	27
1.10 Radiative cooling wood	28
1.11 Radiative cooling fabric	28

- 1.12 Cool Roofs..... 29
- 1.13 Mathematical Background..... 31
 - 1.13.1 Nighttime cooling 31
 - 1.13.2 Cloudless Sky..... 32
 - 1.13.3 Overcast and partly overcast sky 33
 - 1.13.4 Inclined surfaces 34
 - 1.13.5 Convective heat transfer..... 34
 - 1.13.6 Daytime Cooling..... 35
- 1.14 X-ray Diffraction (XRD) Analysis 37
- 1.15 Thermographic camera 39

- 2. State – of - the -art 41

- 3. Experimental 42
 - 3.1 Materials 42
 - 3.2 Fabrication 42
 - 3.2.1 Porous Polymer Coating..... 42
 - 3.2.2 NaZnPO₄ surface..... 46
 - 3.2.2.1 Making the NaZnPO₄ powder..... 46
 - 3.2.2.2 Making the surface 50
 - 3.2.2.3 Waterglass 53
 - 3.3 Measurements and Discussion 63
 - 3.3.1 Porous Polymer Coating 65
 - 3.3.2 NaZnPO₄ surface..... 69
 - 3.4 Thermal Images and Discussion 77

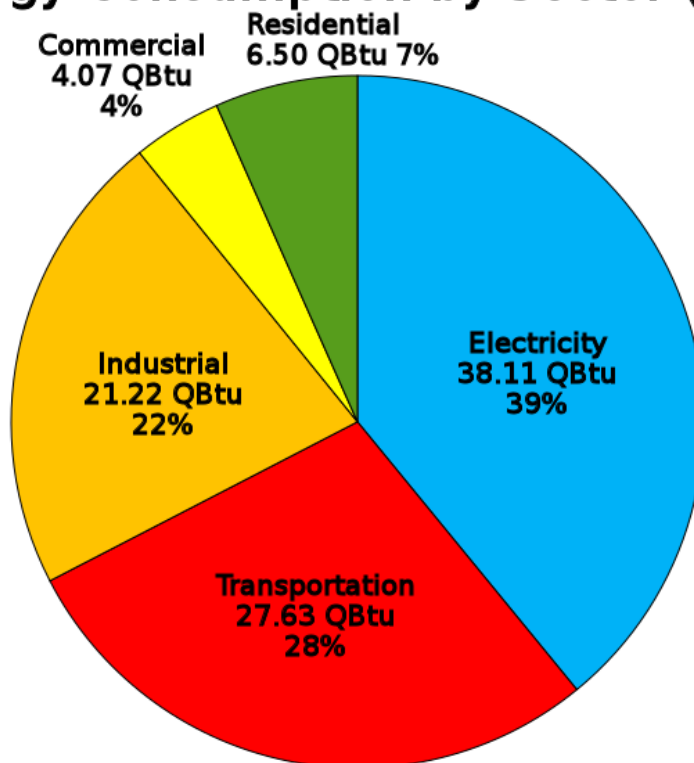
4. Conclusions	95
Bibliography	97

1. Introduction

1.1 Energy consumption in the built environment

As we become more and more aware of the **climate change**, we are looking for energy solutions that are environmental - friendly, sustainable and economically plausible. Important sums of energy are consumed for indoor and vehicular environmental comfort by heating, ventilation, and air conditioning (HVAC) systems in buildings ¹. In the following image², we can see the percentage of energy consumption by sector for the US in 2015

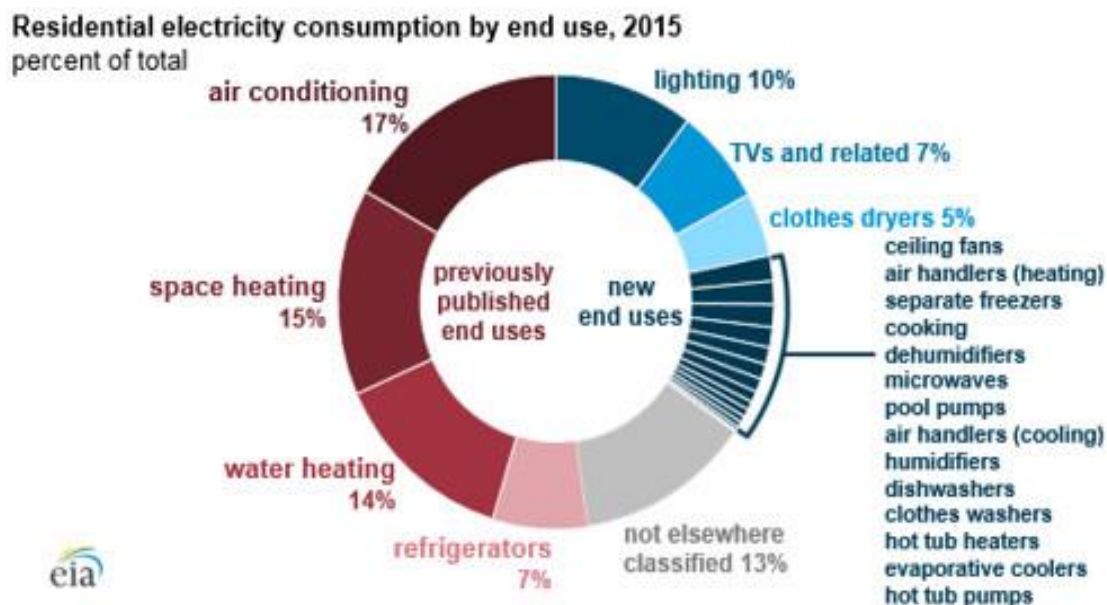
Energy Consumption by Sector (2015)



Picture 1: Percentage of US energy consumption by sector in 2015

We see that 7% of the total energy goes to the residential sector.

In the image below³ we see the residential energy consumption by sector for the same year in the US.



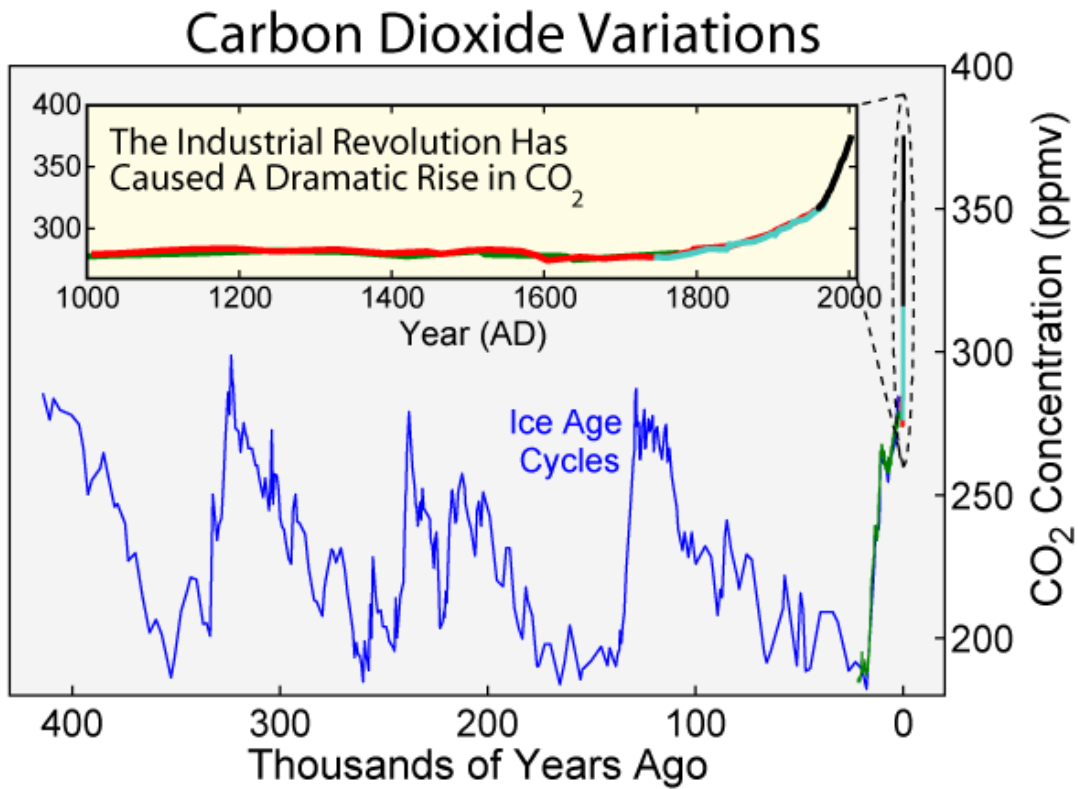
Picture 2: Residential Electricity Consumption in the US for the year 2015

Therefore, the use of HVAC systems that consume less amount of energy in the buildings is going to have positive effects on the reduction of CO₂ emissions created by the energy production and hence on the climate change.

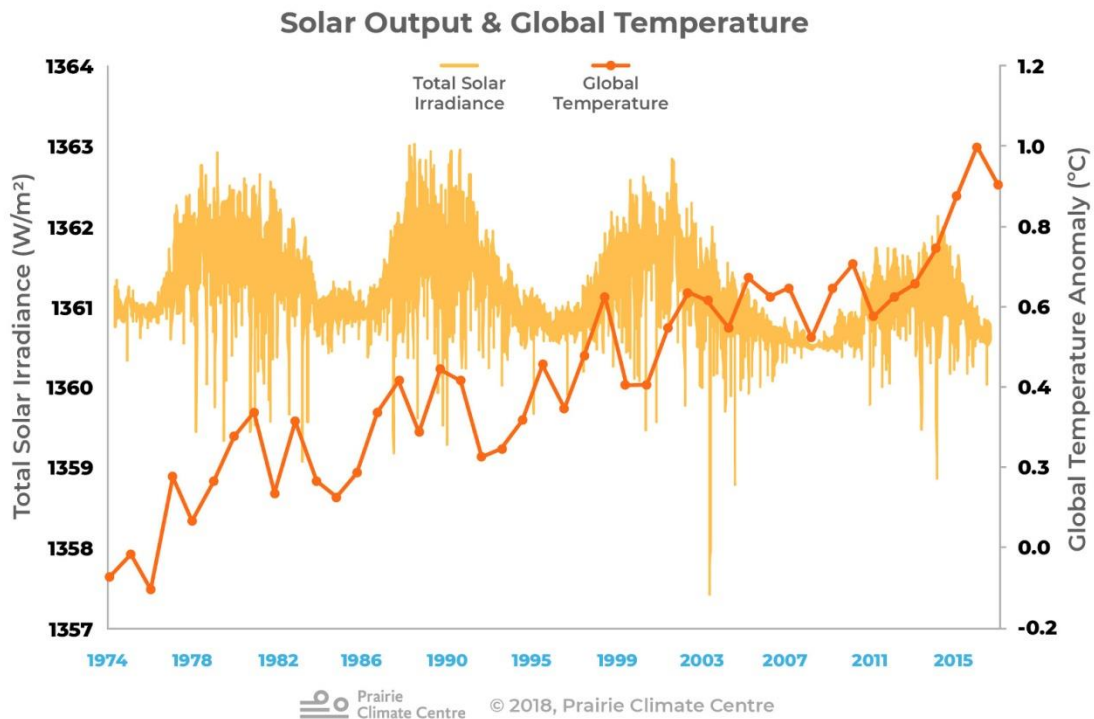
1.2 Climate Change

The climate of the Earth has changed many times along its history. We know a lot about the natural causes and effects of ancient climate change, and this knowledge leads us to state with certainty that modern **climate change is a result of human**

activity.⁴ In Picture 3 we can see the carbon dioxide concentration in the atmosphere along the years⁵ while in Picture 4⁴ we can see the relationship between the solar irradiance (W/m2) ⁶ and the global land – ocean temperature (°C; relative to 1951-1980)⁷ along the past years.



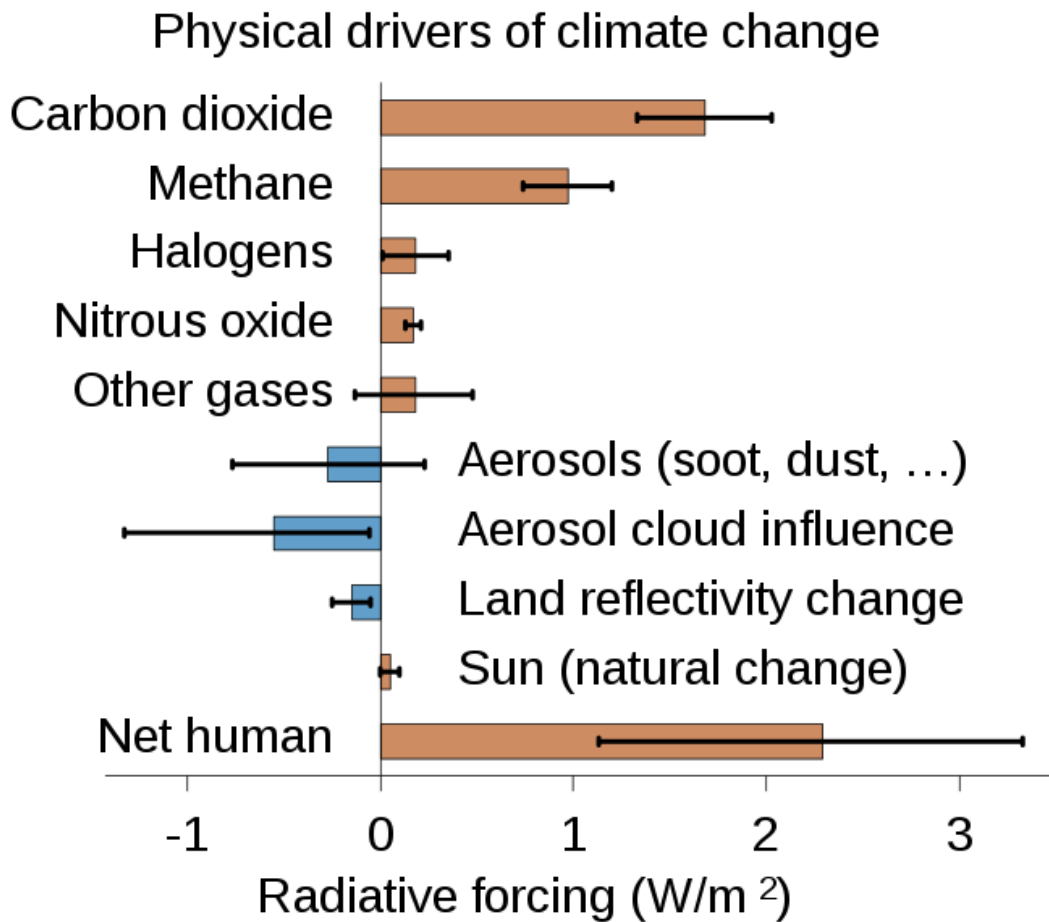
Picture 3: Carbon dioxide (CO₂) record variations



Picture 4: The warming observed around the world compared to the 11-year solar cycle

In Picture 5⁸ we can see the radiative forcing of different contributors to climate change, as taken from the Summary for Policymakers of the fifth IPCC assessment report. Radiative forcing or climate forcing is a measure of how the energy balance of the Earth–atmosphere system is influenced. The word ‘radiative forcing’ is used because these factors change the balance between incoming solar radiation and outgoing IR radiation within the Earth's atmosphere. The term forcing is used to indicate that Earth's radiative balance is pushed away from its normal state⁹.

For the gases and aerosols, the values represent both the effect they have themselves and the effect of any chemical compound they get converted into in the atmosphere. Halogens have both a positive radiative forcing as greenhouse gas and a negative forcing because they can destroy ozone. The other gases are short-lived and include carbon monoxide and NO_x. Aerosols, liquid or solid particles, often block sunlight leading to cooling. Soot, which is also considered an aerosol, has a warming effect due to its ability to absorb sunlight and make surfaces darker. Volcanoes are omitted, following IPCC AR5 because their radiative forcing fluctuates heavily and is therefore difficult to compare to other forcing agents¹⁰.



Picture 5: Radiative forcing of different contributors to climate change.

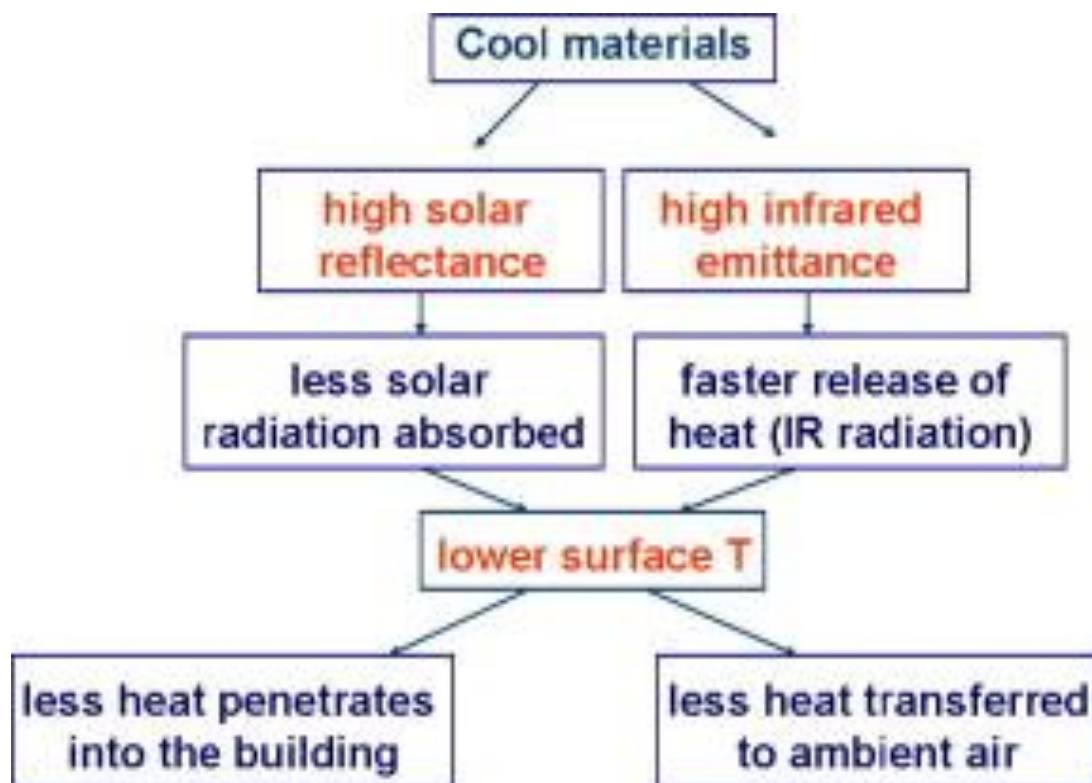
The sun's irradiance fluctuates throughout the years. The sun's irradiance varies over time. From the picture we understand that the solar output does not explain the rise in the global temperature. On the contrary, we are at the low end of the most recent 11-year solar cycle, so the past decade of warming has taken place despite low output from the sun.

Therefore, the more we can find ways to consume less energy, the faster we can mitigate the climate change effect. Passive radiative cooling systems as a way to cool

a building, is a tempting idea that could create the aforementioned results since **they operate with no power input.**

1.3 Cool Materials

Passive radiative cooling materials are a subcategory of cool materials. Cool materials are well - known for years and have the characteristics of **high solar reflectance coefficients and high infrared emittance coefficients** of the incident radiation. In that way, less solar radiation is absorbed overall and they release heat (IR radiation) faster than common materials. Thus, they manage to acquire surface temperatures lower than conventional materials so less heat penetrates into the building. In Picture 6¹¹ we see a diagram with the basic principles of cool materials.



Picture 6: The basic principles of cool materials

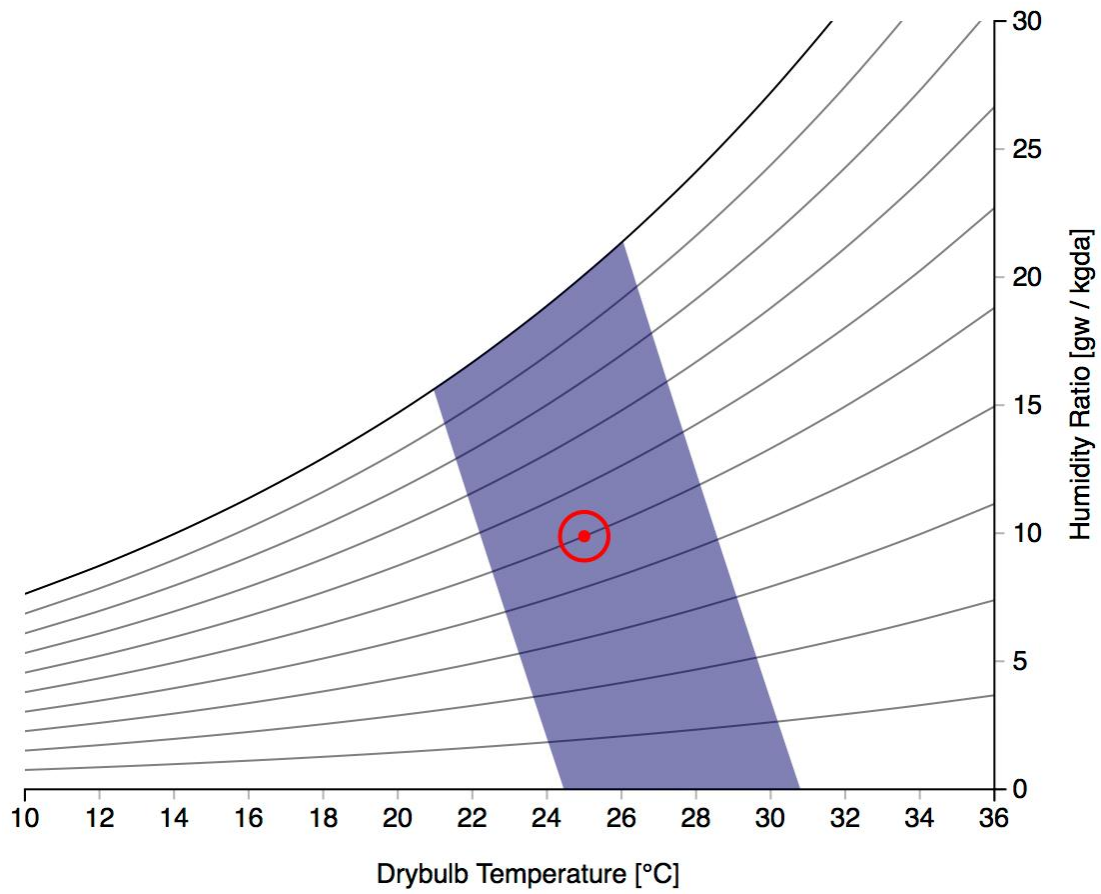
1.4 Thermal Comfort

Of course, the temperature at which different people feel comfortable can have great deviations. **The main factors that influence thermal comfort are those that determine heat gain and loss**, namely metabolic rate, clothing insulation, air temperature, mean radiant temperature, air speed and relative humidity. Psychological parameters, such as individual expectations, also affect thermal comfort¹².

Thermal comfort is defined by the American Society of Heating, Refrigerating and Air-Conditioning Engineers (ASHRAE) as “the condition of mind that expresses satisfaction with the thermal environment and is assessed by subjective evaluation¹³”. The human body gives off about 100 Watts of energy on average. It will generate excess heat into the environment and this heat transfer is proportional to temperature difference. In cold environments, the body loses more heat to the environment and in hot environments the body does not exert enough heat. Both the hot and cold scenarios lead to discomfort. Maintaining this standard of thermal comfort for occupants of buildings or other enclosures is one of the important goals of HVAC (heating, ventilation, and air conditioning) systems. Most people will feel comfortable at a range of temperatures around 20 to 25 °C¹⁴.

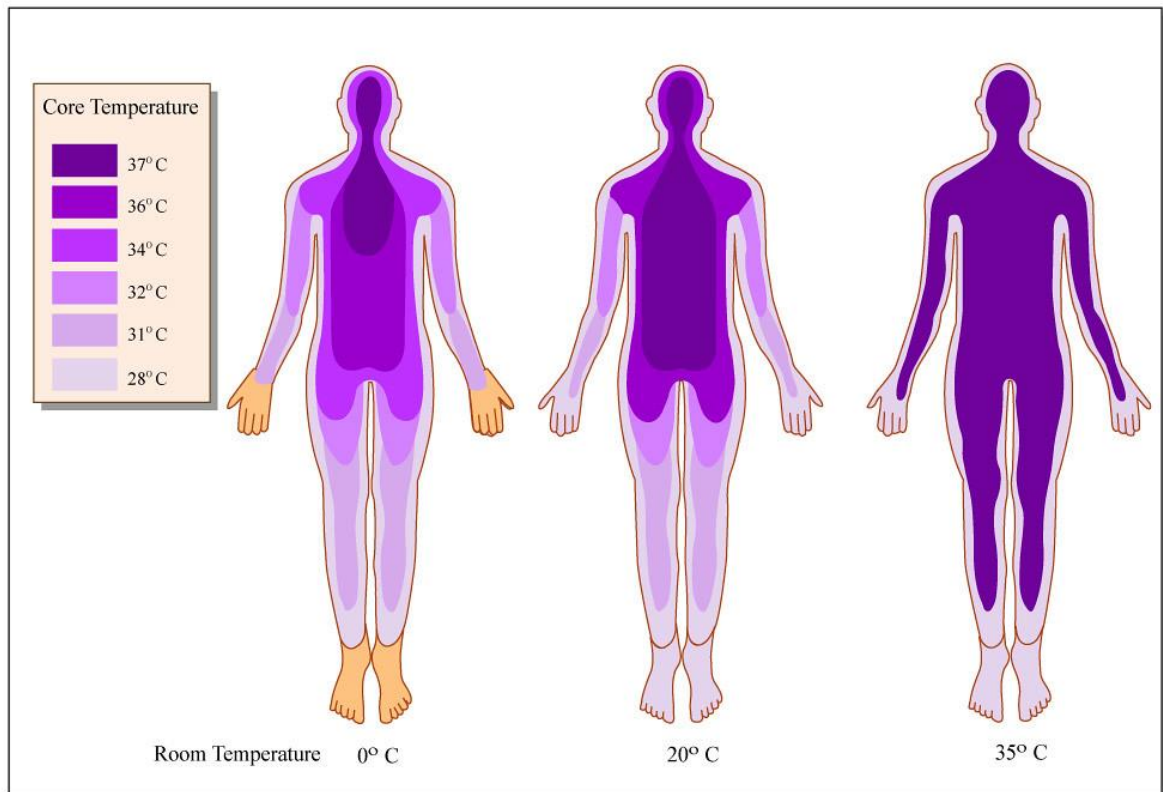
The predicted mean vote (PMV) was developed by Povl Ole Fanger at Kansas State University and the Technical University of Denmark as an empirical fit to the human sensation of thermal comfort. It was later adopted as an ISO standard. It predicts the average vote of a large group of people on a seven-point thermal sensation scale¹⁵

A **psychrometric chart** (Picture 7¹⁶) represents the acceptable combination of air temperature and humidity values, according to the PMV/PPD method in the ASHRAE 55-2010 Standard. In the picture below, the comfort zone in blue represents the 90% of acceptability¹⁶.



Picture 7: Psychrometric chart

In Picture 8¹⁷ we see how room temperature affects body temperature



Picture 8: Human body temperature at a variety of room temperatures.

Maybe the most serious problem with old cold materials is that some of them send the excess heat to the area close to the building. So yes, a building built with cold materials will be cooler than a building built with conventional materials but the excess heat will be directed to the periphery of the building augmenting the **urban heat island effect** phenomenon.

1.5 Urban Heat Island Effect

Generally, an **urban heat island** occurs when a city experiences much warmer temperatures than nearby rural areas. The difference in temperature between urban and less – developed rural areas has to do with how well the surfaces in each environment absorb and hold heat¹⁸. In Picture 9 we can see an illustration of the heat island effect¹⁸.

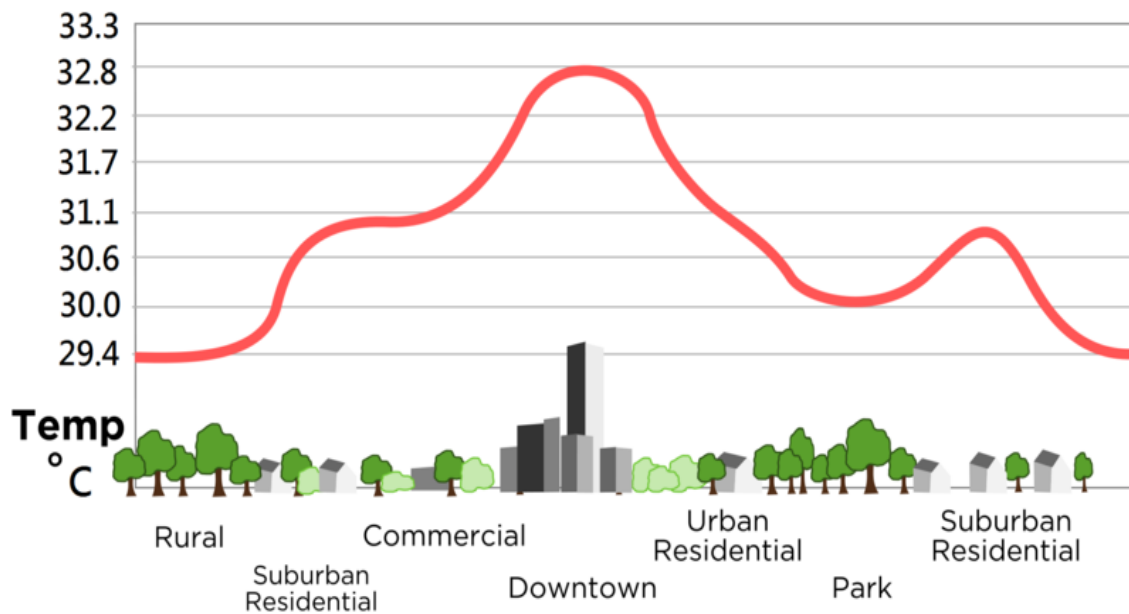


Picture 9: Illustration of urban heat island effect

In a rural area most of the region is covered with vegetation. Plants take up water from the ground and they store the water in their stems and leaves. The water eventually travels to small holes on the underside of leaves. There, the water turns into water vapor and it is released into the air, a process that is called transpiration. It acts as nature's air conditioner¹⁸.

In Picture 10¹⁹ we see the change in temperature in relation to the type of the area.

URBAN HEAT ISLAND PROFILE



Picture 10: Urban Heat Island profile

In a big city the abundance of vegetation is very limited. Instead there are structures which are made up of materials such as cement, asphalt, brick, glass, steel and dark roofs. Urban building materials are one of the reasons that urban areas trap heat. Many modern building materials are impervious surfaces so the water cannot flow through surfaces like it would through a plant. Without a cycle of flowing and evaporating water, these surfaces have nothing to cool them down¹⁸.

On the contrary, **the use of radiative cooling materials does not contribute to the heat island effect for the excess heat is reemitted to space and not to an area close by.** All in all, we could say that passive radiative cooling could be used to acquire sub – ambient surface material temperatures if the material has a certain key specific: **it emits radiation selectively within the atmospheric window while suppressing emission and absorption for wavelengths outside this range²⁰.**

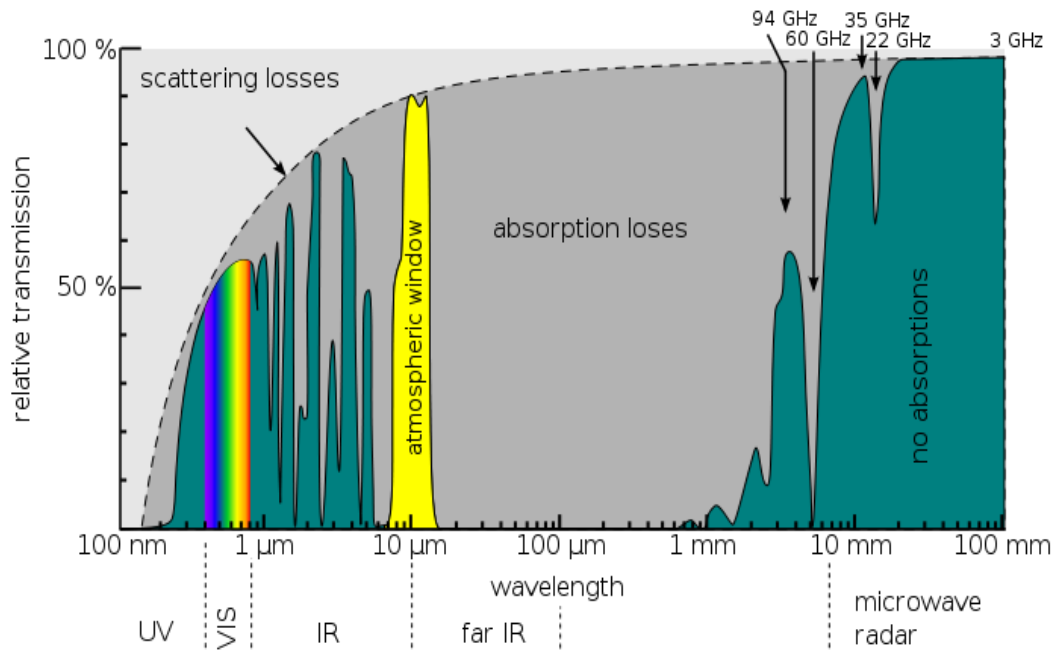
1.6 Atmospheric window

Practically, all bodies at finite temperatures emit electromagnetic radiation. The radiative characteristics of the atmosphere depend strongly on the wavelength. It has been noted that in the clear sky atmosphere, there is a **transparency window that is in the range of 8 μm – 13 μm** . This is called **atmospheric window**²¹. The infrared atmospheric window is the overall dynamic property of the earth's atmosphere, taken as a whole at each place and occasion of interest, that lets some infrared radiation from the cloud tops and land-sea surface pass directly to space without intermediate absorption and re-emission, and thus without heating the atmosphere. It cannot be defined simply as a part or set of parts of the electromagnetic spectrum, because the spectral composition of window radiation varies greatly with varying local environmental conditions, such as water vapour content and land-sea surface temperature, and because few or no parts of the spectrum are simply not absorbed at all, and because some of the diffuse radiation is passing nearly vertically upwards and some is passing nearly horizontally. A large gap in the absorption spectrum of water vapor, the main greenhouse gas, is most important in the dynamics of the window. Other gases, especially carbon dioxide and ozone, partly block transmission²¹.

The infrared atmospheric window is critical for life on Earth. In a scenario where this window does not exist, our planet would become much too warm to support life, and possibly so warm that it would lose its water (as Venus did early in solar system history). Thus this would render Earth an inhabitable planet²².

This atmospheric window also coincides with the peak thermal radiation wavelengths at average ambient temperatures²³. Therefore, **it is possible to dissipate heat from a terrestrial body to the outer space by radiative heat transfer**. From the thermal radiation point of view, we could see the outer space as a black body which has a temperature close to absolute zero, so we could say that **the outer space is the ultimate heat sink**²³

In Picture 11²⁴ we see the transmission of radiation in the earth's atmosphere as a function of wavelength. The main species that contribute to radiative absorption in the atmospheric window are CO₂, O₂ and H₂O²⁴.



Picture 11: The transmittance in the infrared atmospheric window 8 – 13 μm

From the picture above, we notice that as the main part of the ‘window’ spectrum, a clear electromagnetic spectral transmission ‘window’ can be seen between 8 and 13 μm. A fragmented part of the ‘window’ spectrum (one might say a louvred part of the ‘window’) can also be seen in the visible to mid-wavelength infrared between 0,2 and 5,5 μm²⁵

1.7 Which climates are best for passive cooling technologies?

The level of transparency of the atmospheric window depends on the local content of water vapor in the atmosphere and on the optical depth of clouds in the local sky. Optical depth (optical thickness) is how transparent a cloud is or how much the cloud modifies light passing through it. A thick cloud is optically thick especially if it has a high density of moisture. A thin cloud or a very cold cloud (low moisture density) is

optically thin. An optically thick cloud cannot be seen through as easily. An optically thin cloud can be seen through easier²⁶.

Thus, the radiative cooling capacity of solar reflectors not only depends on the optical properties of their surfaces but also on local meteorological conditions. M. Li et al²⁷ constructed detailed radiative cooling resource maps for the contiguous United States with the goal of determining the best climates for large-scale deployment of passive radiative cooling technologies.

The passive cooling potential is estimated based on ideal optical properties, i.e., zero shortwave absorbance (maximum reflectance) and blackbody long – wave emittance. They used recently calibrated correlations, experimental data and models for ground values of water vapor and temperature with sky emissivity to map out the places in the U.S. where we can most effectively reject heat from the ground to outer space. They came to the conclusion that because of the physical processes involved, locations with **drier atmospheres and the most frequent clear skies are the most appropriate** for deploying passive cooling technologies.

1.8 What happens in winter?

Another challenge is that radiative-cooling systems might increase heating costs in winter. To address this problem, scientists trying to introduce a liquid layer on top of the super-cool materials that would freeze when the temperature drops low enough. Once the liquid solidifies, radiation can no longer escape to space, so the cooling effect is cut off. And last October, Mandal and Yang reported another way to stop overcooling²⁸. If they fill the pores of their polymer coating²⁹ with isopropanol, the coating starts to trap heat rather than shed it. This can be reversed by blowing air through the pores to dry them out³⁰.

1.9 Types of passive cooling materials

A type of technology used very commonly as radiative cooling materials are advanced **nano photonics, such as photonic crystals, plasmonics, and metamaterials**. It has been shown that photonic and plasmonic selective emitters as well as metamaterials could be tuned in such a way, that they emit heat to the outer space in order to cool terrestrial objects providing passive cooling³¹.

1.9.1 Photonic emitters

Photonic emitters are nanophotonic structures that have thermal radiation properties different from conventional thermal emitters. Conventional thermal radiators have typical characteristics including a broad frequency bandwidth and a near-isotropic emission pattern. Also, they are subject to a set of fundamental constraints. For example, the spectral density of the thermal emission per unit emitter area is upper bounded by Planck's law of thermal radiation. In addition, thermal radiators are typically subject to Kirchhoff's law, which states that the angular spectral absorptivity and emissivity must be equal to each other. These characteristics and constraints impose strong restrictions on the capability for controlling thermal radiation with conventional structures³².

The field of thermal photonics utilizes thermal photonic structures with characteristics that are drastically different from those of conventional thermal radiators. A defining aspect of these thermal photonic structures is that at least one of the structural features of the radiator is comparable with or even smaller than the thermal wavelength³².

The key to daytime radiative cooling is the capability of a thermal photonic structure to control the radiation property over a very broad-band wavelength range spanning from UV to mid-wave infrared³². By utilizing multiple resonances, photonic structures can enhance or suppress their thermal emissivity in a specific frequency range and thus achieve radiative cooling³³.

1.9.2 Plasmonics

The coupling between light and collective oscillations of free carriers at metallic surfaces and nanostructures is at the origin of one of the main fields of nanophotonics: **plasmonics** (Picture 12³⁴).



Picture 12: Categories of Nanoscience & Nanotechnology

The potential applications offered by plasmonics range from biosensing to solar cell technologies and from nonlinear optics at the nanoscale to light harvesting and extraction in nanophotonic devices. Heavily doped semiconductors are particularly appealing for the infrared spectral window due to their compatibility with microelectronic technologies, which paves the way toward their integration in relatively low-cost, mass-fabricated devices. In addition, their plasma frequency can be tuned chemically, optically, or electrically over a broad spectral range³⁵.

Plasmonic emitters are usually hybrid metal structures (mostly gold and silver, but also many other materials that show metal - like optical properties in specific wavelength ranges) where by altering the composition of the materials we can tune the surface plasmons' wavelengths in a way that they resonate in the infrared region. In that way we can achieve a high factor of thermal emittance³⁶

Picture 13³⁷ depicts a surface plasmon resonance device.



Picture 13: Surface plasmon resonance device

The unique properties of plasmonic materials stem from the resonant collective oscillations of charge carriers – so-called plasmons – which can be induced by external light sources, embedded emitters or thermal fluctuations. The collective dynamics of volume plasmon oscillations is driven by the long-range Coulomb forces, and can be controlled by tailoring the spatial region filled by electron plasma³⁸.

Additionally, unlike most dyes and pigments, plasmonic nanoparticles have a color that depends on their size and shape and can be tuned to optimize performance for individual applications without changing the chemical composition of the material: for example, the solutions may contain gold or silver nanoparticles with controlled size and shape that tunes their optical response, resulting in vibrantly colored dispersions³⁶.

1.9.3 Metamaterials

The prefix meta indicates that the characteristics of the material are beyond what we see in nature. Metamaterials are artificially crafted composite materials that derive their properties from internal microstructure, rather than chemical composition found in natural materials³⁹

The core concept of metamaterials is to craft materials by using artificially designed and fabricated structural units to achieve the desired properties and functionalities. These structural units – the constituent artificial 'atoms' and 'molecules' of the metamaterial – can be tailored in shape and size, the lattice constant and interatomic interaction can be artificially tuned, and 'defects' can be designed and placed at desired locations.

By engineering the arrangement of these nanoscale unit cells into a desired architecture or geometry, one can tune the refractive index of the metamaterial to positive, near-zero or negative values. Thus, metamaterials can be endowed with properties and functionalities unattainable in natural materials.

For instance, in order for invisibility cloak technology to obscure an object or, conversely, for a 'perfect lens' to inhibit refraction and allow direct observation of an individual protein in a light microscope, the material must be able to precisely control the path of light in a similar manner. Metamaterials offer this potential.

Although metamaterials already have revolutionized optics, their performance has been limited by their inability to function over broad bandwidths of light. Designing a metamaterial that works across the entire visible spectrum remains a considerable challenge³⁹.

1.10 Radiative cooling wood

T. Li et al⁴⁰ newly engineered a wood-based material which successfully reflects heat, or infrared radiation, and could cut the energy costs associated with cooling buildings by up to 50%, according to a modeling analysis of its application in 16 U.S. cities. The white "cooling wood," which is more than eight times stronger than natural wood, is both highly reflective and capable of passive radiative cooling.

By compressing wood that has been stripped of its lignin (polymers that help make plant cells rigid), Tian Li and colleagues enhance the qualities of the already widely used, sustainable construction material and imbue it with impressive mechanical and radiative cooling properties. According to Li et al., the complete delignification and densification process not only makes the wood significantly stronger, but also results in partially aligned cellulose nanofibers, which gives the cooling wood its highly solar reflective surface, and high infrared emissivity. Testing of the cooling wood's radiative flux demonstrated continuous sub-ambient cooling during day and night. What's more, a cooling cost evaluation across 16 U.S. cities finds savings between 20% and 50%⁴¹.

1.11 Radiative cooling fabric

Peng Y. et al (2018)⁴² report an energy-saving fabric constructed from nanoporous polyethylene microfibrils using economically viable materials and industrial fabrication technologies. The embedding of nanocavities into the polyethylene microfibre not only ensures the visible opacity, but also achieves cotton-like softness. Compared with the commercial cotton fabric, the nano - polyethylene fabric's superior cooling effect brings about a 2,3 °C drop of the indoor set - point, which corresponds to a 20% energy saving. Besides the enticing cooling effect, the nano – polyethylene fabric also exhibits a collection of compelling wearability features. With

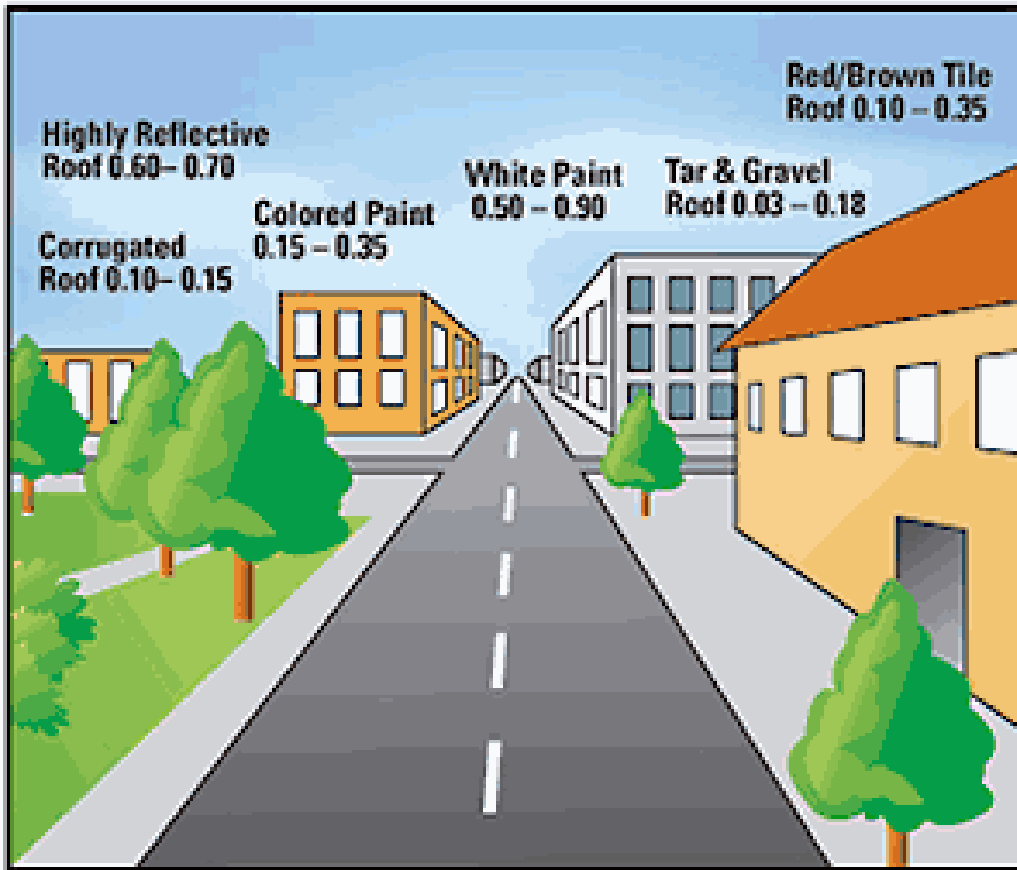
large - scale production, it can be immediately and extensively adopted as a sustainable energy - saving solution to improve our way of living. It is expected that the nano - polyethylene fabric will not only revolutionize textile for radiative cooling, but also achieve a breakthrough in reducing energy consumption for global sustainability.

P. Hsu et al (2017)⁴³ constructed a dual-mode textile that can perform both passive radiative heating and cooling using the same piece of textile without any energy input. The dual-mode textile is composed of a bilayer emitter embedded inside an infrared - transparent nanoporous polyethylene (nanoPE) layer. They demonstrated that the asymmetrical characteristics of both emissivity and nanoPE thickness can result in two different heat transfer coefficients and achieve heating when the low-emissivity layer is facing outside and cooling by wearing the textile inside out when the high-emissivity layer is facing outside. This can expand the thermal comfort zone by 6,5°C. Numerical fitting of the data further predicts 14,7°C of comfort zone expansion for dual-mode textiles with large emissivity contrast.

It is evident that daytime radiative cooling is more challenging than nighttime radiative cooling due to the incident solar radiation. Applications for radiative cooling include **low – grade heat dissipation from power stations** and **ice making** in developing countries (India and Iran) through apparatuses that permit nocturnal radiative cooling⁴⁴.

1.12 Cool roofs

Other applications are included in the architectural domain in **cool roofs** where there is a need for heat removal by passive cooling of residential and commercial buildings²³. A cool roof is one that has been designed to reflect more sunlight and absorb less heat than a standard roof. Cool roofs can be made of a highly reflective type of paint, a sheet covering, or highly reflective tiles or shingles⁴⁵. Picture 14⁴⁶ shows some roof types of surfaces and their reflectance coefficients



Picture 14: Roof surfaces and their reflectance coefficients

Cool roof coatings are white or special reflective pigments that reflect sunlight. Coatings are like very thick paints that can protect the roof surface from ultra-violet (UV) light and chemical damage, and some offer water protection and restorative features⁴⁵.

Cool roofs provide a number of benefits beyond urban heat island mitigation, including:

- *Reduced energy use:* A cool roof transfers less heat to the building below, so the building stays cooler and uses less energy for air conditioning.
- *Reduced air pollution and greenhouse gas emissions:* By lowering energy use, cool roofs decrease the production of associated air pollution and greenhouse gas emissions.

- *Improved human health and comfort:* Cool roofs can reduce air temperatures inside buildings with and without air conditioning, helping to prevent heat-related illnesses and deaths⁴⁷.

Cool roofs deflect some desired heat gain during the winter. In general, though, cool roofs result in net energy and cost savings⁴⁷

1.13 Mathematical background

1.13.1 Nighttime cooling

The heat loss of an uncovered night-sky radiator is caused by radiation and convection. The heat loss related to conductive heat transfer between radiator and surrounding can be neglected, so that

$$P_c = P_{rad} + P_{conv}$$

where

P_c is the total cooling power and

P_{conv} the convective cooling power of the radiator.

The long-wave radiative cooling power, P_{rad} , of a radiator with aperture area A and an emittance ε_r is given by

$$P_{rad} = A \cdot \varepsilon_r (\sigma T_{rad}^4 \times 2R)$$

where

R is the long-wave radiation incident on the radiator's surface and

T_{rad} the mean temperature of the radiator at a given time.

For a horizontal surface, the down welling long-wave radiation originates mainly from a few hundred meters thick atmospheric layer near the ground ($R=R_A$). The air

temperature near the ground, T_a , is fairly representative for this layer. In order to describe the radiant heat transfer of the atmosphere R_A , the term ‘sky temperature’ T_{sky} is introduced. It is defined as the temperature of a black body radiator emitting the same amount of radiative power as the sky according to

$$R_A = \sigma \cdot T_{sky}^4 = \sigma \cdot \varepsilon \cdot T_a^4$$

Where

the sky emittance ε is independent on wavelength and

σ is the Stefan–Boltzmann constant.⁴⁸

1.13.2 Cloudless sky

Several simple formulae for the estimation of the long-wave atmospheric irradiance have been compared to experimental and computed data by Skartveit et al. (1996)⁴⁹. For normally stratified, cloud-free atmospheres, it was found that the description by Berdahl and Fromberg (1982) adequately reflects the radiation physics over a wide range of T and RH . There is also the extended formula by Berdahl and Martin (1984)⁵⁰ which expresses the emittance of the night sky as a function of the temperature and the relative air humidity for cloudless atmospheres ($\varepsilon = \varepsilon_0$)

$$\varepsilon_0 = 0,711 + 0,0056 \cdot T_{dp} + 0,000073 \leq T_{dp}^2 + 0,013 \cdot \cos\left(\frac{2\pi t_m}{24}\right)$$

$$\text{and } T_{dp} = C_3 \frac{[\ln(RH) + C_1]}{C_2 - [\ln(RH) + C_1]}$$

where

t_m is the number of hours from midnight in solar time,

T_{dp} the dew point temperature in ($^{\circ}\text{C}$),

RH the relative humidity, $0 \leq RH \leq 1$,

$$C_1 = \frac{C_2 \cdot T_{dry}}{C_3 + T_{dry}}, C_2 = 17,08085, C_3 = 234,175 \text{ and}$$

the dry bulb temperature $T_{\text{dry}} = T_a$.

The experimental data by Berdahl and Martin (1984) covered for T_{dp} a range of -20 °C to +30 °C and for $(T_{\text{sky}} - T_a)$ a range of 5 K in a hot, humid climate and 30 K in a cold, dry climate⁴⁸.

1.13.3 Overcast and partly overcast sky

The presence of clouds increases the atmospheric absorbance and hence the emittance. Martin and Berdahl (1984) describe ε as an empirical adjustment of the cloudless model given in Equations (5) and (6). For overcast conditions, ε is a function of the fractional cloud cover, the cloud emittance and the temperature difference between surface and cloud base:

$$\varepsilon = \varepsilon_0 + (1 - \varepsilon_0) \varepsilon_c n \exp\left(-\frac{z_c}{z_*}\right), 0 \leq n \leq 1$$

where

z_c is the cloud base height (in km) and

$z_* = 8,2$ km.

The hemispherical cloud emittance ε_c is assumed to be ~ 1 for low and medium high clouds. For cirrus clouds, $\varepsilon_c = 0,74 - 0,084(z_c - 4)$ for $11 > z_c > 4$ km, and $\varepsilon_c = 0,15$ for $z > 11$ km⁴⁸.

1.13.4 Inclined surfaces

The long-wave radiation incident upon an inclined surface is given by the sum of the atmospheric R_A and ground components R_G . In the model by Unsworth and Monteith (1975)^{51 52}, the ground component has an isotropic angular distribution while the atmospheric radiance has an additional anisotropic term:

$$R(a) = R_A(a) + R_G(a) \quad (8)$$

where
$$R_A(a) = R_A \cos^2(a/2) + bI_7\sigma T_a^4 \quad (9)$$

and
$$R_G(a) = \sin^2(a/2) \cdot (\varepsilon_g \sigma T_g^4 + \rho_g R_A) \quad (10)$$

b is a parameter,

I_7 is a function of the tilt angle a ,

T_g is the ground surface temperature,

ε_g the emittance and

ρ_g the reflectance of the ground.

1.13.5 Convective heat transfer

The convective heat transfer can be described by

$$P_{cool}(T) = P_{rad}(T) - P_{atm}(T_{amb}) - P_{sun} - P_{cond+conv}$$

For surfaces without wind screen the coefficient for convection h is in the first order a linear function of the wind speed V which has the form $h_{conv} = a + bV$. Previous studies show a large variety in assigning values to a and b . The best fit was obtained by using h_{conv} as suggested by the Australian standards of 1989, reported and discussed by Molineaux et al. (1994)⁵³ with V in $m\ s^{-1}$.⁴⁸

$$h_{conv} = 3,1 + 4,1V [Wm^{-2} K^{-1}]$$

1.13.6 Daytime cooling

We showed the case of nighttime cooling, now as far as daytime cooling is concerned, things get more complicated. Consider a radiative cooler of area A at temperature T , whose spectral and angular emissivity is $\varepsilon(\lambda, \theta)$. When the radiative cooler is exposed to a daylight sky, it is subject to both solar irradiance and atmospheric thermal radiation (corresponding to ambient air temperature T_{amb})⁵⁴.

The net cooling power P_{cool} of such a radiative cooler is given by:

$$P_{cool}(T) = P_{rad}(T) - P_{atm}(T_{amb}) - P_{sun} - P_{cond+conv} \quad (1)$$

In equation (1) the power radiated out by the structure is:

$$P_{rad}(T) = A \int d\Omega \cos\theta \int_0^{\infty} d\lambda I_{BB}(T, \lambda) \varepsilon(\lambda, \theta) \quad (2)$$

Here $\int d\Omega = 2\pi \int_0^{\pi/2} d\theta \sin\theta$ is the angular integral over a hemisphere.

$I_{BB}(T, \lambda) = \frac{2hc^2}{\lambda^5} \frac{1}{e^{hc/(\lambda k_B T)} - 1}$ is the spectral radiance of a blackbody at temperature T , where h is Planck's constant, k_B is the Boltzmann constant, c is the speed of light and λ is the wavelength.

$$P_{atm}(T_{amb}) = A \int d\Omega \cos\theta \int_0^{\infty} d\lambda I_{BB}(T_{amb}, \lambda) \varepsilon(\lambda, \theta) \quad (3)$$

is the absorbed power due to incident atmospheric thermal radiation, and:

$$P_{sun} = A \int_0^{\infty} d\lambda \varepsilon(\lambda, \theta_{sun}) I_{AM1.5}(\lambda) \quad (4)$$

is the incident solar power absorbed by the structure. We arrive at equation (3) and equation (4) by using Kirchhoff's radiation law to replace the structure's absorptivity with its emissivity $\varepsilon(\lambda, \theta)$. The angle dependent emissivity of the atmosphere is given by $\varepsilon_{atm}(\lambda, \theta) = 1 - t(\lambda)^{1/\cos\theta}$ where $t(\lambda)$ is the atmospheric transmittance in the zenith

direction. In equation (4), the solar illumination is represented by $I_{AM1.5}(\lambda)$, the AM1.5 spectrum. We assume the structure is facing the Sun at a fixed angle θ_{sun} . Thus, the term P_{sun} does not have an angular integral, and the structure's emissivity is represented by its value at θ_{sun} .

$$P_{cond+conv}(T, T_{amb}) = Ah_c(T_{amb} - T) \quad (5)$$

is the power lost due to convection and conduction. $h_c = h_{cond} + h_{conv}$ is a combined non-radiative heat coefficient that captures the collective effect of conductive and convective heating owing to the contact of the radiative cooler with external surfaces and air adjacent to the radiative cooler.

Equation (1) in general relates the cooling power $P_{cool}(T)$ of the surface, that is, the net power outflow of the surface, as a function of its temperature. Such a surface becomes a daytime cooling device if there is a net positive power outflow when $T = T_{amb}$ under direct sunlight, that is, if it radiates more heat out to space than it gains by absorbing sunlight and atmospheric thermal radiation. The power outflow $P_{cool}(T = T_{amb})$ then defines its cooling power at ambient air temperature. In the absence of net outflow, a radiative cooler's temperature should reach a steady - state temperature below ambient. The solution of equation (1) with $P_{cool}(T) = 0$ defines the steady-state temperature T_s .

To achieve daytime radiative cooling, the device must satisfy a very stringent set of constraints as dictated by the power balance equation of equation (1). First, it must reflect sunlight strongly to minimize P_{sun} . Therefore, it must be strongly reflecting over visible and near-infrared wavelength ranges. Second, it must strongly emit thermal radiation P_{rad} while minimizing incident atmospheric thermal radiation P_{atm} by minimizing its emission at wavelengths where the atmosphere is opaque. Thus, the device must emit selectively and strongly only between 8 μm and 13 μm , where the atmosphere is transparent, and reflect at all other wavelengths. These constraints are formidable and fundamentally thermodynamic in nature. Radiative power scales as T^4 , and the Sun, at 5.777 K, far outstrips the radiation of room-temperature objects on Earth, which are typically around 300 K. Even with an ideally selective emitter that emits only in the atmospheric transparency window, over 90% of incident sunlight must be reflected to remain at ambient temperature. In practice, to achieve meaningful daytime radiative cooling more than 94% of sunlight must be reflected, especially given variation in atmospheric conditions across different geographic regions. This is particularly challenging when combined with the goal of emitting strongly and selectively in the atmospheric window.

1.14 X-ray Diffraction (XRD) Analysis

1.14.1 Introduction

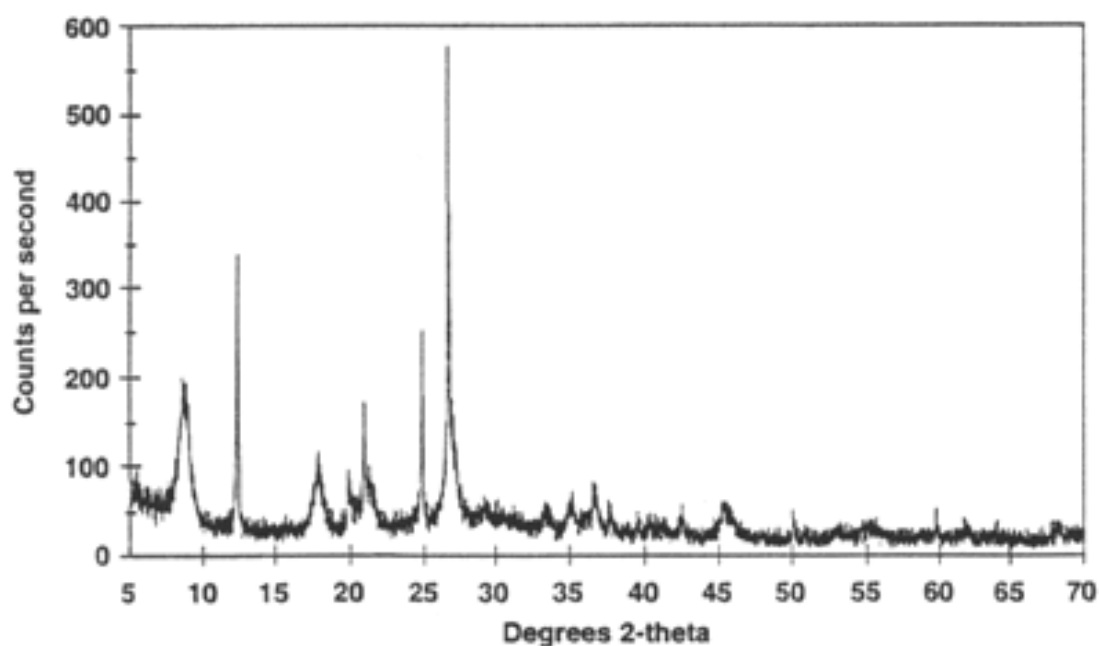
X-ray powder diffraction analysis (XRD) is perhaps the most widely used X-ray based analytical technique for characterizing materials. As the name suggests, the sample is usually in a powdery form, consisting of fine grains of crystalline material to be studied. The term 'powder' really means that the crystalline domains are randomly oriented in the sample. Therefore, when the 2-D diffraction pattern is recorded, it shows concentric rings of scattering peaks corresponding to the various d spacings in the crystal lattice. The positions and the intensities of the peaks are used for identifying the underlying structure (or phase) of the material. For example, the diffraction lines of graphite would be different from diamond even though they both are made of carbon atoms. This phase identification is important because the material properties are highly dependent on structure.

1.14.2 Theory and Methodology

The three-dimensional structure of crystalline materials, such as minerals, is defined by regular, repeating planes of atoms that form a crystal lattice. When a focused X-ray beam interacts with these planes of atoms, part of the beam is transmitted, part is absorbed by the sample, part is refracted and scattered, and part is diffracted. Diffraction of an X-ray beam by a crystalline solid is analogous to diffraction of light by droplets of water, producing the familiar rainbow. X-rays are diffracted by each mineral differently, depending on what atoms make up the crystal lattice and how these atoms are arranged. When an X-ray beam hits a sample and is diffracted, we can measure the distances between the planes of the atoms that constitute the sample by applying Bragg's Law. Bragg's Law is: $n\lambda = 2d \sin\theta$, where the integer n is the order of the diffracted beam, λ is the wavelength of the incident X-ray beam, d is the distance between adjacent planes of atoms (the d -spacings), and θ is the angle of incidence of the X-ray beam. Since we know and we can measure, we can calculate the d -spacings. The geometry of an XRD unit is designed to accommodate this measurement. The characteristic set of d -spacings generated in a typical X-ray scan provides a unique "fingerprint" of the mineral or minerals present in the sample.

When properly interpreted, by comparison with standard reference patterns and measurements, this "fingerprint" allows for identification of the material. In X-ray

powder diffractometry, X-rays are generated within a sealed tube that is under vacuum. A current is applied that heats a filament within the tube; the higher the current the greater the number of electrons emitted from the filament. This generation of electrons is analogous to the production of electrons in a television picture tube. A high voltage, typically 15-60 kilovolts, is applied within the tube. This high voltage accelerates the electrons, which then hit a target, commonly made of copper. When these electrons hit the target, X-rays are produced. The wavelength of these X-rays is characteristic of that target. These X-rays are collimated and directed onto the sample, which has been ground to a fine powder (typically to produce particle sizes of less than 10 microns). A detector detects the X-ray signal; the signal is then processed either by a microprocessor or electronically, converting the signal to a count rate⁵⁵. Changing the angle between the X-ray source, the sample, and the detector at a controlled rate between preset limits is an X-ray scan. The geometry of an X-ray diffractometer is such that the sample rotates in the path of the collimated X-ray beam at an angle θ while the X-ray detector is mounted on an arm to collect the diffracted X-rays and rotates at an angle of 2θ . The instrument used to maintain the angle and rotate the sample is termed a goniometer. For typical powder patterns, data is collected at 2θ from $\sim 5^\circ$ to 70° , angles that are preset in the X-ray scan (see Picture 15)⁵⁶.



Picture 15: Example of an XRD analysis

1.14.3 Applications

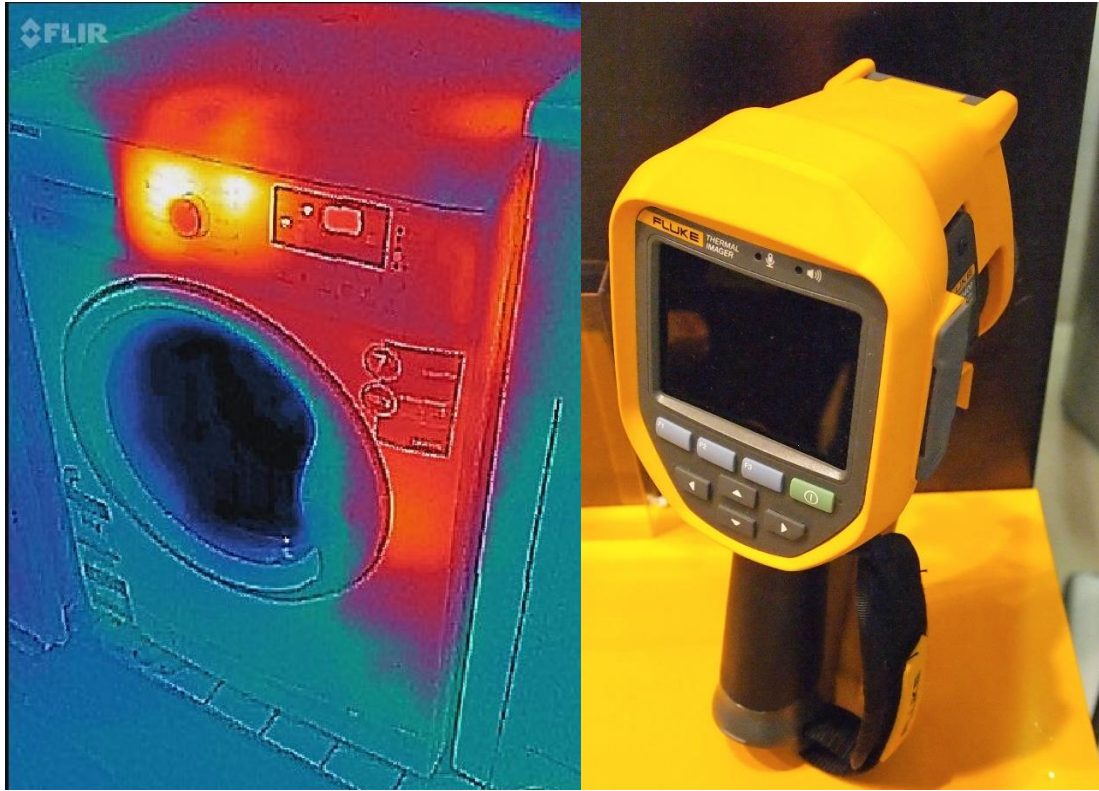
Applications XRD analysis has a wide range of applications in material science, chemistry, geology, environmental science, forensic science, and the pharmaceutical industry for characterizing materials. Amorphous materials are readily recognized by the absence of peaks in an XRD chart. The technique is also used for studying particles in liquid suspensions or polycrystalline solids (bulk or thin film materials). Other applications of XRD analysis include determination of phase transitions in a given substance, semi-quantitative determination of phases present in a sample, measurement of crystallite size particularly in nanomaterials, analysis of stress and crystal structure analysis by Reitveld refinement⁵⁵.

1.15 Thermographic camera

A thermographic camera (also called an infrared camera or thermal imaging camera or thermal imager) is a camera that creates an image using infrared radiation, similar to a common camera that forms an image using visible light. Instead of the 400–700 nanometer range of the visible light camera, infrared cameras are sensitive to wavelengths from about 1.000 nm (1 μm) to about 14.000 nm (14 μm). The art of capturing and analyzing the data they provide is called thermography.

Optical glass that is transparent to a human eye is just about perfectly opaque in the thermal infrared bands. Hence, thermal camera lenses are made out of occasionally exotic, typically expensive and frequently toxic materials like silicon crystal, germanium and zinc selenide. In order to make thermal cameras even remotely affordable, not only the imagers had to become affordable (enter microbolometers), but also the lenses⁵⁷⁵⁸⁵⁹.

Picture 16⁶⁰ shows a washing machine as an example of a thermal image whilst Picture 17⁶¹ depicts a thermal camera



Picture 16 & 17: Example of a thermal picture of a house (left) and a thermographic camera (right)

2. State-of-the-art

Most of the designs for passive radiative cooling materials comprise sophisticated emissive coatings like photonic structures, polymers, dielectrics and polymer – dielectric composites on metal mirrors. The disadvantages of these techniques are the high cost, the fragility of the material and the fact that they cannot be applied to existing roofs or walls but have to be pre – fabricated²⁹.

Hierarchically porous polymer coatings could be applied as cool – roof paints while they are not as expensive. Their performance equals or surpasses those of the state – of – the - art radiative cooling designs, while the technique offers a paint – like simplicity. Using a simple, scalable and cheap phase – inversion based process, we can produce a coating that exhibits both high solar reflectance coefficient and long – wave infrared (LWIR) thermal emittance²⁹.

Conventional cool – roof paints (CRPs) usually comprise dielectric pigments (e.g. titanium and zinc oxide) implanted in a polymer matrix. The pigments have high ultraviolet (UV) absorbance and low near – to - short wavelength infrared reflectance ($\lambda \sim 0,7\mu\text{m} - 2,5 \mu\text{m}$). By replacing the pigments in CPRs with light - scattering air voids (porous), it is possible to refrain from the environmental damages linked with the pigments while simultaneously surging up the optical characteristics and overall optical performance⁶².

The second material we are constructing is a NaZnPO_4 surface. It is also easy to be manufactured and all the devices needed for producing it are common and cheap.

3. Experimental

Based on the most recent research papers, **we fabricate two radiative materials and we study their performances.**

3.1 Materials

3.1.1 Porous Polymer Coating

Acetone, water, PVdF, green mineral powder, blue food color

3.1.2 NaZnPO₄ surface

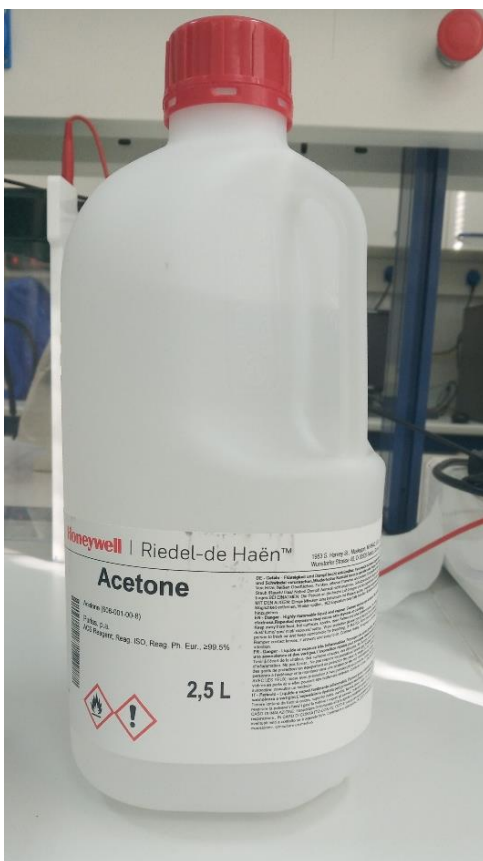
Zn(NO₃)₂·6H₂O, deionized water, H₃PO₄, Na₂CO₃, powder potassium silicate anhydrous, water

3.2 Fabrication

3.2.1 Porous polymer coating

After studying the literature in the theme of passive radiative cooling techniques, we tried to reproduce the aforementioned coating based on the research paper by J. Mandal et al²⁹.

We combined 6, 4 ml of acetone with 0, 8 ml H₂O



Lab Photo 1: Acetone

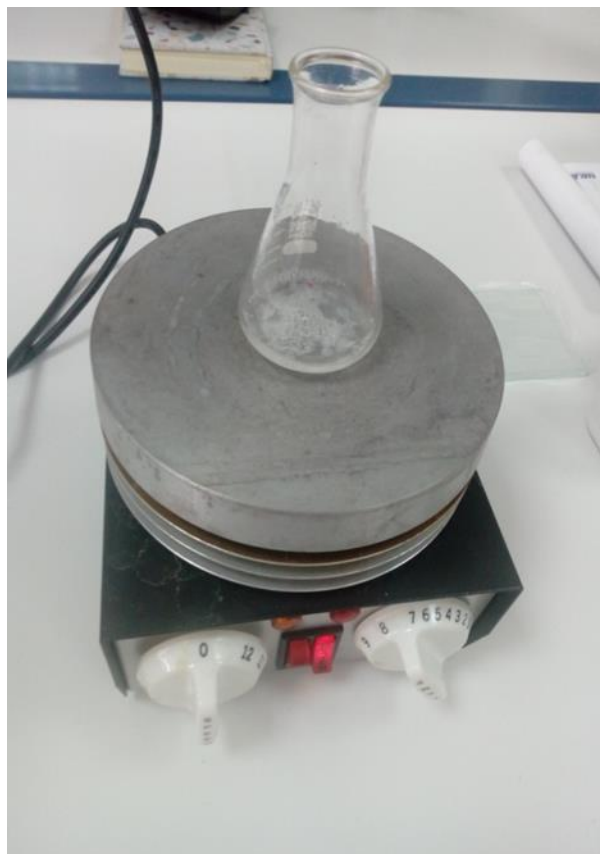
and we added 0,8 gr of the polymer.





Lab Photos 2 & 3: The polymer that we used (PVdF)

We heat the mixture in temperature around 60 °C and stirred throughout the whole process. The first two batches were not successful as the polymer did not dissolve while the acetone fully evaporated. In the third batch, we augmented the quantity of the acetone, adding now 8 ml instead of the previous 6,4 ml. However, that was not helpful either; the polymer was again not fully dissolved.



*Lab Photo 4: Preparing the mixture;
heating while stirring*

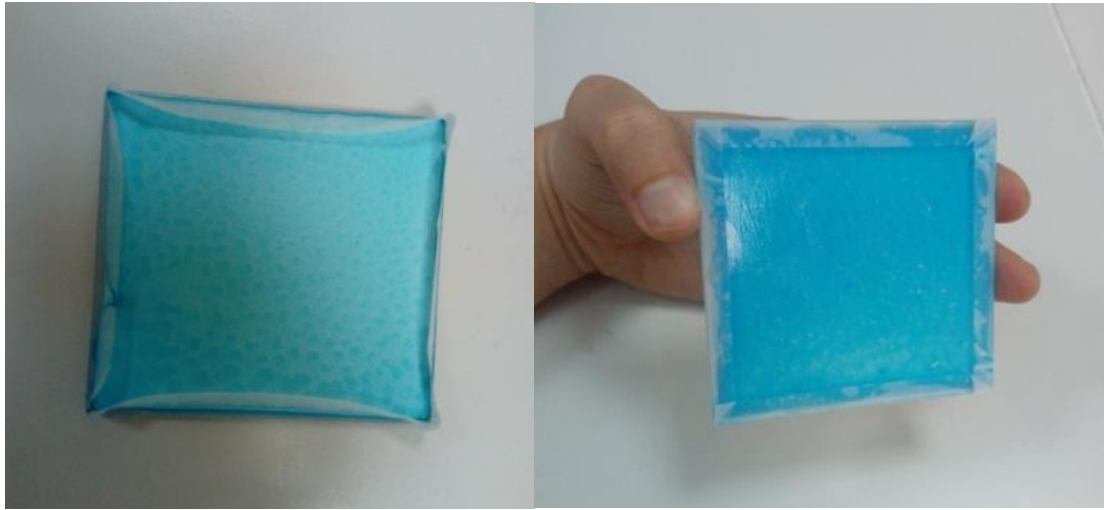
After that, we made a batch only with 8 ml of acetone and 0,8 gr of the polymer and we heat to lower temperatures (around 30 – 40 °C) while stirring. When the polymer was dissolved, we added 0,8 ml H₂O, we poured the mixture in a glass sample and let it cool and solidify. Then we tried the same procedure three times with dyes. First, we tried adding 0,8 ml of blue food color, then we tried with mineral green color and lastly, we added 1 ml of blue food color. In the green mineral color case, the dye sunk to the bottom of the sample after it dried. In the last batch, while in the beginning after a few hours, the blue dye seemed to be sinking at the bottom as well, after one day's wait the color seemed to have been equally distributed in the sample.



Lab Photo 5: The first batches. On the left we can see the sample with 0,8 ml of blue food color put on a PET basis while on the right we can see the green mineral color sample which was placed on a glass carrier.



Lab Photo 6: The second blue color batch where we added 1 ml of food blue color. After the first few hours the dye seemed to be staying at the bottom, so the front surface developed a lighter shade of blue color than the back side.



Lab Photos 7 and 8: The same sample (front side in picture 14 and back side in picture 15) after one day. The sample developed an homogenous color distribution along the surface

3.2.2 NaZnPO₄ surface

The **second material** is a diffuse surface material for daytime radiative cooling based on the research paper “Preliminary experimental study of a specular and a diffuse surface for daytime radiative cooling” by Ao, X. et al⁶³. We first make the NaZnPO₄ powder⁶⁴ and out of the powder we chemically prepare the surface.

3.2.2.1 Making the NaZnPO₄ powder

28,766 grams of Zn(NO₃)₂ · 6H₂O are dissolved in a 400 ml beaker by 100 ml deionized water and the solution is scattered in an ultrasonic oscillations instrument for 10 minutes.



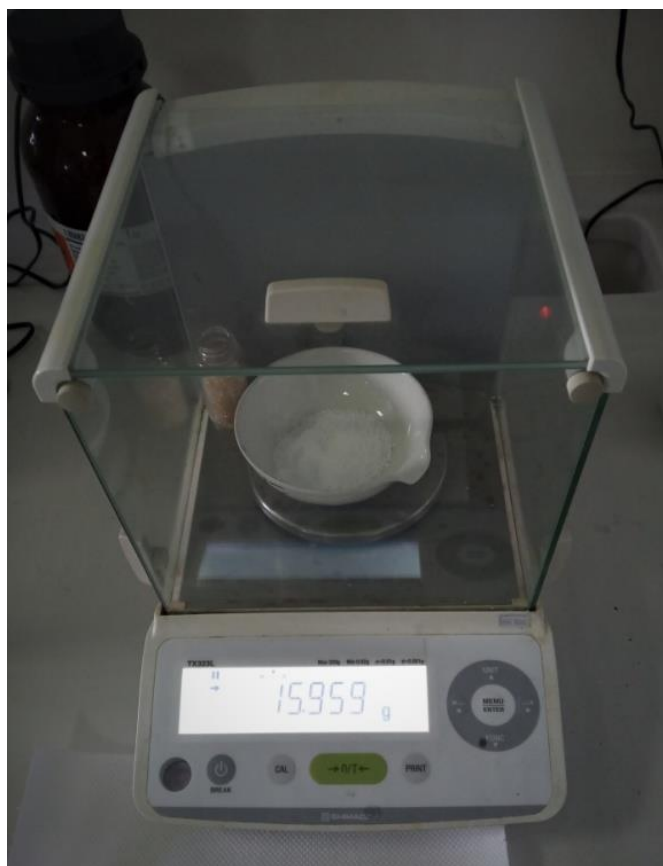
Lab Photo 9 (left): Ultrasonic oscillation instrument

Lab Photo 10 (right): Solution scattered in ultrasonic oscillation instrument

Furthermore, we added 10ml of H_3PO_4 and the solution is stirred for about ten minutes at moderate speed.

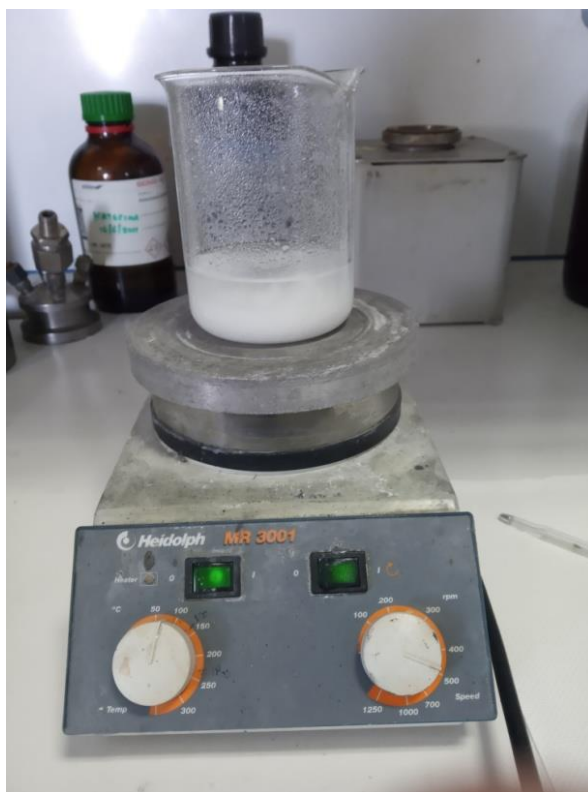


Lab Photo 11: Stirring the solution after adding the H_3PO_4



Lab Photo 12: 15,959 grams of Na_2CO_3 are weighted with electronic balance

We heat the solution at 30 °C and gradually mix it with 15,959 grams of Na_2CO_3 while stirring and elevating the temperature till 60 °C. It took us around 15 minutes to throw all the quantity of Na_2CO_3 to the solution.



Lab Photo 13: Adding the Na_2CO_3 to the solution

After that, we left the solution for 2 hours at 60 °C while stirring.

Once the solution is stewed, the precipitation is formed and it is afterwards filtered and dried for about two and a half hours in an 80 °C drying oven. The powder is heated at 600 °C for about two hours in the resistance furnace and so the product of zinc phosphate sodium is prepared by co-precipitation. After heating, we take the powder out and leave it at room temperature to get cool.



Lab Photos 14 & 15: We leave the powder to cool at room temperature

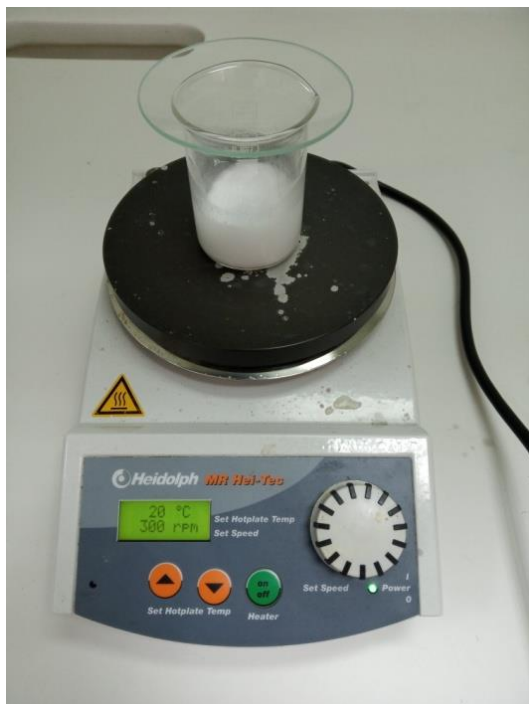
3.2.2.2 Making the surface

We pestle the powder (Lab Photo 16) in order to smash it and make it softer and homogenous.



Lab Photo 16: Pestling the powder

NaZnPO_4 powder and isopropyl alcohol are mixed with a volume ratio 1:3 and specifically, we put 7 gr. of NaZnPO_4 powder and 21 gr. of isopropyl alcohol. The solution is stirred at 250 - 300 r/min for about 80 minutes. The layer of deposited film is dried at 60 °C for 30 min.



Lab Photo 17: Stirring the solution at room temperature

After that, it is deposited on an aluminum substrate by spraying coating methods.



Lab Photo 18: We put aluminum foil on top of microbiological glasses



Lab Photo 19: We created the surface by spraying the solution on the aluminum foil



Lab Photo 20 & 21: Front and back surface of the sample

We put another glass on top once we took the samples out of the oven because the powder did not stick to the foil. However, we lost most of it while transferring them to the lab. It did not become like a surface, it was like powder on an aluminum foil, so **it**

was too vulnerable even to measure. So, we tried to look for alternative ways to turn the powder into a surface.

3.2.2.3 Waterglass

Looking for alternative ways to turn the powder into surface, we thought the use of waterglass might be a good idea.

Based on the paper “Self - Cleaning Mineral Paint for Application in Architectural Heritage”⁶⁵, the use of potassium silicate as binder not only prevents the coating from self - degradation but also offers high percentage of reflectivity in the visible to near – infrared region. In the paper, they constructed a silicate paint containing potassium silicate as the inorganic binder and colloidal silica. After measuring the paint, the total solar reflectance was calculated according to the ASTM E903 standard (weighted ordinates method), by integrating the spectral reflectance $\rho(\lambda_i)$ over the solar spectral irradiance distribution, E_λ , as follows:

$$TSR = \frac{\sum_{i=1}^n \rho(\lambda_i) E_{\lambda_i} \Delta\lambda_i}{\sum_{i=1}^n E_{\lambda_i} \Delta\lambda_i}$$

where n is the number of wavelengths for which E_λ is known.

So for the silicate paint, they found

Wavelength range (nm)	Reflectivity
	TSR = 91.0
UV (300 – 380 nm)	= 16.7
Visible (380–700 nm)	= 94.6
NIR (700–2500 nm)	= 91.2

So since the use of waterglass as a binder seems to go in line with a high reflectance quality, we decided to use it as a binder for the NaZnPO_4 powder.

Before mixing the waterglass with our powder, we tried to construct the waterglass alone.

We mixed 6 gr. of powder potassium silicate anhydrous (Lab Photos 22 & 23) with 9 gr. H_2O . The ratio is based on research from bibliography⁶⁶.



Lab Photo 22 & 23: Potassium silicate anhydrous, the powder for constructing the waterglass

We heat the mixture in a material temperature of about 80°C in order to be dissolved. We were manually stirring with a small spoon at the same time. After some minutes we realized that the solution could not be dissolved and we added 9 gr. of water more. We increased the temperature of the plate (about 180 °C). After some time, we added some more water (+ 5gr. H₂O) and increased again the temperature of the plate a bit more (~ 220 °C)



Lab Photo 24: Heating and stirring of waterglass

After an overall time of about 30 minutes of heating and manually stirring, the solution became homogeneous. We poured the liquid solution onto a glass substrate



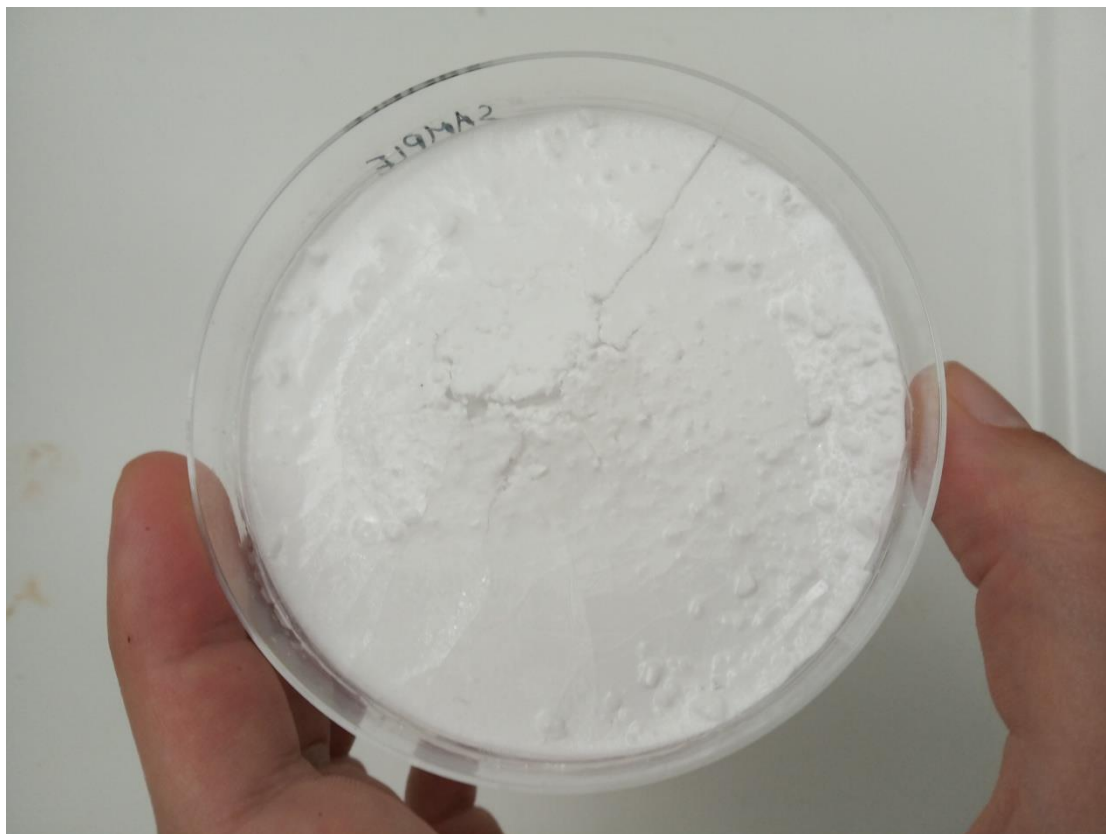
Lab Photo 25 & 26: The solution poured onto the substrate turning into a surface

We repeated the same procedure (6 gr of powder potassium silicate anhydrous and 9 gr H₂O) but this time we poured the solution onto a plastic substrate. The previous (glass) substrate had no peripheral edges, we put plastic tape around it but again, the liquid solution could not be maintained on the substrate.



Lab Photo 27 & 28: The waterglass on a plastic substrate

We followed the same procedure but this time we added 5,1 gr of NaZnPO_4 powder to the liquid solution and we dried it at 60°C for 3 days.



Lab Photo 29: The NaZnPO_4 surface with waterglass as the binder

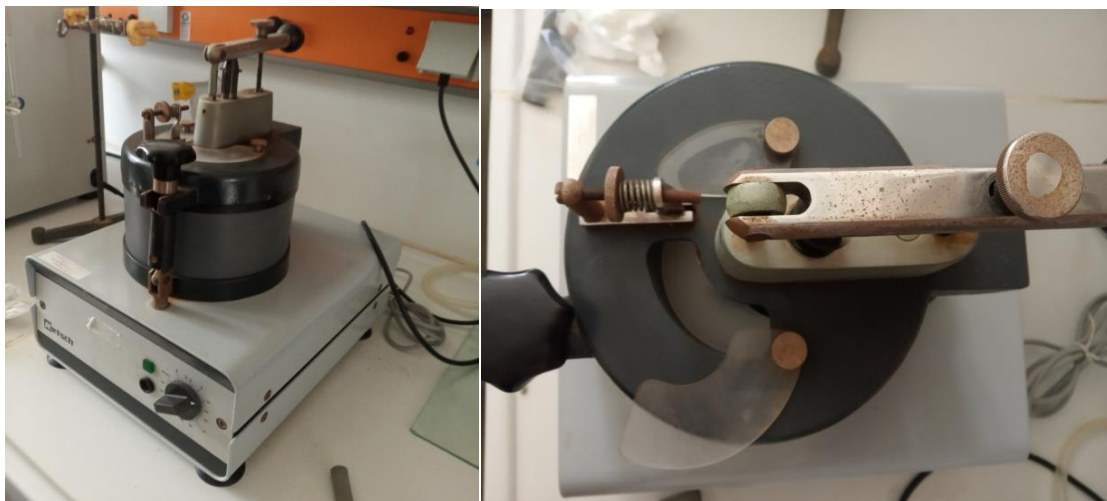
Unfortunately, during the measurement procedures, the sample broke as there was already a crack in the middle. However, we did manage to measure it before it broke. We believe we left the surface for drying longer than it needed and that is the reason why it cracked.

In order to make the surface again, we took the sample for crashing in order to make it into powder again. First, we smashed it with a hand mortar and pestle (Lab Photo 30)



Lab Photo 30: Mortar and pestle

and then we tried to make it even finer by smashing it mechanically



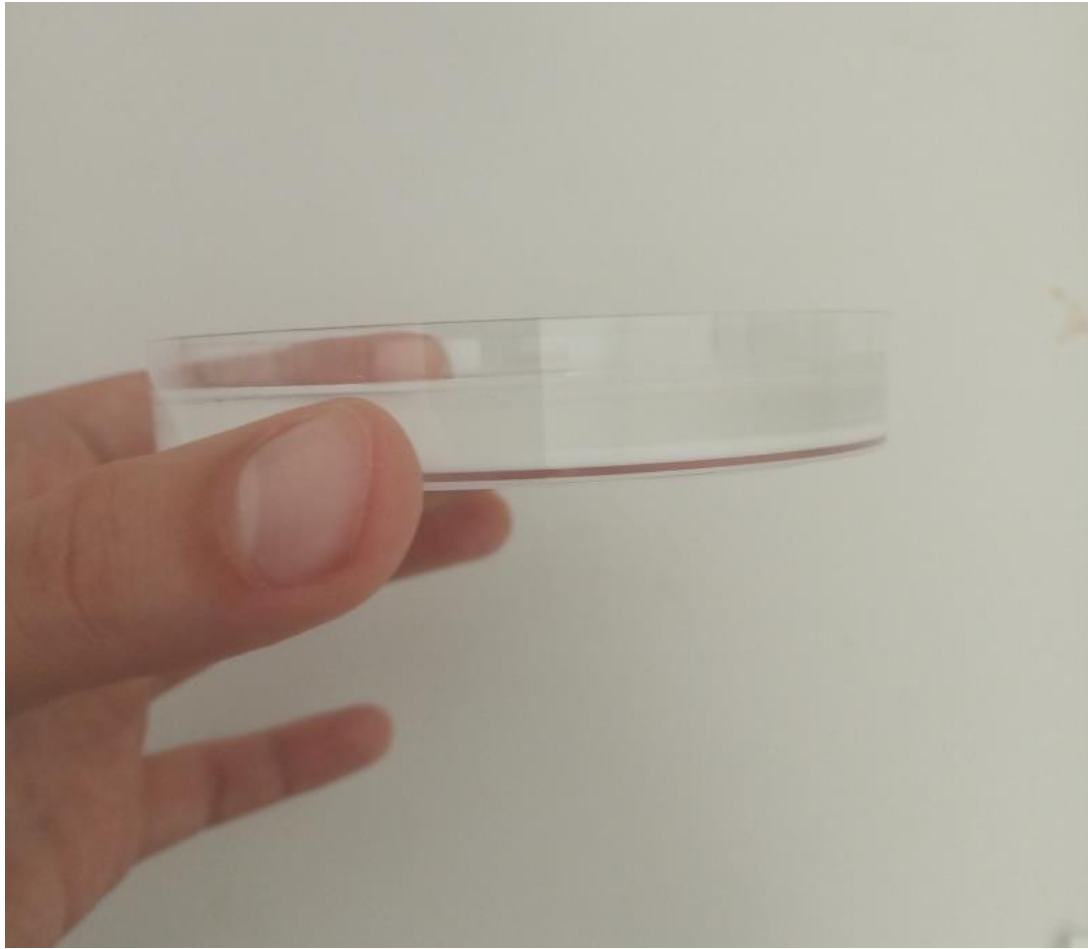
Lab Photos 31 & 32: Pestling mechanically

Unfortunately, although we cleaned the machine before using it, there were still some impurities that got mixed up with the powder

So, we tried again from the beginning to mix the powder with the waterglass. This time, we changed the analogy NaZnPO₄ powder: potassium silicate to 1: 3. So we manufactured the surface using 5 gr of NaZnPO₄ powder and mixing it with 15 gr waterglass. The surface became rather thick so we let it dry at room temperature for one week. We did not want to dry it in the oven due to fear of breaking it again.

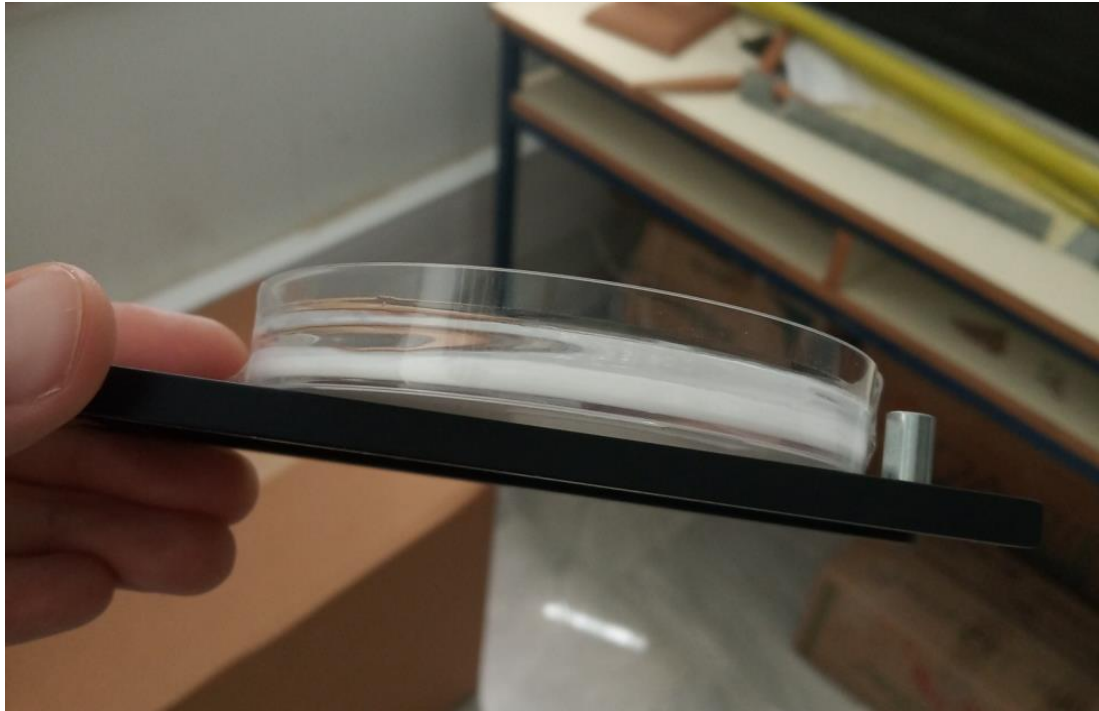
In the photos below, we can see the surface on the plastic substrate as well as its thickness.





Lab Photos 33 & 34: The second NaZnPO_4 surface. We can see its thickness and the fact that it is not distributed homogeneously. The powder is at the bottom and the waterglass is on top.

We notice that the surface is not distributed homogeneously. Most of the powder sank to the bottom and the waterglass is on top.



Lab Photo 35: Preparing the NaZnPO_4 sample (#2) to be measured by the spectrophotometer.

This was not the case when the surface was thinner, the first time we manufactured it.

After constructing the materials, we measured their reflective properties using a spectrophotometer and we tested how the materials behave under the sun. We placed some samples on the roof of the building K3 and we checked their thermal qualities using a thermo camera.



Lab Photo 36: Placing the samples on the rooftop in order to be measured with a thermal camera. From top to bottom and from left to right: porous polymer (no dye), green porous polymer, blue porous polymer (#2), blue porous polymer, waterglass and NaZnPO₄ (thick) surface (#2)

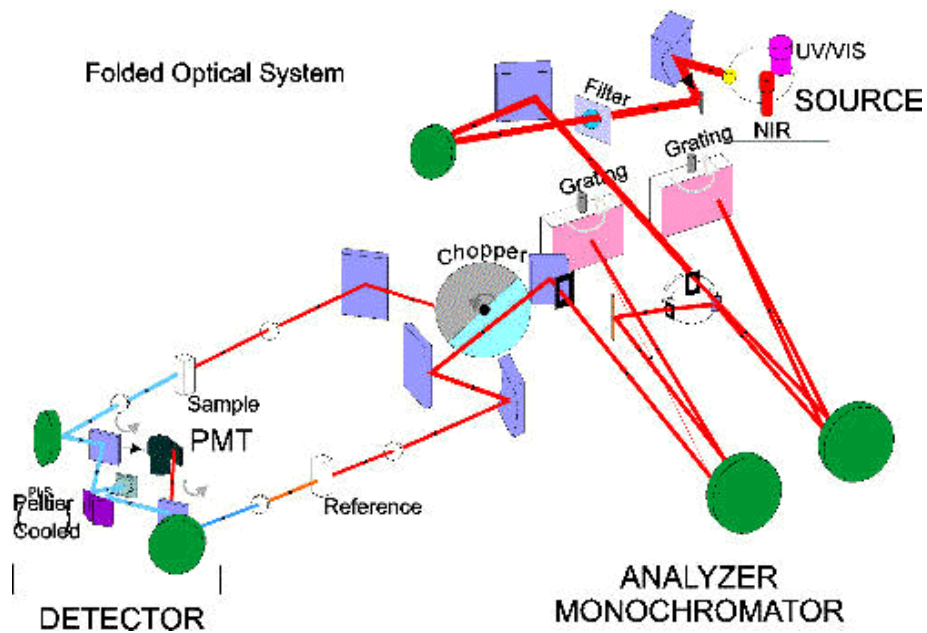
3.3 Measurements and discussion

Using a UV – Visible – Near – Infrared Spectrophotometer we took measurements of the samples. The structure can be seen in the photos below.



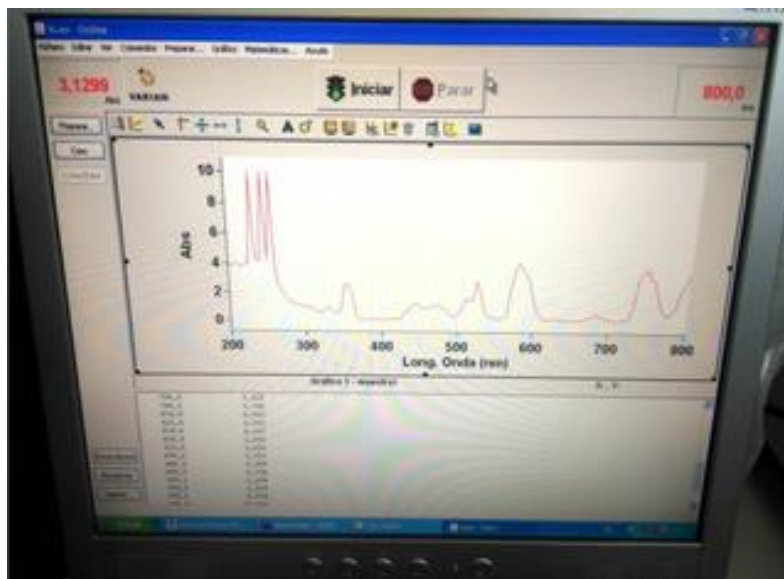
Lab Photos 37 & 38: UV – Visible – Near – Infrared Spectrophotometer and the associated computing system

This device allows the collection of UV – Vis – NIR spectra so it can specify the characteristics of optical components, thin films and coatings. It allows us to measure in the area from 200 nm to 2500 nm, though its photometric performance is greatest in the 175 nm – 900 nm range. In the picture below, we can see the specifics of the structure on the inside. The beam from the source passes from a filter and after grating it passes from a chopper in order to meet the sample. A Pb detector then is able to identify the reflected particles after the interaction of the beam with the sample.



Picture 18: The spectrophotometer in detail

The device is connected with a Windows – based modular software that is called Cary WinUV⁶⁷.



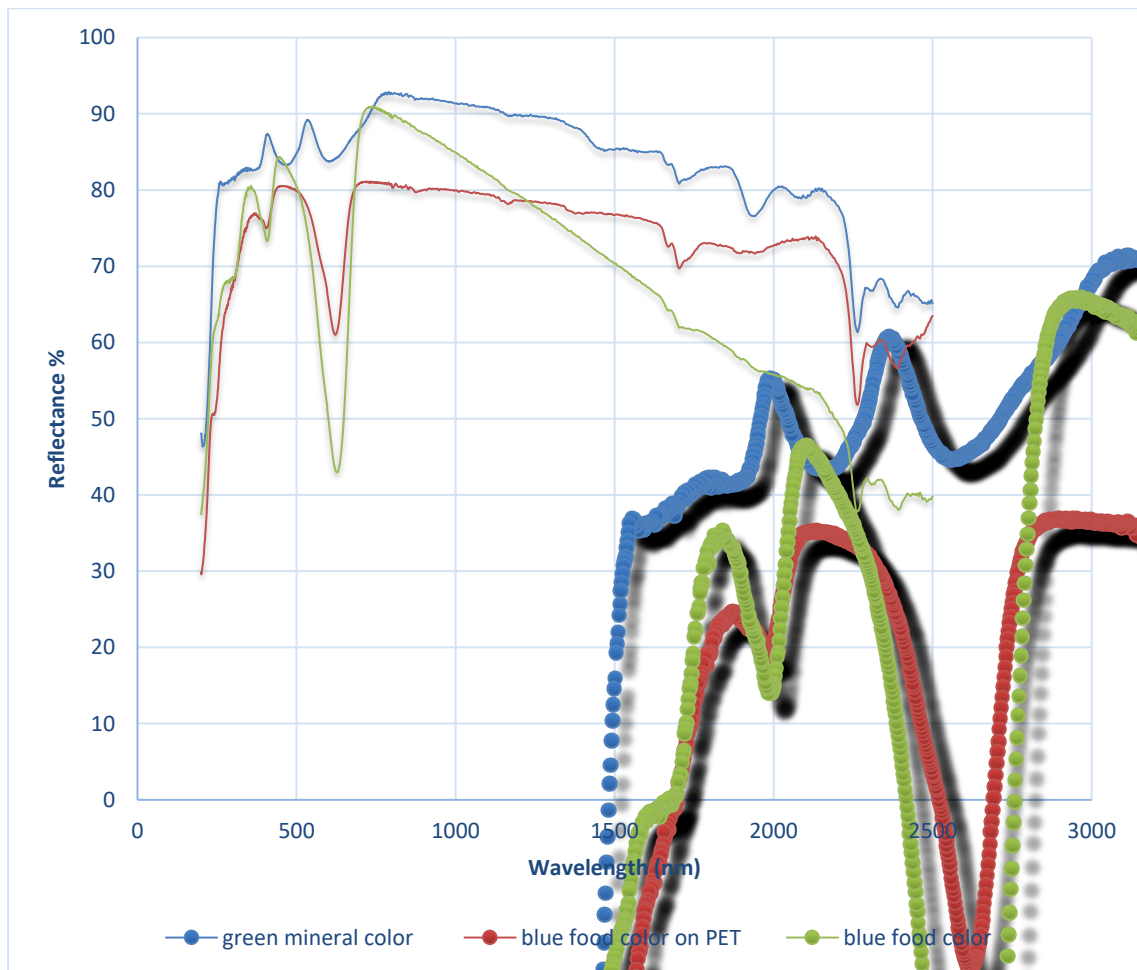
Lab Photo 39: Cary Win UV program

First, we identify the baseline by putting specific samples that demonstrate the 100 % of reflectance. Then we do the opposite by blocking the beam in order to specify the 0 % of reflectance. As long as we determine the two borderlines, we are ready to measure the reflectance percentage of our samples. We took measurements for the

blue food color and the green mineral color samples on glass substrate as well as the blue food color sample on plastic substrate.

3.3.1 Porous polymer coatings

We measured the coatings' performance using the UV – Visible – Near – Infrared spectrophotometer. On the graph below, we can see the % reflectance curves in relation to the wavelength for the three porous polymer samples.



Graph 1: Reflectance percentage in relation to the wavelength for the three porous polymer samples measured by a Cary UV Spectrophotometer.

We notice that overall, the green mineral color sample appears to demonstrate the highest reflectance percentage along this range. As for the other two samples, the blue food color is a little higher in the range ~ 300 nm – 450 nm but then its curve

demonstrates a big drop in between ~ 450 nm - 800 nm where the blue food color on PET shows a higher percentage of reflectance. Then in the area from 800 nm till ~ 1200 nm the blue food color curve is again higher but after that, it drops below the blue food color on PET curve for the rest of the wavelengths.

Then for the porous coatings, by using a quantum cascade laser, we tried to measure the diffuse reflectance in relation to the wavenumber. Quantum cascade lasers (QCLs) are semiconductor lasers where laser emission happens through interband transitions in a repeated stack of semiconductor multiple quantum well heterostructures. These lasers are comprised of dozens of alternating layers of semiconductor material which form quantum energy wells. These wells confine the electrons to particular energy states. By applying a voltage difference along the device, each electron travels from one quantum well to the next as it passes through the medium of the laser. We call “active regions” the specific positions where the electron jumps from one valence band energy state to a lower one. Simultaneously a photon is emitted. As the electron continues through the medium it finds the next active region where the same procedure takes place; the electron passes across a lower energy state and another photon is emitted. Different QCLs contain different amounts of active regions and they may have up to 75 active regions. So each electron emits the same number of photons as it travels through the device^{68 69}.

QCL can be constructed to operate in wavelengths that diode lasers cannot reach. The structure of the layers rather than the lasing material is what determines the output wavelength. So in contrast with diode lasers where the output wavelength is around 2,5 μm , QCLs run at longer wavelengths. There are devices with mid – infrared production that go till 11 μm while there are also for 25 μm although still in experimentation. So, these lasers emit in the mid – to – far – infrared region of the electromagnetic radiation⁶⁹. Specifically, the quantum cascade laser that we used operates well in the area 7 μm – 13 μm . We should remind the fact that the atmospheric window is at 8 μm – 13 μm

Perhaps the most important application for QCLs is in gas sensing and measurement. In order to measure multiple gas species, we can use systems based on widely-tunable QCLs and narrowly targeted systems can detect and measure gas concentrations in the parts-per-trillion range⁶⁹.

Distributed feedback QCLs (DFB QCL) are capable of wavelength tuning up to a few tens of cm^{-1} . External cavity QCLs (EC - QCL) expand the tuning range to $\sim 1000 \text{ cm}^{-1}$, and are used for sensing and measuring multiple gas species. These types of QCLs are used for both local and remote sensing of numerous gas species, including CO, CO₂, NH₃, CH₄, NO_x, and SO₂.

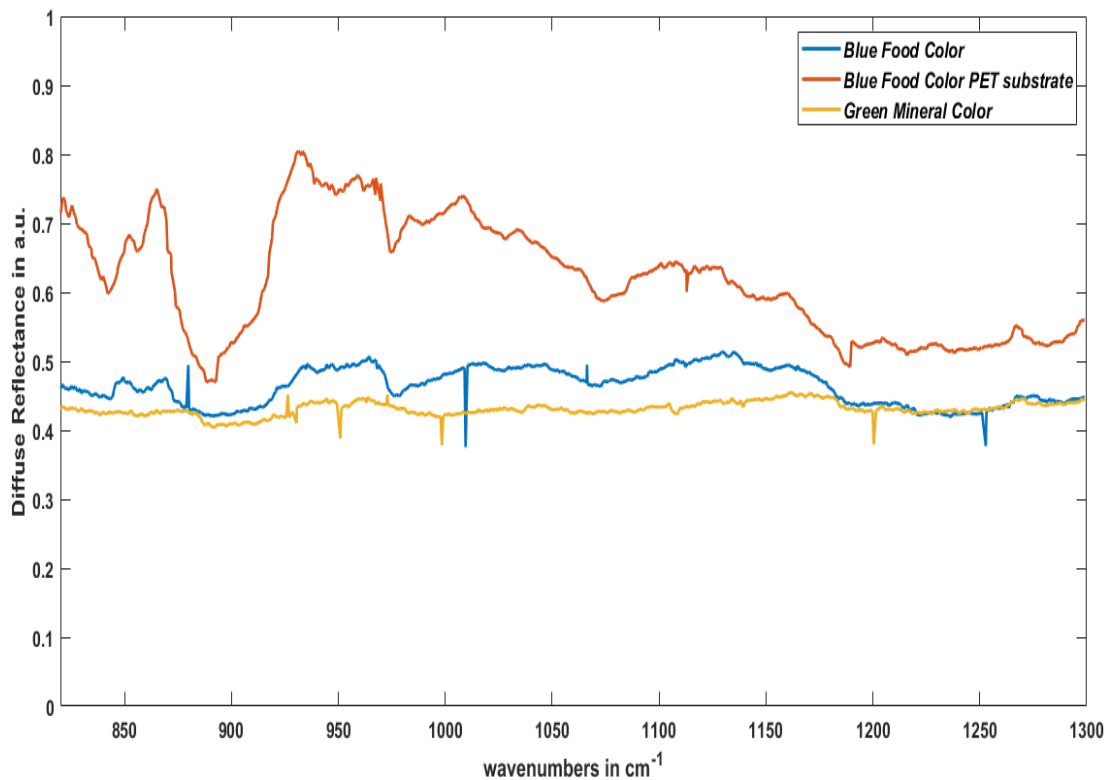
Because they require relatively low power and are so small, QCL - based systems replace larger and slower FTIR and mass spectroscopy systems for both lab and field work. Some applications include continuous exhaust monitoring on an industrial basis, such as in – the - stack measurements of pollutants, or well - head detection of byproduct gases at petroleum drilling platforms.

QCL - based systems are also finding application in the growing field of medical diagnostics. Trace gases present on a patient's breath can indicate diabetes, asthma and other respiratory issues, kidney and liver dysfunction, and other indicators are being discovered regularly. Such an application requires extremely fast sampling times, relatively small size, and accurate results in order to avoid misdiagnosis⁶⁹.

At present QCLs are still somewhat specialized devices. Manufacturing is difficult to optimize, and small batch sizes result in high unit cost. As the value of these devices is more widely realized and more applications are created, QCLs is believed to become more and more readily available and affordable.

Implementing QCLs requires system designers to pay particular attention to the driver and temperature control electronics. Current noise from the QCL driver causes the laser linewidth to broaden, which reduces the overall system sensitivity and precision, and temperature change causes the wavelength to drift. In order to fully realize the precision made possible by QCLs it is important that they are powered by ultra-low noise drivers and highly stable temperature controllers⁶⁹.

We firstly measured the sample with the blue food color put on a glass basis, then the green mineral color one and in the end, we measured the sample with the blue food color put on a plastic substrate. We can see the results in the graph below. The blue curve represents the blue food color sample on glass, the red curve shows the blue food color sample on plastic basis and the yellow one represents the green mineral color sample. The x – axis shows the wavenumber. The wavenumber and the wavelength are inversely proportional ($\text{wavelength} = 1 / \text{wavenumber}$). So for the atmospheric window, the wavelength range is $8 \mu\text{m} - 13 \mu\text{m}$ while the corresponding wavenumber range is $\sim 760 \text{ cm}^{-1} - 1250 \text{ cm}^{-1}$.



Graph 2: Diffuse reflectance in relation to the wavenumber for the three samples in the infrared

In the graph, we see that the reflectance is measured in atomic units (a.u.). Atomic units are the units in the electron's world. The four main constants are

- ✓ Reduced Planck constant, also known as the atomic unit of action
- ✓ Elementary charge, also known as the atomic unit of charge
- ✓ Bohr radius, also known as the atomic unit of length
- ✓ Electron mass, also known as the atomic unit of mass

They all equal to 1 by definition⁷⁰.

We notice that the highest curve belongs to the blue food color sample with the plastic substrate. That was expectable since the different material basis was undeniably going to affect the reflectance factor. Glass absorbs highly in the infrared, so relatively between the two materials, plastic is expected to demonstrate a greater reflectance factor. The reflectance curves of the two samples that were placed on glass substrates are closer together. However, although the difference is small, most of the time the blue food color curve is higher than the green mineral color one. On average the reflectance percentage of the blue food color sample is around 50 % while the reflectance percentage of the green mineral color sample is around 40 %. The spikes

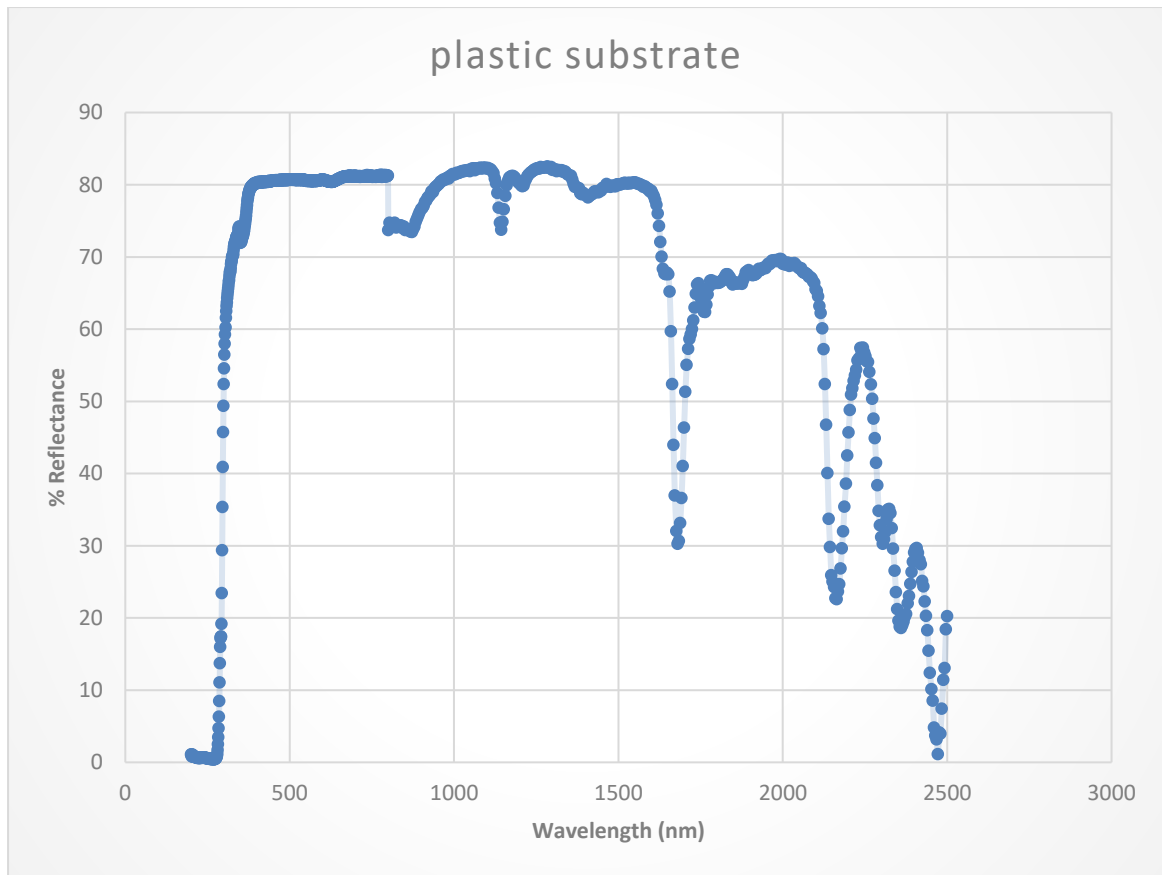
of the curves do not demonstrate anything significant as they are caused by the QCL's random fluctuations.

From the two graphs, we cannot exclude a clear conclusion on which coating demonstrates the optimal performance in terms of the reflectance factor. The green mineral color sample shows greater reflectance in the area from 200 nm to 2500 nm (UV, visible, near – infrared spectra) whilst in the area 8 000 – 13 000 nm (the atmospheric window) the same sample reflects less than the blue food color sample although by a smaller difference.

3.3.2 NaZnPO₄ surface

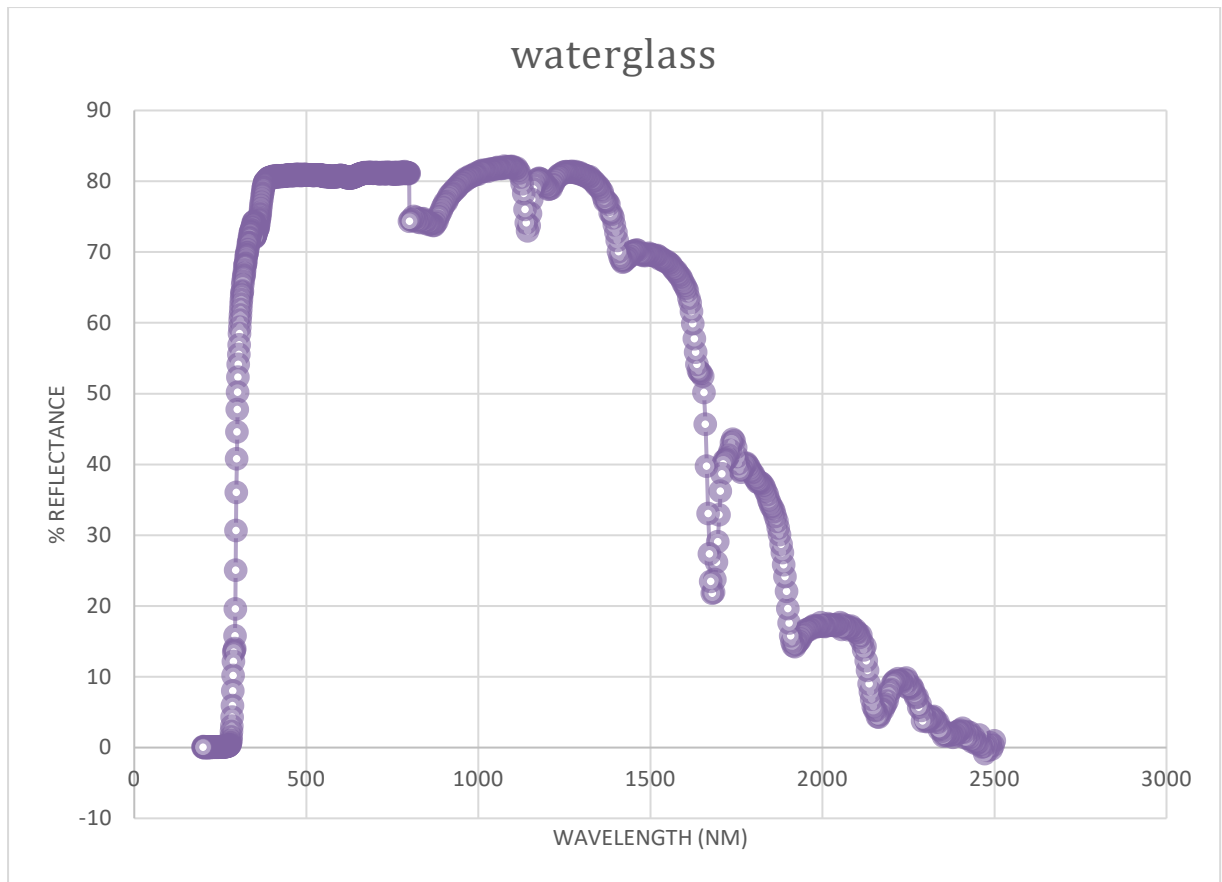
In continuation, we measured the NaZnPO₄ surface in relation to its thermal qualities. The measurements were performed by the Cary UV Spectrophotometer.

On the graph below, we can see the % reflectance curve in relation to the wavelength for the plastic substrate that we used for the NaZnPO₄ surface.



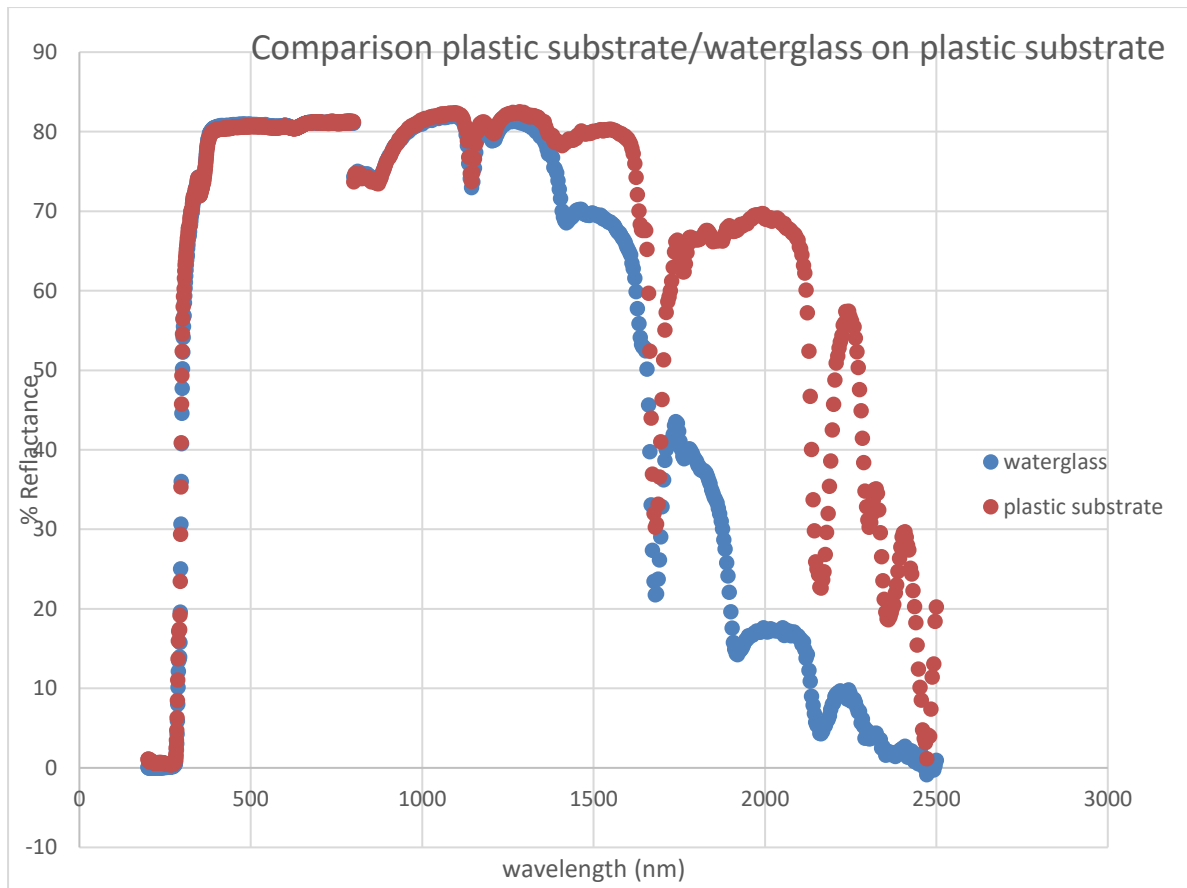
Graph 3: Reflectance percentage in relation to the wavelength for the plastic substrate alone, measured by a Cary UV Spectrophotometer.

We also measured the waterglass alone, on a plastic substrate. The aforementioned graph is shown below.



Graph 4: Reflectance percentage in relation to the wavelength for the waterglass on plastic substrate, measured by a Cary UV Spectrophotometer.

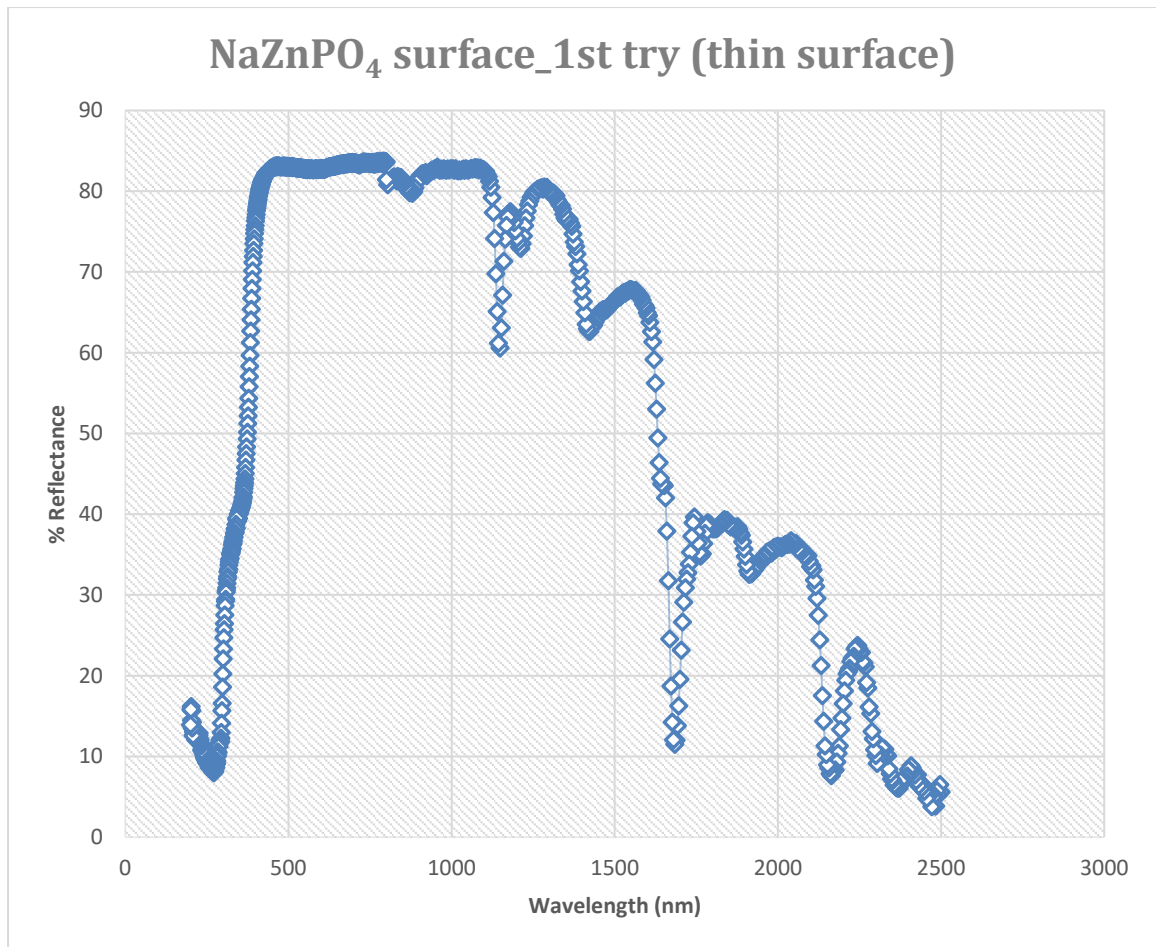
Followingly, we put the two graphs in one.



Graph 5: Comparison of the reflectance percentage of the plastic substrate with the waterglass measured on the plastic substrate

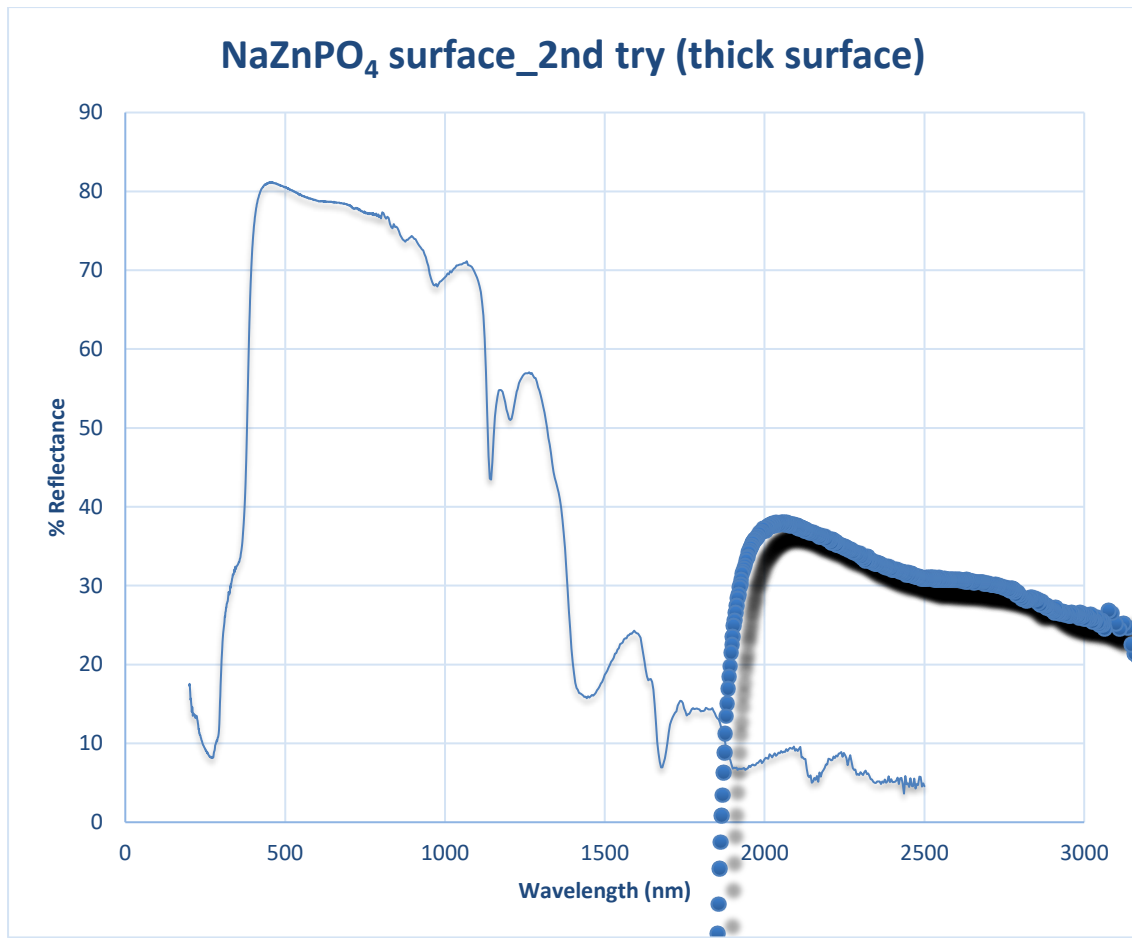
Comparing the curves of the reflectance percentage of the plastic substrate and the waterglass measured on the same kind of plastic substrate, we can see that the waterglass has fairly high reflectance, so choosing it as a binder seems to have been a wise choice. Of course, we bear in mind that this only concerns the area 200 – 2500 nm. We have not measured the waterglass’s reflectivity at the other wavelengths.

Finally, on the graph below, we see the percentage reflectance – wavelength curve for the first surface NaZnPO₄ we created.



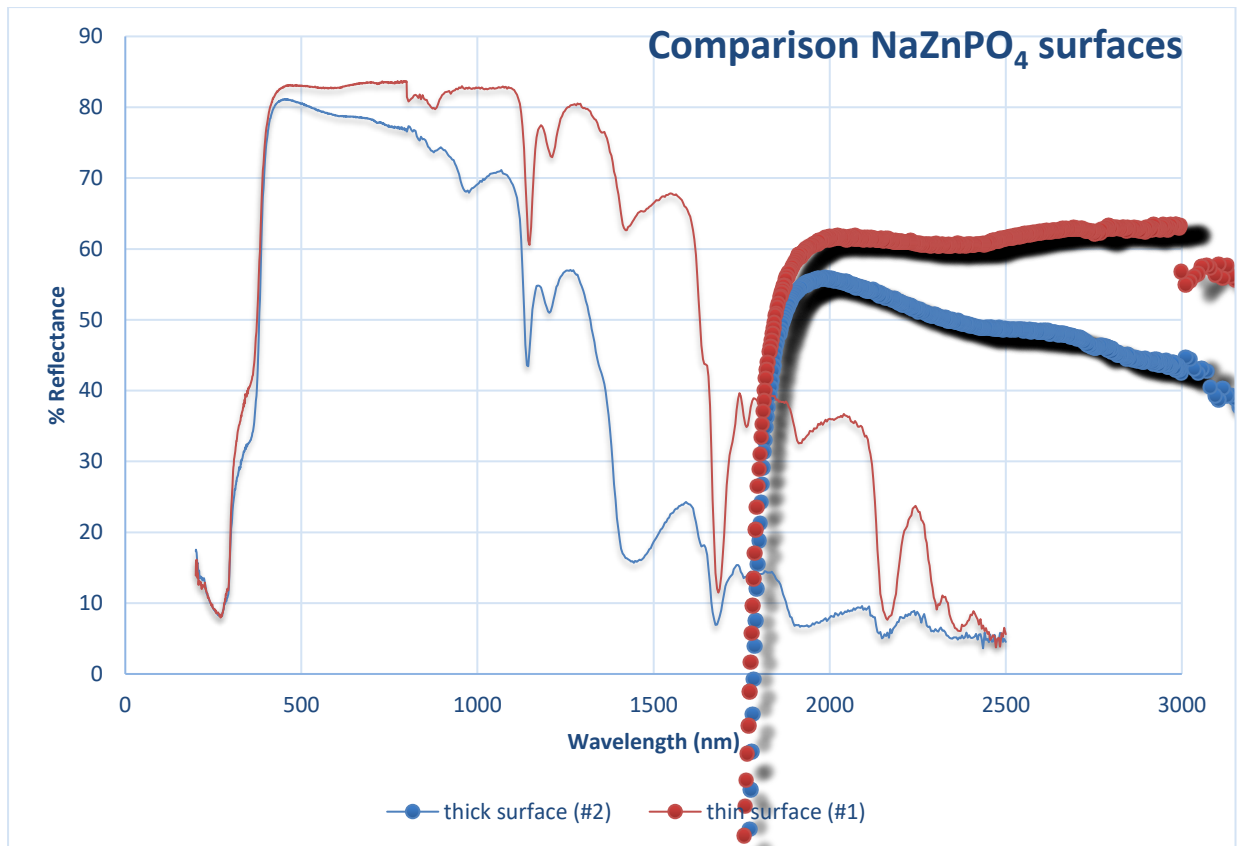
Graph 6: Reflectance percentage in relation to the wavelength for the first surface NaZnPO₄, measured on plastic substrate by a Cary UV Spectrophotometer.

Furthermore, we will now see the same curve for the second NaZnPO₄ surface we manufactured (the thick one).



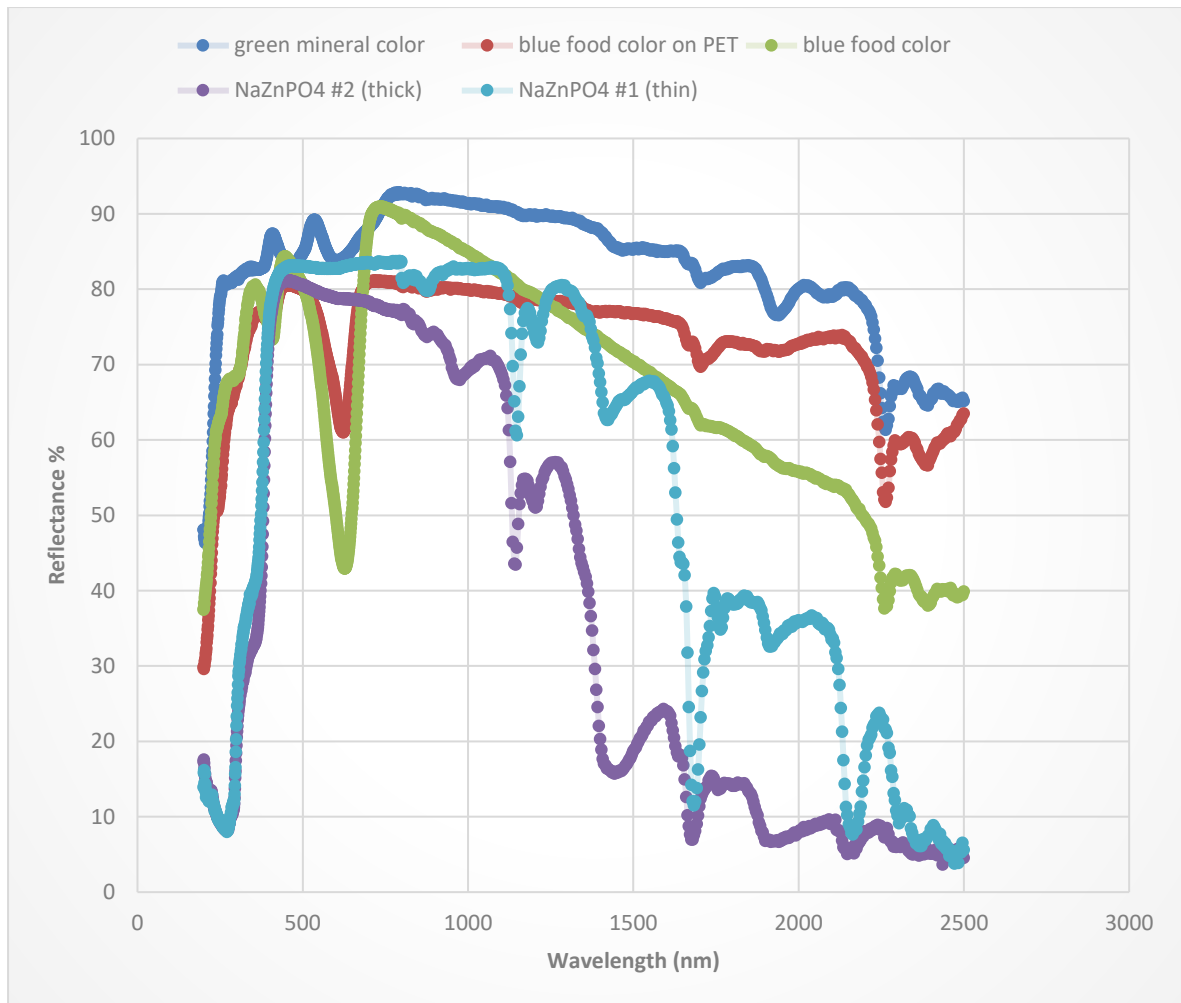
Graph 7: Reflectance percentage in relation to the wavelength for the second NaZnPO₄ surface, measured on plastic substrate by a Cary UV Spectrophotometer.

We understand that the thicker the surface, the lower the percentage of reflectance in this area. The two curves are shown on one diagram below.



Graph 8: Reflectance percentage in relation to the wavelength for the two (thick and thin) NaZnPO₄ surfaces, measured on plastic substrate by a Cary UV Spectrophotometer.

Finally, in the graph below we can see the curves for all the samples together.



Graph 9: Reflectance percentage in relation to the wavelength for all the samples together, measured on plastic substrate by a Cary UV Spectrophotometer.

We can say that the sample with the highest reflective behavior in the range 200 - 2500 nm is the green mineral color. The one with the lowest reflectance is the thick NaZnPO₄ surface. The performances of the other coatings are hard to compare, one may have higher reflectance percentage at some wavelengths and one at others.

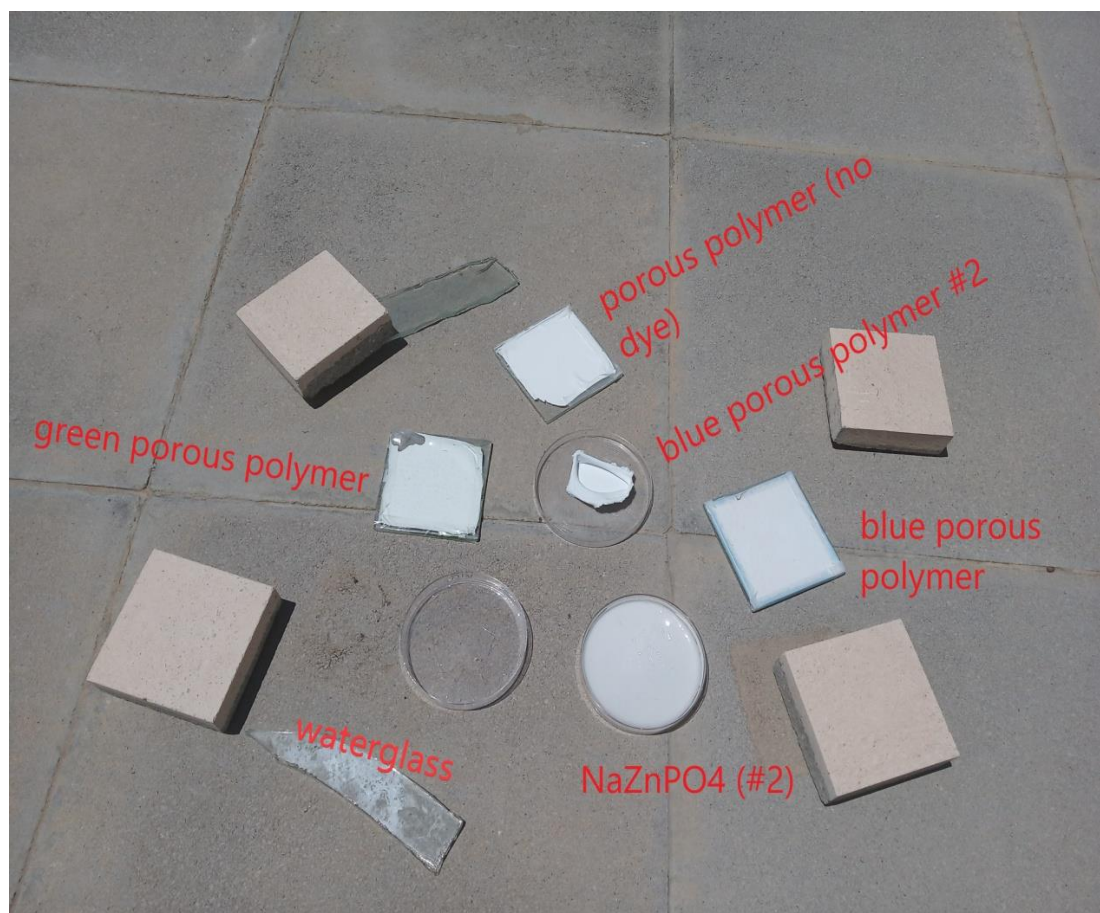
3.4 Thermal Images and Discussion

After measuring them, we placed the samples on the rooftop of K3 building and we took thermal photos every 20-30 minutes. The thermocamera shooting took place on Monday 29th of June 2020.



Lab Photos 40 & 41: The thermal camera that we used.

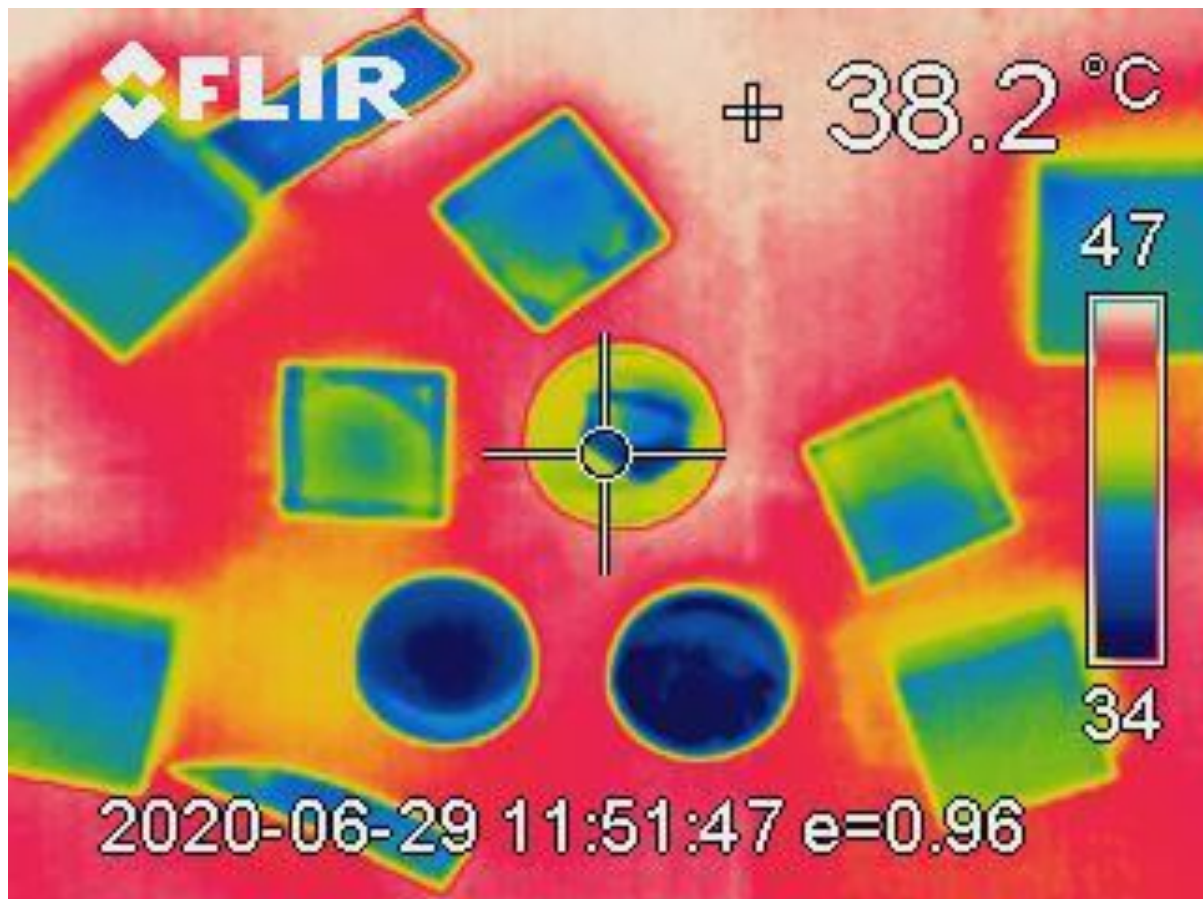
On the picture below, we can see the samples that were placed on the roof for testing. The porous polymer coating without any dyes was not manufactured now and we just took it for comparison reasons. The green porous polymer coating is the one where the green mineral dye was used, the blue porous polymer is the one with the blue food color which was placed on a glass substrate. The blue porous polymer #2 is the same but placed on a plastic substrate and it is kind of distorted, the coating is not well – distributed on the full surface of the substrate (see picture). The last two samples are the ones with the waterglass alone, placed on a plastic substrate and the NaZnPO_4 #2 surface. This is the second batch of NaZnPO_4 surface, so it is the thick coating.



Lab Photo 36 (29_06_2020 at 12h51) : From top to bottom and from left to right: porous polymer (no dye), green porous polymer, blue porous polymer (#2), blue porous polymer, waterglass and NaZnPO_4 (thick) surface (#2)

Below we can see the thermal images of the above setting.

1. The first thermophoto was taken at 12h51 (The thermocamera's clock is set one hour behind)



Thermal picture 1 (29_06_2020 at 12h51) : From top to bottom and from left to right: porous polymer (no dye), green porous polymer, blue porous polymer (#2), blue porous polymer, waterglass and NaZnPO₄ (thick) surface (#2)

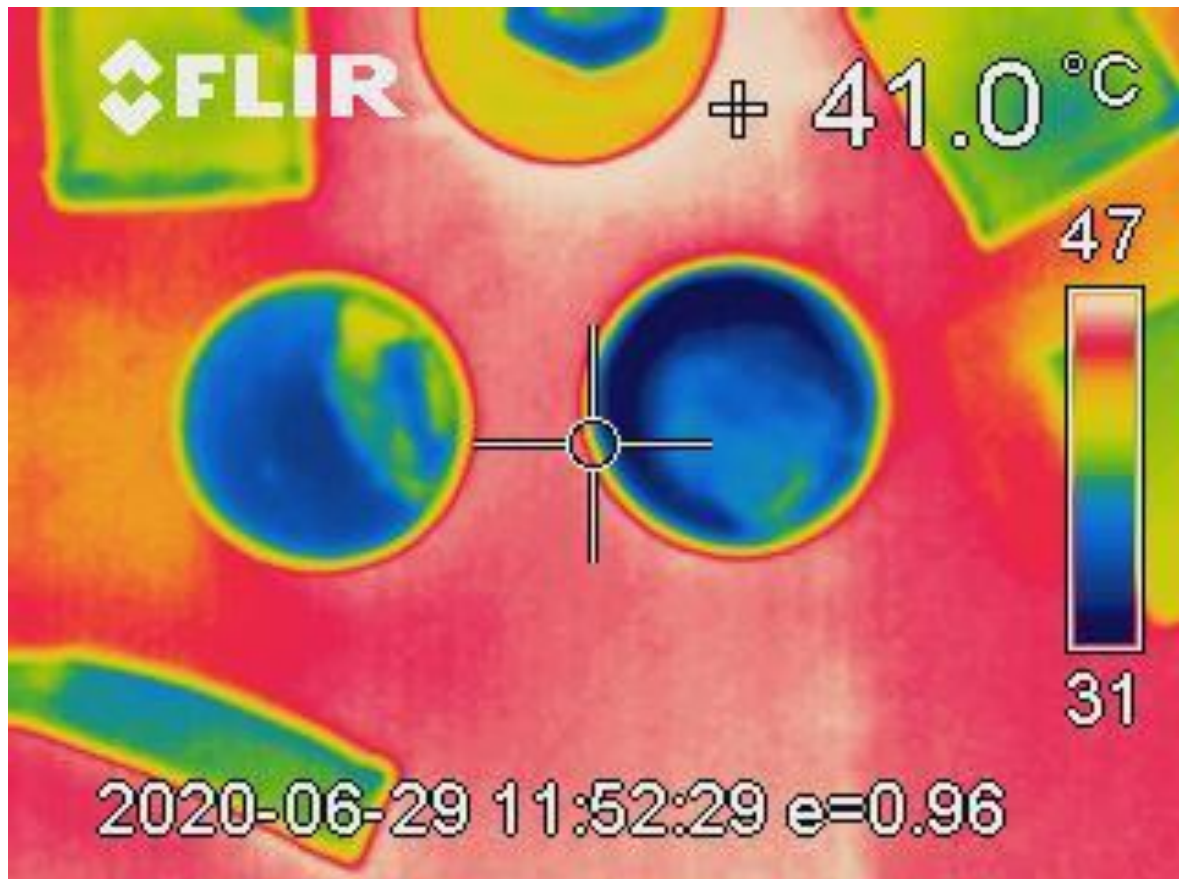
The temperatures that the colors represent are depicted at the scale on the right of the image.

We observe that the waterglass on the plastic substrate and the NaZnPO₄ surface demonstrate the best thermal behavior. Based on the bibliography, that was expected for the waterglass and that is the reason why it was chosen as the binder.

As for the porous polymer samples, we can see that the one without dye stays cooler than the ones with dyes. We also notice some thermal unevenness on the surfaces. We believe that the distribution of the material on the substrates may be more on some

regions of the substrate and less on others which could be the reason why some regions are hotter than others.

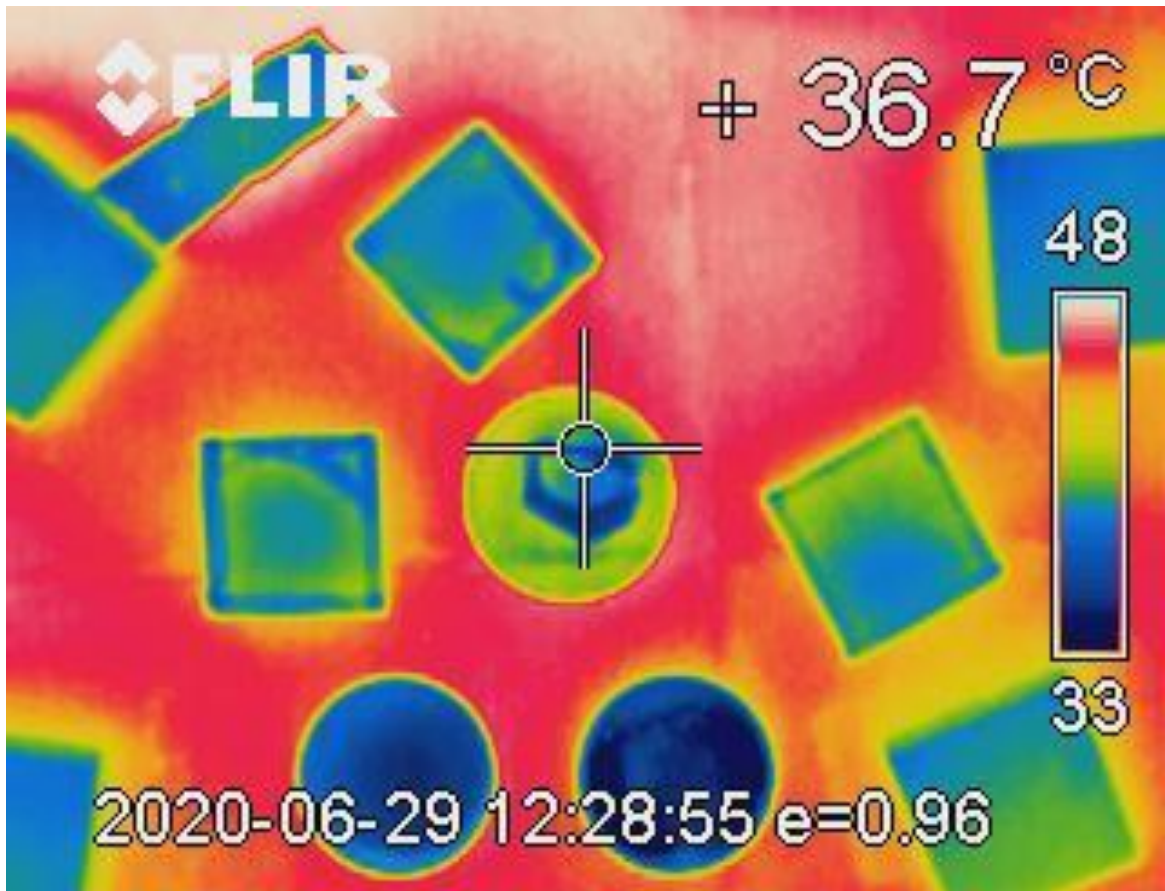
As the solar radiation, the humidity and the wind currents fluctuate, we can see below the waterglass and NaZnPO₄ surface thermal image the next minute.

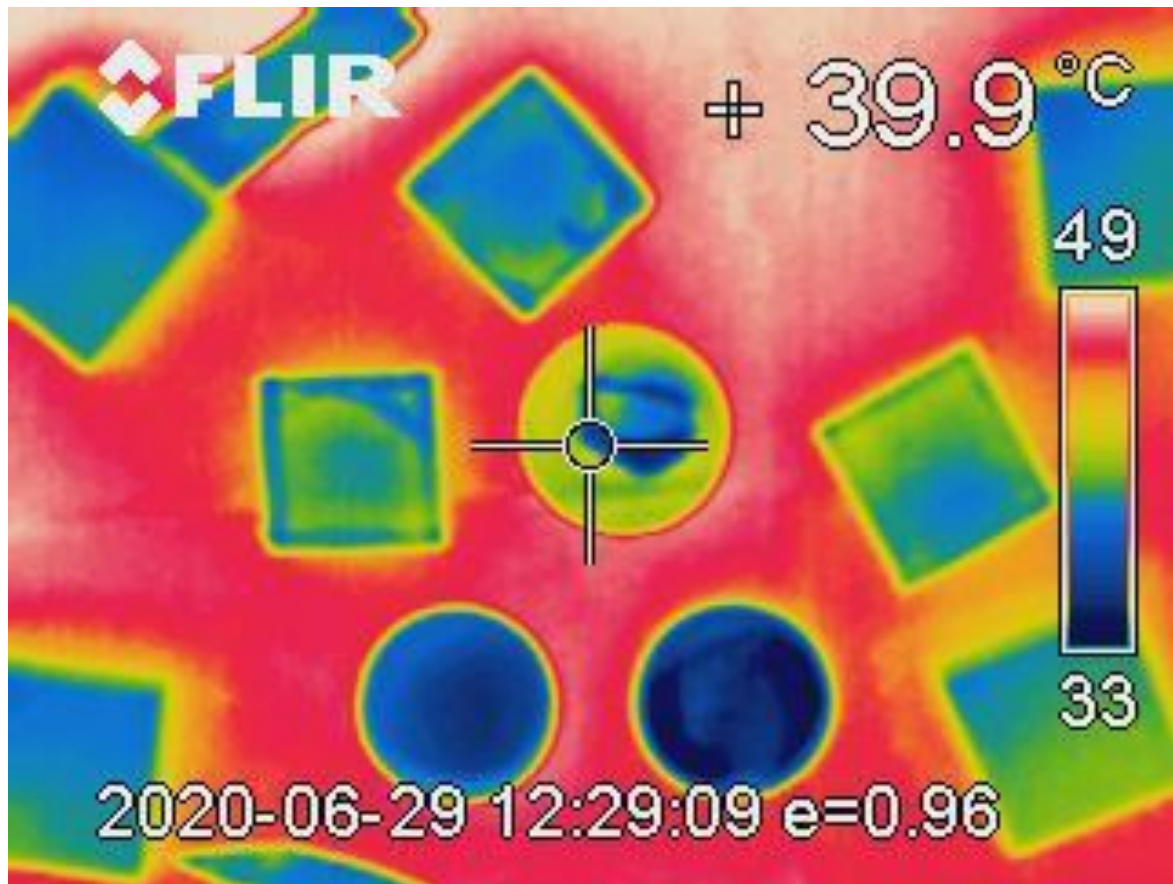


Thermal picture 2 (29_06_2020 at 12h52): Comparison of waterglass (left) and NaZnPO₄ surface (right)

From the last picture, it is evident that the NaZnPO₄ surface stayed at lower temperatures than the waterglass.

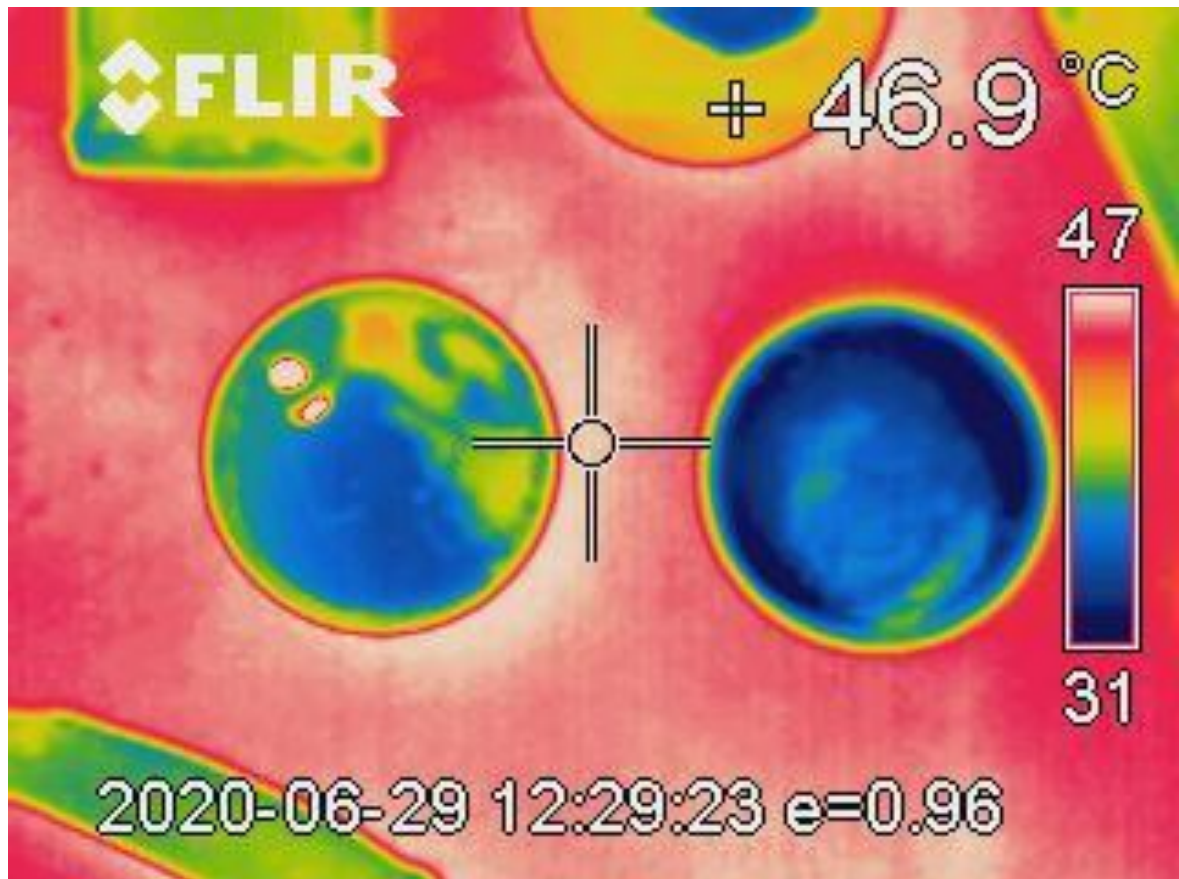
2. The next thermal images were taken at 13h28 the same day.



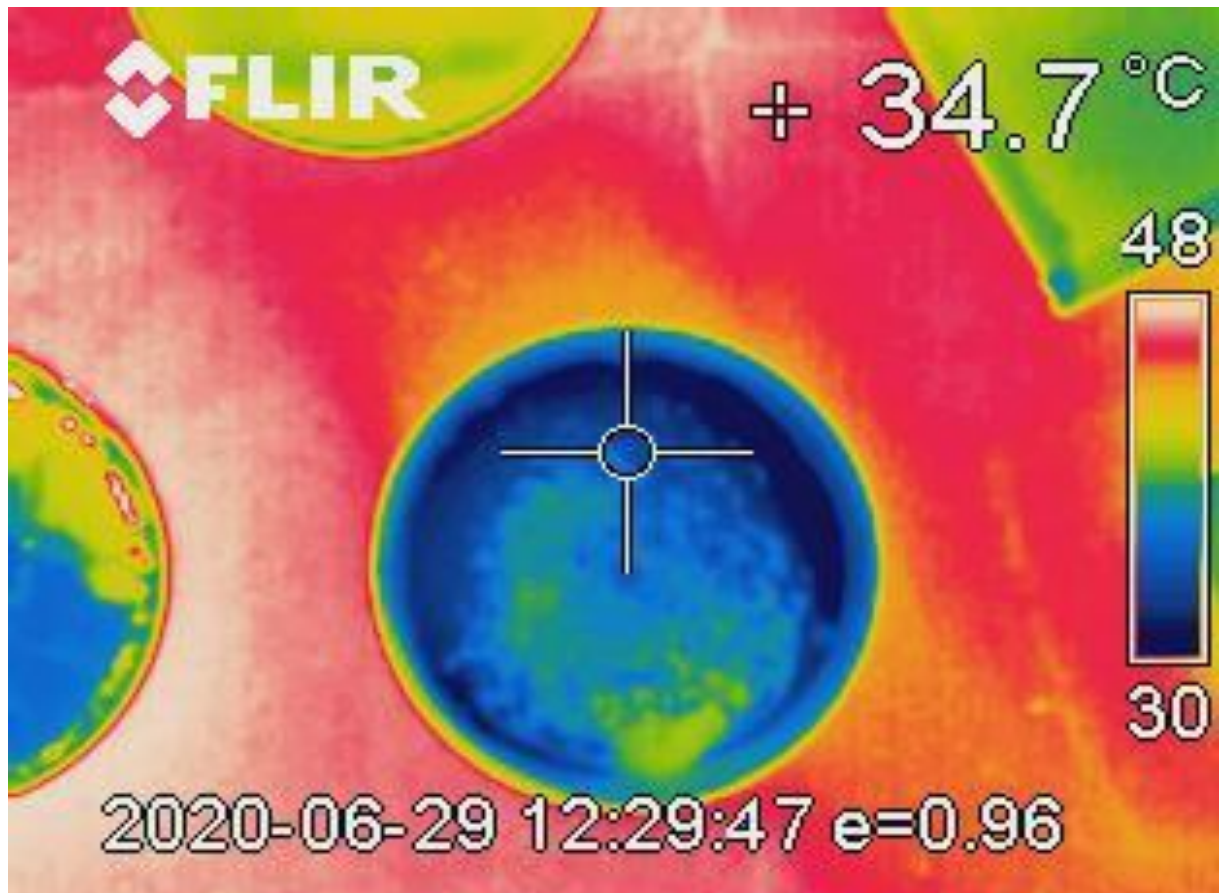


Thermal picture 3 & 4 (29_06_2020 at 13h28): From top to bottom and from left to right: porous polymer (no dye), green porous polymer, blue porous polymer (#2), blue porous polymer, waterglass and NaZnPO₄ (thick) surface (#2)

Again, we notice that the NaZnPO₄ surface has the best thermal attitude in relation to all the other samples. From the porous polymer samples, again the one without any dyes seems to have the best thermal attitude.



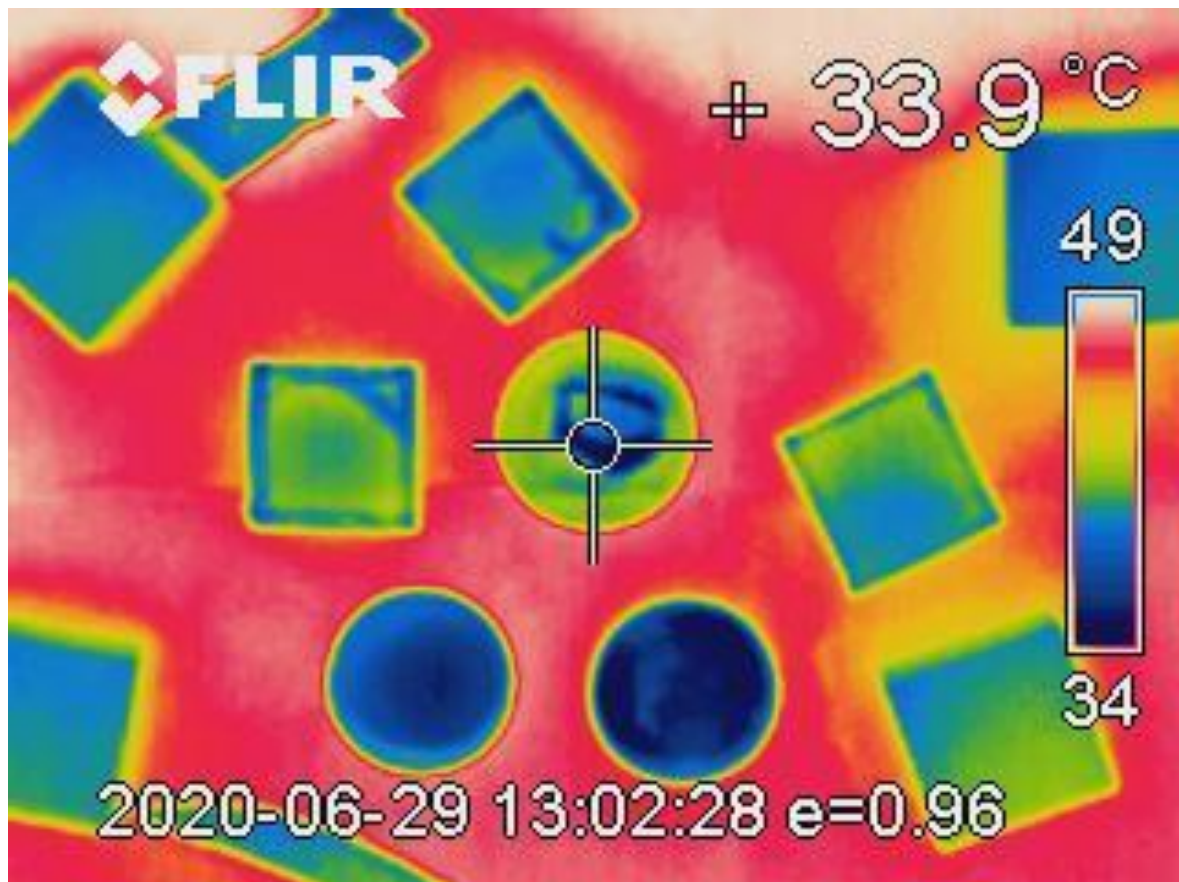
Thermal picture 5 (29_06_2020 at 13h29): Comparison of waterglass (left) and NaZnPO₄ surface (right)



Thermal picture 6 (29_06_2020 at 13h29): NaZnPO₄ surface

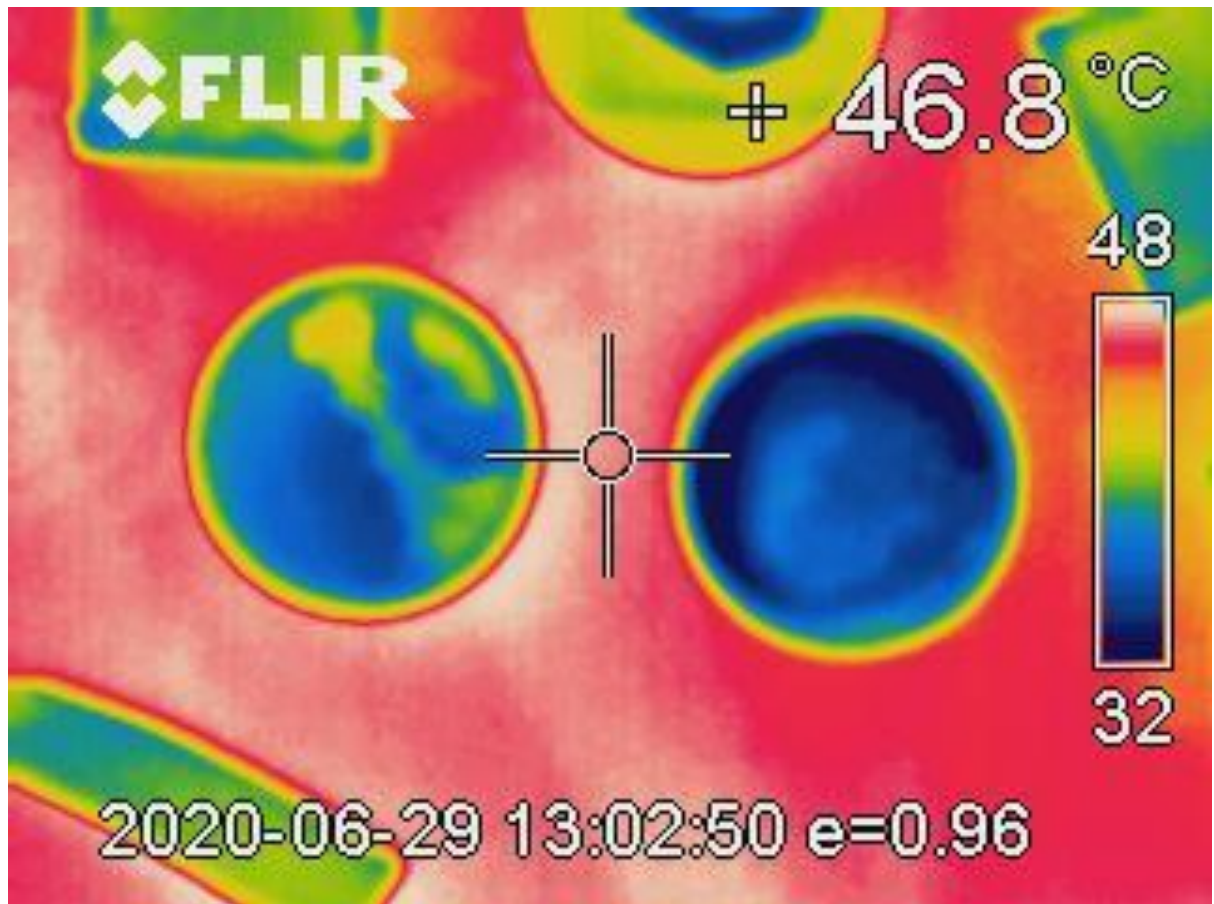
We notice from the picture above that the temperature of the NaZnPO₄ surface is between more or less between 30 – 38 °C

3. The third thermal image was taken at 14h02

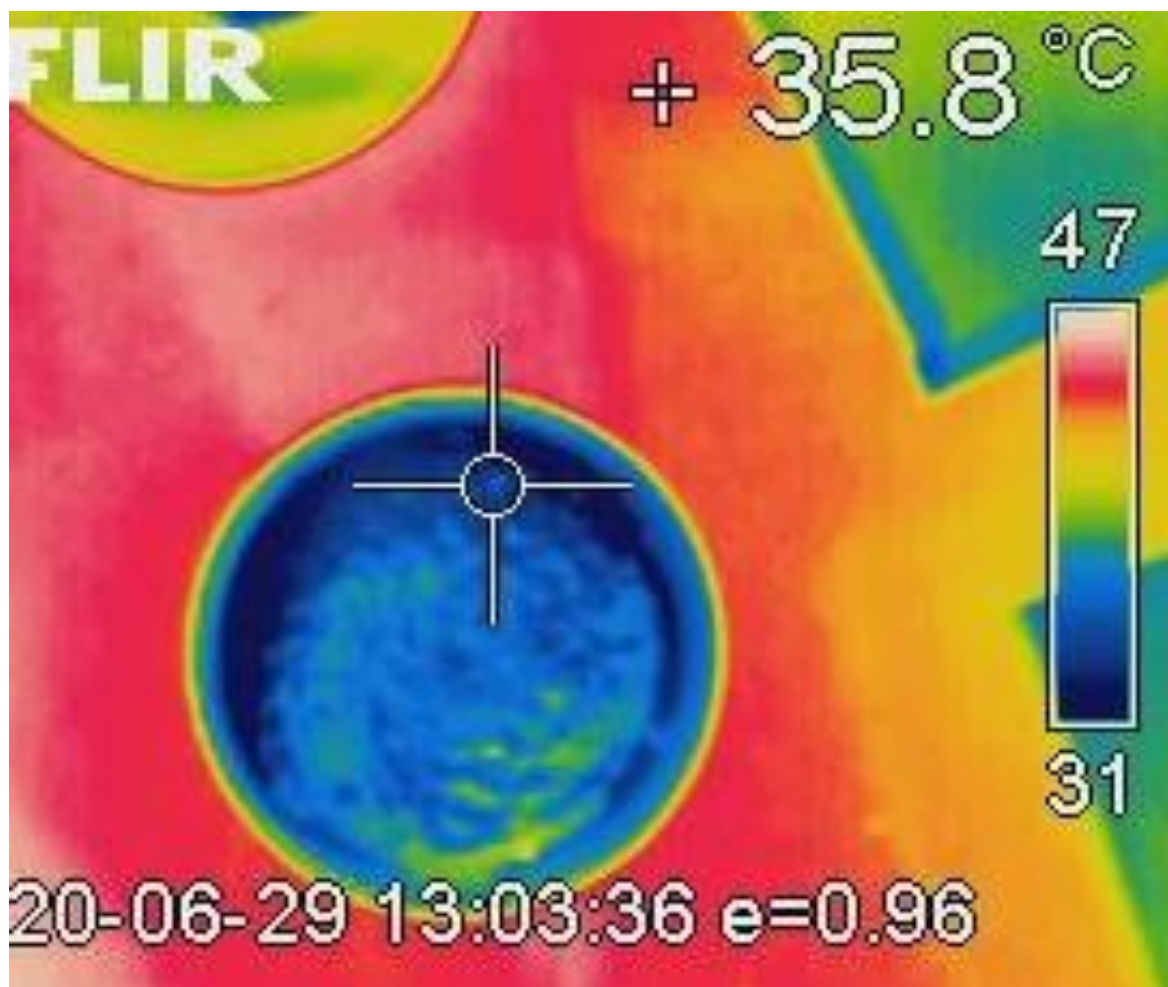


Thermal picture 7 (29_06_2020 at 14h02): From top to bottom and from left to right: porous polymer (no dye), green porous polymer, blue porous polymer (#2), blue porous polymer, waterglass and NaZnPO₄ (thick) surface (#2)

We see that the NaZnPO₄ surface keeps being cooler than the other surfaces.

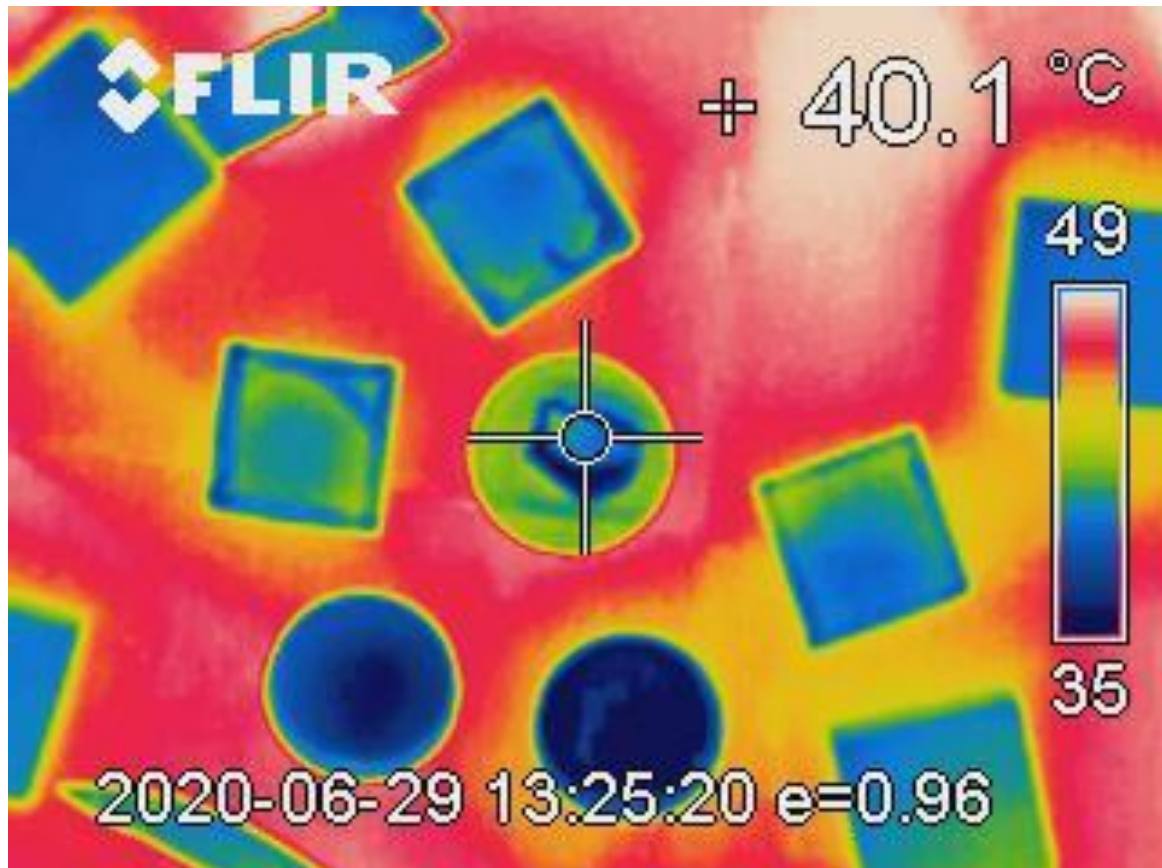


Thermal picture 8 (29_06_2020 at 14h02): Comparison of waterglass (left) and NaZnPO₄ surface (right)



Thermal picture 9 (29_06_2020 at 14h03): NaZnPO₄ surface

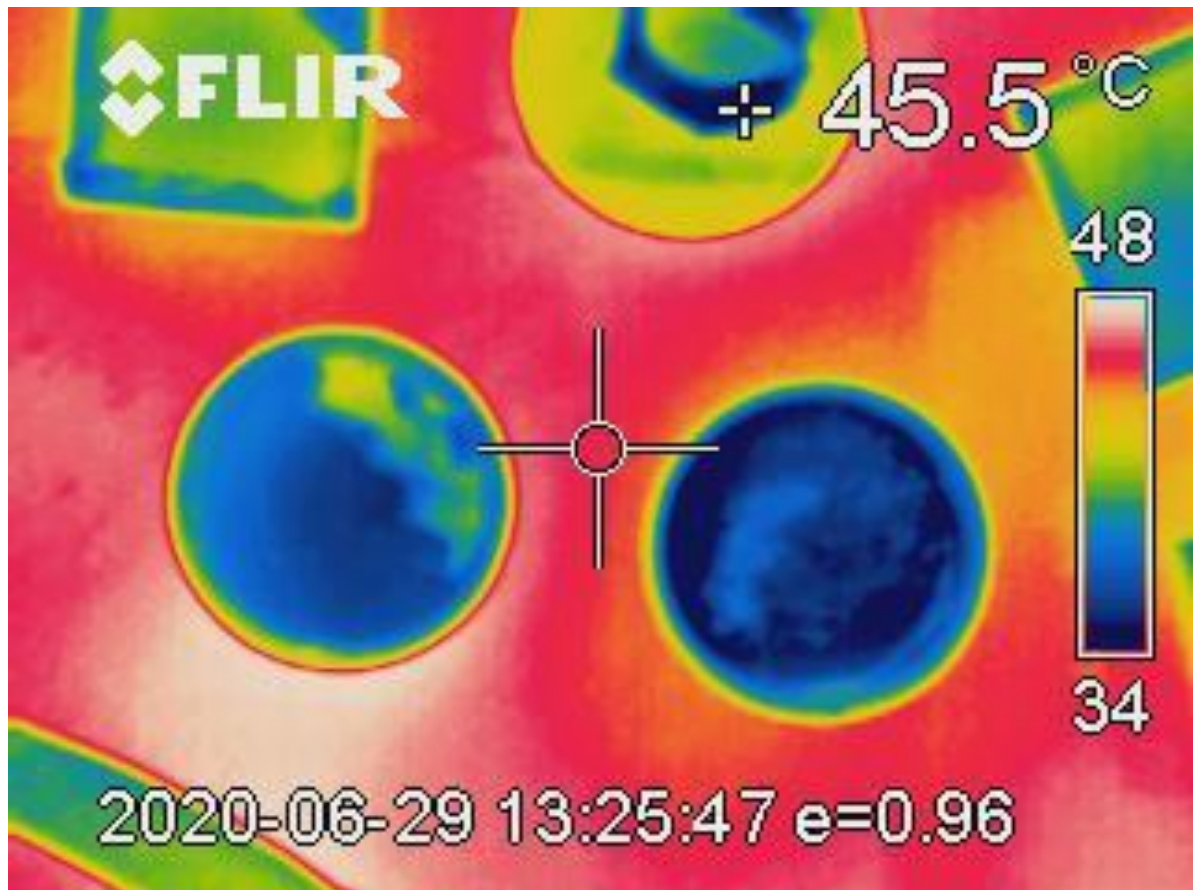
4. The fourth thermal image was taken at 14h25



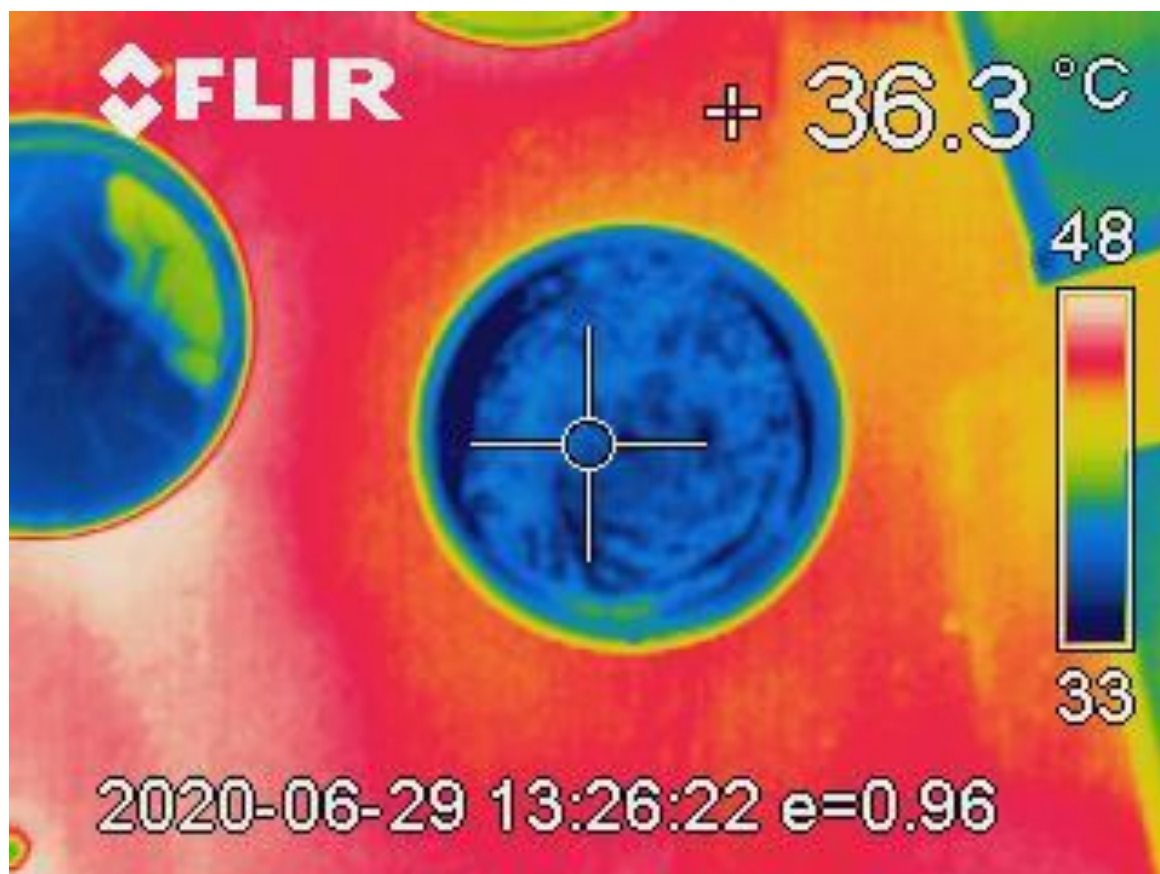
Thermal picture 10 (29_06_2020 at 14h25): From top to bottom and from left to right: porous polymer (no dye), green porous polymer, blue porous polymer (#2), blue porous polymer, waterglass and NaZnPO₄ (thick) surface (#2)

We observe that the temperature of the NaZnPO₄ surface rises as time passes. However, it always maintains temperatures lower than the other coatings.

As far as the porous coatings are concerned, the sample without any dye keeps maintaining lower temperature than the ones with the green mineral dye and the blue food dye.

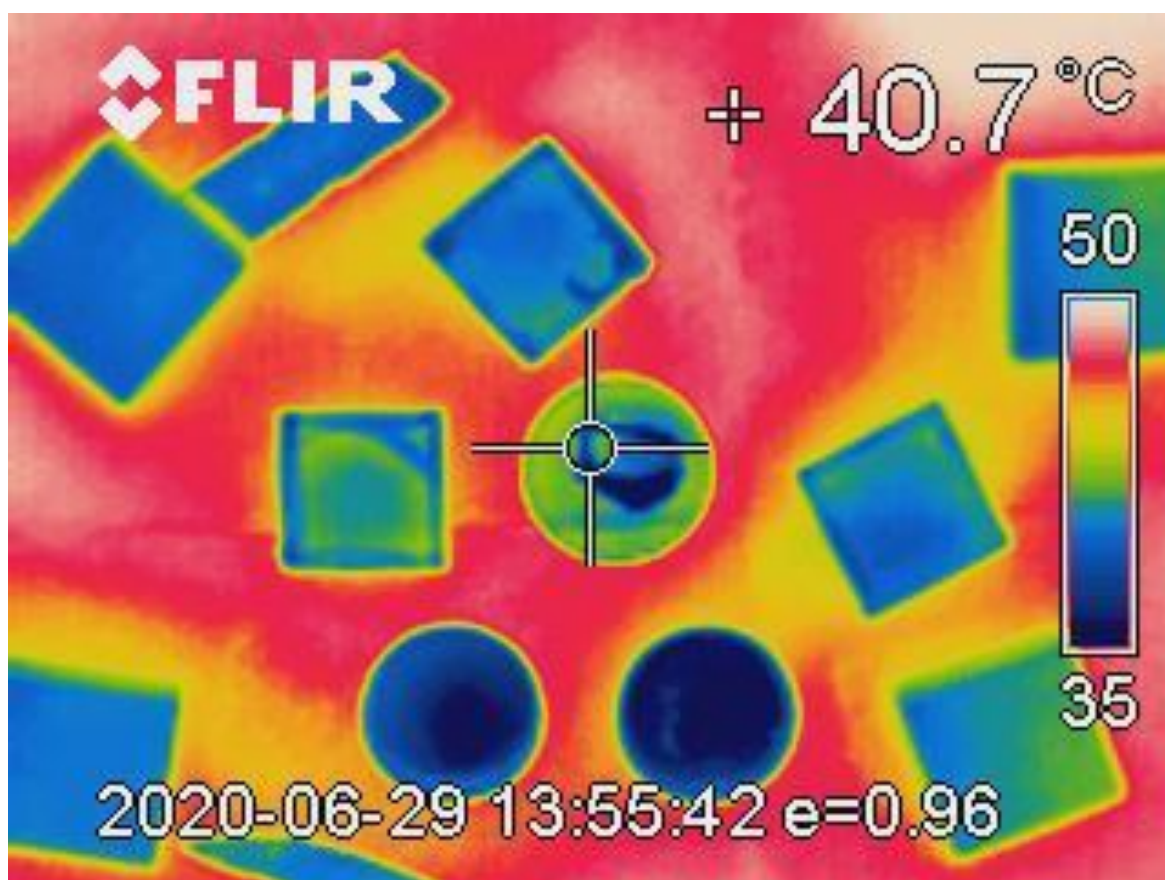


Thermal picture 11 (29_06_2020 at 14h25): Comparison of waterglass (left) and NaZnPO₄ surface (right)

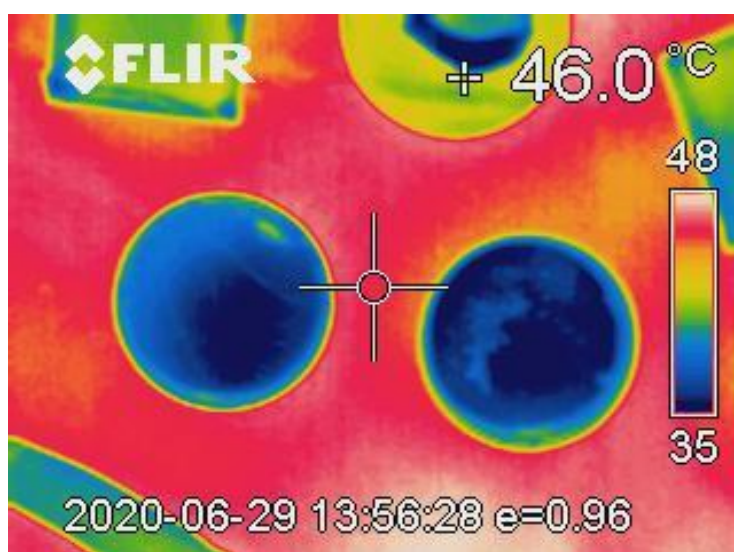


Thermal picture 12 (29_06_2020 at 14h26): NaZnPO₄ surface

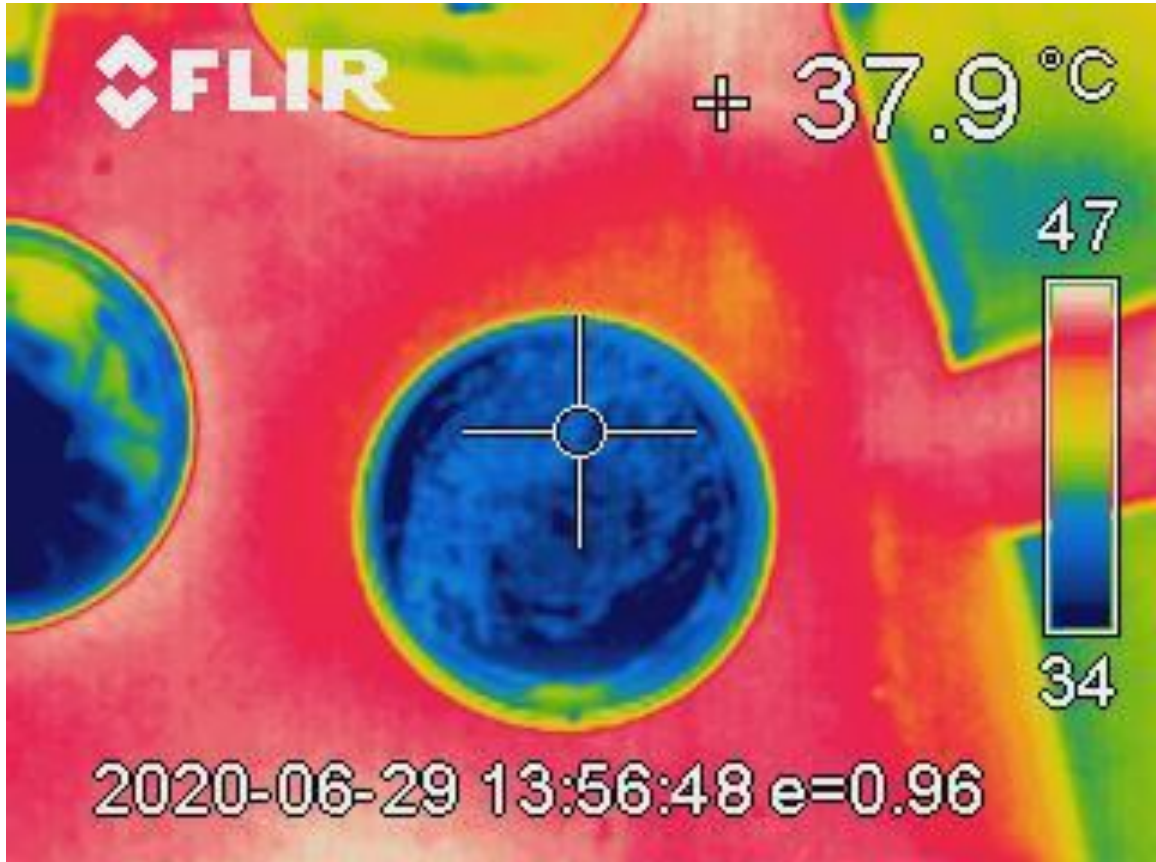
5. The fifth measurement with the thermocamera took place at 14h55

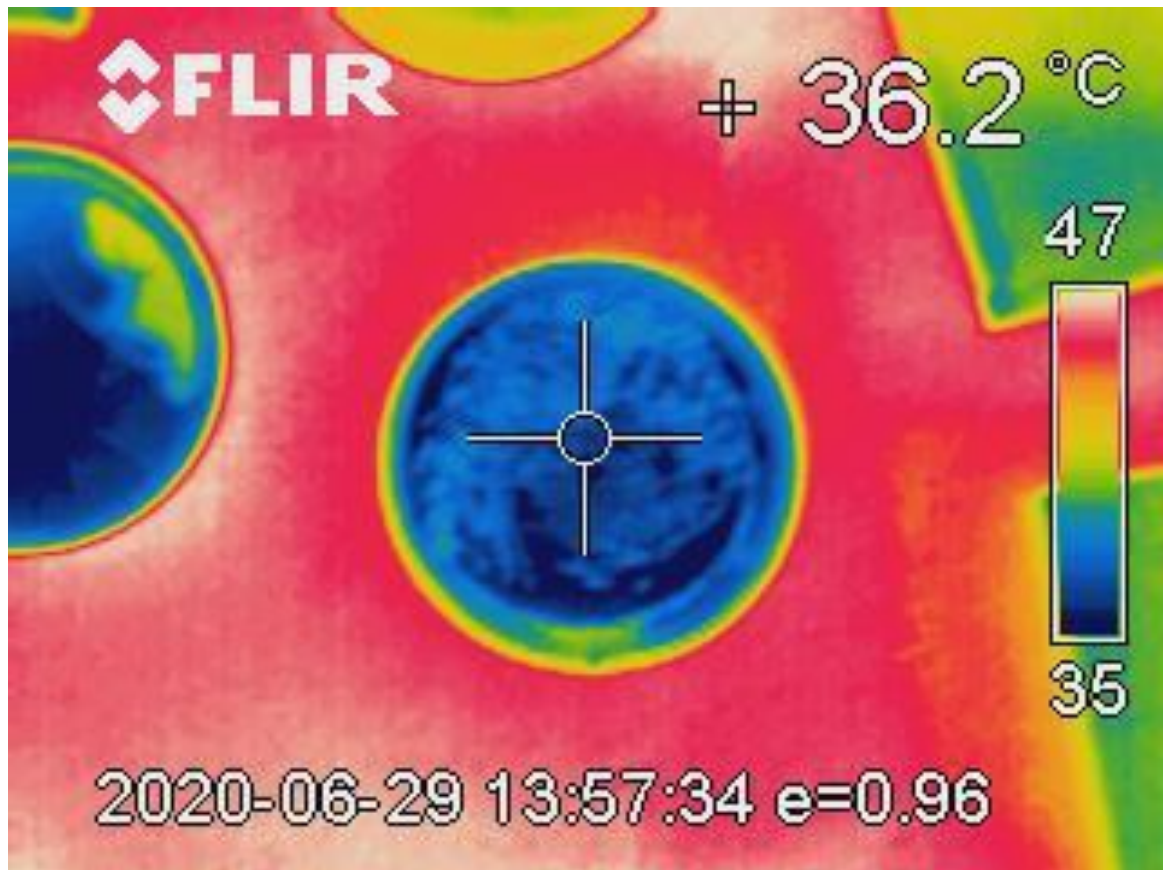


Thermal picture 13 (29_06_2020 at 14h55): From top to bottom and from left to right: porous polymer (no dye), green porous polymer, blue porous polymer (#2), blue porous polymer, waterglass and NaZnPO₄ (thick) surface (#2)



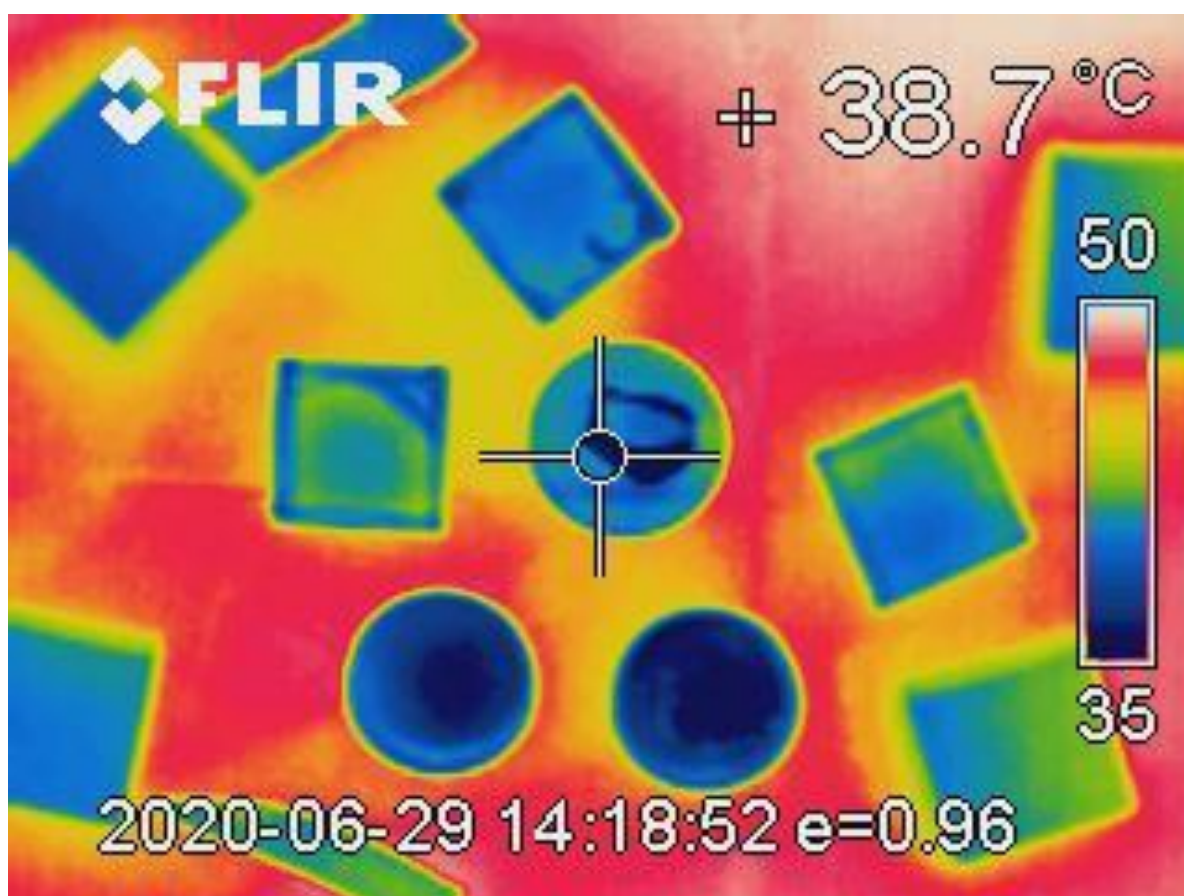
Thermal picture 14 (29_06_2020 at 14h56): Comparison of waterglass (left) and NaZnPO₄ surface (right)





Thermal pictures 15 & 16 (29_06_2020 at 14h57): NaZnPO₄ surface

6. The sixth thermal image was taken at 15h18



Thermal picture 17 (29_06_2020 at 15h18): From top to bottom and from left to right: porous polymer (no dye), green porous polymer, blue porous polymer (#2), blue porous polymer, waterglass and NaZnPO₄ (thick) surface (#2)

We observe that at all times, the NaZnPO₄ surface has managed to keep its temperature lower than the rest of the samples by at least a couple of degrees Celsius. Although from the graphs, we notice that in the range 200 – 2500 nm the higher percentage reflection curve belongs to the green mineral color sample, the atmospheric window does not belong in that range. We assume that overall, taking into consideration all wavelengths, the reflective properties of the NaZnPO₄ surface are higher than the rest of the samples.

4. Conclusions

Looking for alternative ways for a greener and sustainable future, we tried the idea of passive cooling through the use of radiative coatings. After trying to reproduce them in the lab, we managed to create four samples, based on two different kinds of materials. The first kind of material is a porous polymer coating, for which we created three samples mixed with dyes (two samples with blue food color; one on glass and one plastic carrier, and one with green mineral color on glass carrier) in order to make them more commercially attractive.

The second kind of material is based on the reflective properties of NaZnPO_4 powder, which we made into a surface with a new technique, since the technique described by bibliography was not successful. In continuation, we measured all the samples in terms of their reflectance, with the use of a UV- Visible – Near Infrared spectrophotometer, while the porous polymer coatings were also measured with a Quantum Cascade Laser. Each structure functions in different wavelengths and with distinct optical resolutions.

After studying the graphs of the reflectance performance of the materials, we noticed that the green mineral color coating shows higher reflective properties as far the range 200 – 2500 nm is concerned. Comparing only the three porous polymer coatings, the blue food color sample demonstrates higher reflectance in the infrared range 8 μm – 13 μm (atmospheric window). In continuation, we took thermal photos after placing the samples on the rooftop. The NaZnPO_4 surface has always managed to keep its temperature lower than the other samples. Thus, we estimate that its overall reflective properties are higher than the rest of the samples.

Bibliography

1. Katili, A. R., Boukhanouf, R. & Wilson, R. Space Cooling in Buildings in Hot and Humid Climates—A Review of the Effect of Humidity on the Applicability of Existing Cooling Techniques. *Proc. 14th Int. Conf. Sustain. Energy Technol.* 25–27 (2015) doi:10.13140/RG.2.1.3011.5287.
2. *US Energy consumption 2015*.
<https://www.eia.gov/totalenergy/data/monthly/#consumption>.
3. Residential Electricity Consumption.
<https://www.flickr.com/photos/eiagov/42619691731>.
4. ClimateAtlas. <https://climateatlas.ca/why-climates-change>.
5. Lüthi, D. *et al.* High-resolution carbon dioxide concentration record 650,000–800,000 years before present. *Nature* **453**, 379–382 (2008).
6. Sun Climate Data. <http://www2.mps.mpg.de/projects/sun-climate/data.html>.
7. Global Temperature. <https://data.giss.nasa.gov/gistemp/graphs/>.
8. *IPCC*. <https://www.ipcc.ch/report/ar5/wg1/summary-for-policymakers/figspm-05/>.
9. Radiative Forcing.
10. Radiative Forcing.
https://commons.wikimedia.org/wiki/File:Radiative_forcing_1750-2011.svg.
11. Gobakis, K. Design and development of smart cool materials for the built environment. (2018).
12. Schweiker, M., Huebner, G. M., Kingma, B. R. M., Kramer, R. & Pallubinsky, H. Drivers of diversity in human thermal perception—A review for holistic comfort models. *Temperature* **5**, 308–342 (2018).
13. *ASHRAE. Standard 55-2013 Thermal environmental conditions for human occupancy. Am. Soc. Heating, Refrig. Air-Conditioning Eng. Atlanta, USA. 2013.*
14. Fergus, N., Humphreys, M. & Roaf, S. *Thermal comfort: why it is important. Adaptive Thermal Comfort Principles and Practice* vol. 1 (2012).
15. Predicted Mean Vote (PMV).
https://www.designingbuildings.co.uk/wiki/Predicted_mean_vote.
16. Psychrometric chart - PMV method.
https://en.m.wikipedia.org/wiki/File:Psychrometric_chart_-_PMV_method.png.
17. how room temperature affects body temperature.

- <https://www.flickr.com/photos/mitopencourseware/3029642097>.
18. Urban Heat Island. <https://climatekids.nasa.gov/heat-islands/>.
 19. Urban Heat Island Profile.
[https://commons.wikimedia.org/wiki/File:Urban_heat_island_\(Celsius\).png](https://commons.wikimedia.org/wiki/File:Urban_heat_island_(Celsius).png).
 20. Hossain, M. M. & Gu, M. Radiative cooling: Principles, progress, and potentials. *Adv. Sci.* **3**, 1–10 (2016).
 21. Sun, X., Sun, Y., Zhou, Z., Alam, M. A. & Bermel, P. Radiative sky cooling: Fundamental physics, materials, structures, and applications. *Nanophotonics* **6**, 997–1015 (2017).
 22. Why the Atmospheric Window Matters in Earth Science.
<https://gisgeography.com/atmospheric-window/>.
 23. Zhao, D. *et al.* Radiative sky cooling: Fundamental principles, materials, and applications. *Appl. Phys. Rev.* **6**, (2019).
 24. Atmospheric Window. <https://www.sciencedirect.com/topics/earth-and-planetary-sciences/atmospheric-window>.
 25. Ghenadii Korotcenkov. *Handbook of Humidity Measurement*.
doi:10.1201/b22369-3.
 26. Optical depth.
 27. Li, M., Peterson, H. B. & Coimbra, C. F. M. Radiative cooling resource maps for the contiguous United States. *J. Renew. Sustain. Energy* **11**, (2019).
 28. Mandal, J. *et al.* Porous Polymers with Switchable Optical Transmittance for Optical and Thermal Regulation. *Joule* **3**, 3088–3099 (2019).
 29. Mandal, J. *et al.* Hierarchically porous polymer coatings for highly efficient passive daytime radiative cooling. *Science (80-.)*. **362**, 315–319 (2018).
 30. Lim, X. The super-cool materials that send heat to space. *Nature*.
 31. Zeyghami, M., Goswami, D. Y. & Stefanakos, E. A review of clear sky radiative cooling developments and applications in renewable power systems and passive building cooling. *Sol. Energy Mater. Sol. Cells* **178**, 115–128 (2018).
 32. Fan, S. Thermal Photonics and Energy Applications. *Joule* **1**, 264–273 (2017).
 33. Baranov, D. G. *et al.* Nanophotonic engineering of far-field thermal emitters. *Nat. Mater.* **18**, 920–930 (2019).
 34. *Plasmonics - Jason Hafner, Rice University*.
 35. Taliercio, T. & Biagioni, P. Semiconductor infrared plasmonics. *Nanophotonics* **8**, 949–990 (2019).
 36. The Science of Plasmonics. <https://nanocomposix.com/pages/the-science-of->

- plasmonics#target.
37. Surface plasmon resonance device. https://commons.wikimedia.org/wiki/File:Surface_plasmon_resonance_device.jpg.
 38. Boriskina, S. V, Ghasemi, H. & Chen, G. 2013-10-27 Plasmonic materials for energy from physics to applications.pdf.
 39. Michael Berger. What are metamaterials? <https://www.nanowerk.com/what-are-metamaterials.php>.
 40. Li, T. *et al.* A radiative cooling structural material. *Science* **364**, 760–763 (2019).
 41. SCIENCE, A. A. F. T. A. O. Passive radiative cooling in delignified wood material. https://www.eurekalert.org/pub_releases/2019-05/aaft-prc052019.php.
 42. Peng, Y. *et al.* Nanoporous polyethylene microfibres for large-scale radiative cooling fabric. *Nat. Sustain.* **1**, 105–112 (2018).
 43. Hsu, P. *et al.* A dual - mode textile for human body radiative heating and cooling. 1–8 (2017).
 44. Zhang, S. & Niu, J. Cooling performance of nocturnal radiative cooling combined with microencapsulated phase change material (MPCM) slurry storage. *Energy Build.* **54**, 122–130 (2012).
 45. Cool Roofs. <https://www.energy.gov/energysaver/design/energy-efficient-home-design/cool-roofs>.
 46. Roof albedo. <https://commons.wikimedia.org/wiki/File:Roof-albedo.gif>.
 47. Using Cool Roofs to Reduce Heat Islands. <https://www.epa.gov/heat-islands/using-cool-roofs-reduce-heat-islands>.
 48. Meir, M. G., Rekstad, J. B. & LØvvik, O. M. A study of a polymer-based radiative cooling system. *Sol. Energy* **73**, 403–417 (2002).
 49. Skartveit, A., Olseth, J. A., Czeplak, G. & Rommel, M. On the estimation of atmospheric radiation from surface meteorological data. *Sol. Energy* **56**, 349–359 (1996).
 50. M., B. P. and M. Emissivity of clear skies. *Solar Energy* **32**, 663–664.
 51. Unsworth, M. H. & Monteith, J. L. Long-wave radiation at the ground. *Q. J. R. Meteorol. Soc.* **101**, 1029–1030 (1975).
 52. Unsworth_and_Monteith_Q_J_R_Met_Soc_1975_Long-waveII.pdf.
 53. Molineaux, B., Lachal, B. & Guisan, O. Thermal analysis of five unglazed solar collector systems for the heating of outdoor swimming pools. *Sol. Energy* **53**, 27–32 (1994).

54. Raman, A. P., Anoma, M. A., Zhu, L., Rephaeli, E. & Fan, S. Passive radiative cooling below ambient air temperature under direct sunlight. *Nature* **515**, 540–544 (2014).
55. S, P. M. *M S, Pandian. (2014). X-ray Diffraction Analysis: Principle, Instrument and Applications.*
56. X-ray Powder Diffraction (XRD).
https://serc.carleton.edu/research_education/geochemsheets/techniques/XRD.html.
57. Infrared Technology.
<https://web.archive.org/web/20141108081407/http://thermalscope.com/about-thermal-imaging>.
58. Thermographic picture house. <https://www.dreamstime.com/stock-photo-thermographic-picture-house-image26558230>.
59. Flir b60 Infrared Thermal Imaging Camera. <http://www.merlinlazer.com/b60-Infrared-Thermal-Imaging-Camera-2>.
60. Thermal Image washing machine.
<https://www.flickr.com/photos/neeravbhatt/31991360711>.
61. Thermal Camera.
https://commons.wikimedia.org/wiki/File:Fluke_Thermal_Imager.jpg.
62. How ‘Cool Roofs’ Can Pull the Plug on Water Shortages.
<https://www.nbcnews.com/mach/science/how-cool-roofs-can-pull-plug-water-shortages-ncna814296>.
63. Ao, X. *et al.* Preliminary experimental study of a specular and a diffuse surface for daytime radiative cooling. *Sol. Energy Mater. Sol. Cells* **191**, 290–296 (2019).
64. Zhong, M., Fu, W., Da, W. & Su, D. Study on preparation and near-infrared reflective properties of NaZnPO₄. *Adv. Mater. Res.* **399–401**, 1289–1293 (2012).
65. Pal, S., Contaldi, V., Licciulli, A. & Marzo, F. Self-Cleaning Mineral Paint for Application in Architectural Heritage. *Coatings* **6**, 48 (2016).
66. Krizan, D. & Zivanovic, B. Effects of dosage and modulus of water glass on early hydration of alkali-slag cements. *Cem. Concr. Res.* **32**, 1181–1188 (2002).
67. Spectrophotometers Facilities.
<https://www.lakeheadu.ca/centre/lucas/laboratories/luil/facilities/specs>.
68. Edeagu, S. O. MID-INFRARED QUANTUM CASCADE LASERS. **31**, 227–232 (2012).
69. QUANTUM CASCADE LASER BASICS.
<https://www.teamwavelength.com/quantum-cascade-laser-basics/>.

70. *Atomic Units*. https://www.phys.ksu.edu/personal/cdlin/class/class11a-amo2/atomic_units.pdf.

